EVALUATION OF CHARGED-PARTICLE INDUCED NUCLEAR REACTIONS CROSS-SECTIONS FOR THE PRODUCTION OF NON-STANDARD MEDICAL RADIONUCLIDES ^{55}Co, ^{61}Cu AND ^{186}Re

SAMER KAMAL ISSA ALI

FACULTY OF SCIENCE
UNIVERSITY OF MALAYA
KUALA LUMPUR

2019

EVALUATION OF CHARGED-PARTICLE INDUCED NUCLEAR REACTIONS CROSS-SECTIONS FOR THE PRODUCTION OF NON-STANDARD MEDICAL RADIONUCLIDES ^{55}Co, ^{61}Cu AND ^{186}Re

SAMER KAMAL ISSA ALI

THESIS SUBMITTED IN FULFILMENT OF THE REQUIREMENTS FOR THE DEGREE OF DOCTOR OF PHILOSOPHY

DEPARTMENT OF PHYSICS
FACULTY OF SCIENCE
UNIVERSITY OF MALAYA
KUALA LUMPUR

2019

UNIVERSITY OF MALAYA

ORIGINAL LITERARY WORK DECLARATION

Name of Candidate: **SAMER KAMAL ISSA ALI**

Matric No: **SHC140072**

Name of Degree: **DOCTOR OF PHILOSOPHY**

Title of Thesis: **EVALUATION OF CHARGED-PARTICLE INDUCED NUCLEAR REACTIONS CROSS-SECTIONS FOR THE PRODUCTION OF NON-STANDARD MEDICAL RADIONUCLIDES ^{55}Co, ^{61}Cu AND ^{186}Re**

Field of Study: **THEORETICAL PHYSICS**

I do solemnly and sincerely declare that:

(1) I am the sole author/writer of this Work;
(2) This Work is original;
(3) Any use of any work in which copyright exists was done by way of fair dealing and for permitted purposes and any excerpt or extract from, or reference to or reproduction of any copyright work has been disclosed expressly and sufficiently and the title of the Work and its authorship have been acknowledged in this Work;
(4) I do not have any actual knowledge nor do I ought reasonably to know that the making of this work constitutes an infringement of any copyright work;
(5) I hereby assign all and every rights in the copyright to this Work to the University of Malaya ("UM"), who henceforth shall be owner of the copyright in this Work and that any reproduction or use in any form or by any means whatsoever is prohibited without the written consent of UM having been first had and obtained;
(6) I am fully aware that if in the course of making this Work I have infringed any copyright whether intentionally or otherwise, I may be subject to legal action or any other action as may be determined by UM.

Candidate's Signature Date:

Subscribed and solemnly declared before,

Witness's Signature Date:

Name:

Designation:

EVALUATION OF CHARGED-PARTICLE INDUCED NUCLEAR REACTIONS CROSS-SECTIONS FOR THE PRODUCTION OF NON-STANDARD MEDICAL RADIONUCLIDES ^{55}Co, ^{61}Cu AND ^{186}Re

ABSTRACT

Radioisotopes that emit positrons and beta particles show great potential to be used as an active material in diagnostic and therapeutic radiopharmaceuticals, respectively. The radionuclides ^{55}Co, ^{186}Re and ^{61}Cu can be produced via several pathways, however charged-particle induced nuclear reactions show promising towards no carrier added (NCA) production. Many experiments for the production cross-sections of the aforementioned radionuclides were conducted around the world in the last few decades, and they are available in various platforms such as journals, database etc. The EXFOR library, which is maintained by the International Atoms Energy Agency (IAEA), contains an extensive compilation of experimental nuclear reaction cross-sections reported by various authors throughout the world. Nuclear reaction cross-sections play an important role to determine the possibility of producing a radionuclide in pure form or in NCA form. But production cross-sections for a particular radionuclide measured by different authors and/or in laboratories mostly show considerable discrepancies. However, it is possible to overcome the existing discrepancies among the data sets, if the experimental data could be evaluated precisely. Specifically, a more accurate form of nuclear reaction cross-sections can be obtained by evaluating reported cross-sections considering all relevant parameters with respect to the updated ones, i.e., latest agreed values of standards. In this work, cross-sections for ^{55}Co, ^{61}Cu and ^{186}Re radionuclides measured via light-ion-induced nuclear reactions those available in the EXFOR library are evaluated in low energy range. An effective evaluation technique such as Simultaneous Evaluation on KALMAN (SOK) code are used in this evaluation. SOK code mainly used KALMAN filter combined with least squared method to give values close to the real cross-sections

for the reactions of interest, and also to reduce the reported experimental errors in a mathematically correct way. KALMAN filter combined with least square concept was used to obtain the evaluated data together with covariances matrices, and finally obtained one fitted curve following the concept of spline fitting technique. The evaluated cross-sections obtained via SOK code are compared with the calculated cross-sections obtained via some established nuclear reaction model codes such as TALYS (Developed by NRG in Petten, the Netherlands, and CEA in Bruyères-le-Châtel, France) and EMPIRE (Developed by Brookhaven National Lab, USA and IAEA). Our evaluated cross-sections show partial agreement with the calculated data by Talys and Empire code.

Keywords: Cross-Sections, Medical radionuclides, Isotopes production, Data evaluation, cross-section simulation.

PENILAIAN TINDAK BALAS KERATAS RENTAS NUKLEAR YANG DITIMBULKAN OLEH ZARAH YANG DICAS BAGI PENGELUARAN PERUBATAN TIDAK UMUM RADIONUKLID ^{55}Co, ^{61}Cu DAN ^{186}Re

ABSTRAK

Radioisotop yang memancarkan positron dan zarah-zarah beta menunjukkan potensi yang besar untuk digunakan sebagai bahan aktif dalam pengesanan pengimejan dan terapi radiofarmasitikal. ^{55}Co, ^{61}Cu dan ^{186}Re boleh dihasilkan dalam beberapa tindak balas nuklear, namun begitu reaksi yang disebabkan oleh zarah-zarah dicas menunjukkan ketiadaan pengeluaran pembawa tambahan. Banyak eksperimen-eksperimen penghasilan tindak balas terpilih telah diterbitkan di seluruh dunia dalam beberapa dekad yang lalu, keratan rentas yang disiarkan ini telah disenaraikan dalam perpustakaan EXFOR dan digunakan dalam bahagian kesusasteraan dalam kajian penilaian ini. Perpustakaan EXFOR mengandungi kompilasi menyeluruh data eksperimen tindakbalas nuklear dan dianjurkan dan dikendalikan oleh Agensi Tenaga Atom Antarabangsa (IAEA). Perkara yang paling penting adalah data tepat bagi keratan rentas tindak balas-tindak balas nuklear dimana ia amat penting untuk mendapatkan hasil yang betul dari radionuklid yang dikehendaki. Dalam hasil kerja ini, pengeluaran keratan rentas ^{55}Co, ^{61}Cu dan ^{186}Re dinilai untuk tindak balas akibat zarah yang dicaskan cahaya dalam julat tenaga yang rendah. Tindakbalas terpilih terlibat dalam penilaian ini. Teknik penilaian yang berkesan seperti Penilaian Serentak pada kod KALMAN (SOK) memberikan nilai-nilai yang dekat dengan nilai keratan rentas sebenar untuk tindak balas ini. Kod SOK terutamanya menggunakan penapis KALMAN digabungkan dengan kaedah kuadrat terkecil, yang secara matematik mengurangkan kesilapan dalam data eksperimen yang sudah diterbitkan, penapis KALMAN yang digabungkan dengan konsep paling kurang persegi telah digunakan untuk mendapatkan data yang dinilai bersama-sama dengan matriks kovarians dan satu lengkung dipasang yang dihasilkan oleh konsep teknik kekemasan

spline. Untuk mengesahkan data keratan rentas pengeluaran yang dievaluasi, kod Empire yang dibangunkan oleh IAEA- digunakan untuk mengira keratan rentas untuk tindak balas yang dipilih dan dibandingkan dengan keratan rentas yang disenaraikan di perpustakaan data nuklear berasaskan TENDL TALYS.

Kata kunci: keratan rentas, Radionuklid perubatan, Pengeluaran isotop, Penilaian data, simulasi keratan rentas.

ACKNOWLEDGEMENTS

"All the praises and thanks be to Allah, Who has guided us to this, and never could we have found guidance, were it not that Allah had guided us!" Al-A'raaf:43

I would like to express my special appreciation to my respected supervisors Prof. Dr. Mayeen Uddin Khandaker and Prof. Dr. Hasan Abu Kassim for their invaluable guidance, encouragement, advice and helpful insights.

To my father Kamal Al Manasrah and my Mother, who have provided me by moral, emotional and financial support during my life, because I owe it all to you. Many Thanks!

A very special gratitude goes to my sweetheart Huda for all the feelings she granted me over the years of study.

I am also grateful to my other family members and friends who have supported me along the way, credits to my best friends Baker Al-Sharaa, Fuad Abu-Taha, Ali Abu-Hamad, Ibrahim Al-Junaidi, M. Mansour and A. Razayneh.

And finally, I would like to thank my colleagues at the theoretical lab; Sophia Ahmad, Firas Abed, Lurwan Garba. It was great moments sharing the laboratory work with all of you during my research journey.

Samer K. Issa

August - 2018

TABLE OF CONTENTS

LIST OF FIGURES

LIST OF TABLES

LIST OF SYMBOLS AND ABBREVIATIONS

α	:	Alpha
$\bar{\upsilon}$	:	anti-neutrino
β^-	:	Beta
σ	:	cross-section
λ	:	Decay constant
γ	:	Gamma
$t_{1/2}$	:	Half-Life
υ	:	neutrino
β^+	:	Positron
HDEP	:	(1-hydroxyethylidene) diphosphonate
Bq	:	Becquerel
BGO	:	Bismuth germanate
C	:	Carbon
Co	:	Cobalt
CT	:	Computed Tomography
Cu	:	Copper
Ci	:	Curie
d	:	deuteron
EC	:	Electron Capture
eV	:	electron volt
EOB	:	End of bombardment
EXFOR	:	EXchange FORmat library
F	:	Fluorine
FDG	:	Flurodeoxyglucose
Ga	:	Gallium
GLS	:	Generalized Least Squares
Ge	:	Germanium
GeLi	:	Germanium Lithium
Au	:	Gold
HPGe	:	High-Purity Germanium
IAEA	:	International Atoms Energy Agency
Fe	:	Iron
JAERI	:	Japan Atomic Energy Research Institute

keV	:	kilo electron volt
LINUX	:	Linus Torvald's UNIX (Operating System)
LDL^T	:	Lower Diagonal Lower Transpose
LDU	:	Lower Diagonal Upper decomposition
MeV	:	Mega electron volt
mb	:	millibarn
n	:	Neutron
Ni	:	Nickel
N	:	Nitrogen
NCA	:	no carrier added
OLS	:	Ordinary Least Squares method
O	:	Oxygen
PET	:	Positron Emission Tomography
P	:	Proton
ROS	:	Reactive Oxygen Species
Re	:	Rhenium
Rb	:	Rubidium
SOK	:	Simultaneous Evaluation on KALMAN
SPECT	:	Single Photon Emission Computed Tomography
Na	:	Sodium
Sr	:	Strontium
TOI	:	Table of Isotopes
TENDL	:	TALYS-based evaluated nuclear data library
NaI[Tl]	:	Thallium-doped sodium iodide
SRIM	:	The Stopping and Range of Ions in Matter
W	:	Tungsten
UMC	:	Unified Monte Carlo
Zn	:	Zinc

CHAPTER 1: INTRODUCTION

Throughout the ages, human beings have been mediating and observing the surrounding nature. The early Greek's philosophers tried to understand the matter by dividing it into very simple categories. The fundamentals of time, space, energy and matter seemed to be correct over time. Until Sir Isaac Newton's revolution in natural science and the foundation of classical physics, many phenomena explained through classical physics successfully. For over than 200 years, concepts of structure of the matter gradually became better, by the opening of the 20th century many exciting researches continued with more focusing on atomic and subatomic level. The beginning of nuclear physics may be traced to the discovery of radioactivity by Becquerel in 1896, France. Since the known classical physics wasn't able to explain radioactivity, the desire to understand this and other few exceptions led up to the birth of modern physics, and hence models were proposed to puzzle out the atoms and nucleus. Numerous studies established to further understanding nucleus, its properties, and to employ the nuclear science in various areas and applications. In this chapter briefly introduced general nuclear properties, stability and binding energy, radioactivity, nuclear medicine and Research objectives.

1.1 General Properties of Nuclei

The intense research activity in the last century has resulted in a good knowledge on nuclear physics. Nucleons are the main building blocks of the nucleus, protons (p) give the positively charge to nucleus while neutrons (n) are electrically neutral. The atomic number (Z) which represents the number of protons determines the element and its chemical properties, atomic number may vary from Z=1 Hydrogen to Z=118 Oganesson –first synthesized in 2002 in Russia- and organized in the well-known periodic table (IUPAC, 2016). The number of nucleons (all protons and neutrons) gives the mass

number (*A*) which is also determines nucleus weight and the radius *(R)* of nucleus through the following Equation 1.1.

$$R = r_{\circ} A^{\frac{1}{3}} \tag{1.1}$$

Where $r_{\circ} = 1.2fm$.

1.2 Binding Energy and Nuclear Stability

The energy that binds all nucleons together in nucleus is called binding energy, this energy originated from the nucleus itself. For a nucleus of *Z* protons and *N* neutrons the actual mass is less than the summation of individual masses of protons and neutrons. However, this difference in mass was converted to form binding energy and given in Equation 1.2

$$E_B(Z,N) = \left[\left(Z * m_p\right) + (N * m_n) - m(Z,N)\right] * C^2 \tag{1.2}$$

Where $E_B(Z,N)$ is the binding energy of nucleus with *Z* protons and *N* neutrons, $m_p, m_n \; and \; m(Z,N)$ are the masses of protons, neutrons and nucleus, respectively. C is the speed of light (Bertulani, 2007). However, nuclear stability only found in very narrow range in *Z* – *N* plot close to *Z* = *N* line for the low *Z* nuclides in the stable nuclei distribution Figure 1.1 taken from (Wikimedia Commons, 2015), for higher *Z* nuclides there should be more neutrons to achieve nuclear stability. While other nuclides undergoes spontaneous decay through converting protons to neutrons for rich protons nuclei; conversely, nuclides with extra neutrons tend to convert neutrons to protons. Such transformation called disintegration or decay, and its rate measured by dis/sec or Becquerel (*Bq*). However, all of the heavy (*Z* > 83) elements found in nature are radioactive except $^{209}_{83}Bi$ isotope, the only stable nuclide that its atomic number is greater

than $_{82}$Pb (Turner, 2008), Equation 1.3 shows the conversion from proton to neutron, and Equation 1.4 shows neutron to proton conversion

$$ {}^{1}_{1}p \rightarrow {}^{1}_{0}n + {}^{0}_{1}\beta + \upsilon \tag{1.3} $$

$$ {}^{1}_{0}n \rightarrow {}^{1}_{1}p + {}^{0}_{-1}\beta + \bar{\upsilon} \tag{1.4} $$

Where $({}^{0}_{+1}\beta, {}^{0}_{-1}\beta)$ are positron and beta particle, and $(\upsilon, \bar{\upsilon})$ are neutrino and anti-neutrino

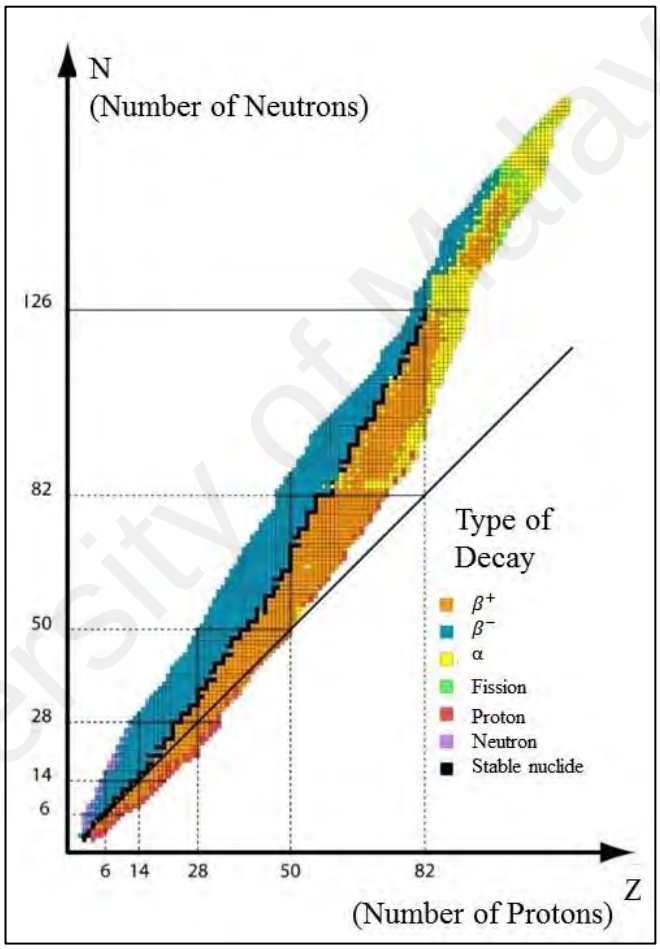

Figure 1.1: Stable nuclei distribution.

1.3 Radioactivity and Radioisotopes in Medicine

As a nucleon may transform to another nucleon in order to achieve stability, other related processes may occurs such as capturing an electron from innermost orbit by nucleus, and hence a proton converts to neutron, nuclei may decay by gamma photon emission. In some rare cases when the nucleus is extremely heavy, probability to

spontaneous fission become higher. For any radioactive material there is a specific decay constant (λ), from this constant half-life $(t_{1/2})$ of that material given by Equation 1.5 and activity at any time (t) can be calculated and given by the exponential decay function Equation 1.6. From Equation 1.7 one can calculate the activity by knowing the number of nuclides (N) in the sample.

$$t_{1/2} = \frac{ln(2)}{\lambda} \tag{1.5}$$

$$A = A_{\circ} e^{-\lambda t} \tag{1.6}$$

$$A = \lambda * N \tag{1.7}$$

Besides Becquerel (Bq), radioactivity can be measured in Curie (Ci) another common unit for radioactivity, which is originally represents the activity ascribed to 1 gm of ^{222}Ra. Now 1 (Ci) is defined as 1.7×10^{10} (Bq), exactly. However, Radionuclides may found naturally either primordial from the creation of the earth or cosmogenic or can be produced artificially by nuclear reactors, accelerators (Froehlich, 2009). The foremost radioisotopes application is nuclear medicine and imaging via Positron Emission Tomography (PET) and gamma camera. The historical backdrop for nuclear medicine isn't confined to one scientific field since many contributions came from physics, engineering, medicine and chemistry. Nuclear medicine can be used for imaging, diagnosis and treatment. Nuclear medicine offers the potential to identify disease in its earliest stage often before symptoms occur or before abnormalities can be detected by other diagnostic tests. Radioisotope with specific properties required to perform the test, however, nuclear medicine can be used in both adults and children to provide informative images of serious physiological processes such as spinal fluid flow or leakage, determination of cancer stage through inspection presence or spread of cancer in various parts of the body.

However, radiopharmaceuticals a medical drugs traced with radionuclide, are taken orally or intravenously. Then images were captured by external gamma detectors using the gamma rays emitted by that radionuclide. In order to achieve good treatment results or informative images, we need also to take into account radiation dose deposited to the patient and the cost as well. Hence, the demand to find out new options of radionuclides become considerable. More description about nuclear medicine and radionuclides production for medical purposes later in chapter two.

1.4 Research Objectives

This study aims to evaluate production cross-sections of non-standard but promising radionuclides for medical applications. The aim and objectives are planned and carried out by combination of computational codes and basic mathematical programs. The objectives of this work are:

- To investigate the production routes for non-standard medical radionuclides ^{55}Co, ^{61}Cu and ^{186}Re.
- To normalize the literature data based on the latest decay data, monitor reactions, isotopic abundances etc.
- To construct experimental correlation matrices using systematic and statistical uncertainties
- To apply SOK code combined with least-squares method on the corrected data for the reactions of interest
- To obtain evaluated data together with covariance matrix for the reactions of interest and recommend cross-section values very close to real excitation functions for the reactions of interest.

- To compare the evaluated data with the predictions of the nuclear reaction model codes TALYS and EMPIRE, and to see how the modelling codes calculated results deviate from the recommended cross-sections.

1.5 Thesis Outline and Organization

This thesis has been divided into six chapters, first chapter contains selected general concepts of nuclear physics, Radioactivity, Radioisotopes in medicine. Research Objectives also listed in the introduction chapter.

Chapter two provides a brief overview of nuclear reactions and continues with nuclear medicine and radiopharmaceuticals. We have introduce the ^{55}Co, ^{61}Cu and ^{186}Re radioisotopes involved in the study.

However, all literature data (experimental results) on ^{55}Co, ^{61}Cu and ^{186}Re production reactions extracted from the EXFOR database maintained by the International Atomic Energy Agency (IAEA). Chapter 3, investigates these experiments and select, exclude some of these experiments for this study.

Mathematical framework used in this study including KALMAN, Generalized Least Squares methods, Linear and Quadratic Spline fitting functions and Variance-Covariance matrices are described in Chapter 4. EMPIRE and TALYS nuclear reaction model codes also discussed in this chapter.

Chapter 5 presents the evaluated cross-sections for the ^{56}Fe(p,2n)^{55}Co reaction in the first subsection "Section 5.1". In Section 5.2, evaluated cross-sections for ^{61}Cu production reactions considered in this work: ^{58}Ni(α,p)^{61}Cu, ^{59}Co(α,2n)^{61}Cu, ^{60}Ni(d,n)^{61}Cu, ^{64}Zn(p,α)^{61}Cu. Evaluated cross-sections for ^{186}W(p,n)^{186}Re and ^{186}W(d,2n)^{186}Re reactions were discussed in Section 5.3. Obtained evaluated Cross-sections and/or excitation

functions of this work were compared with other theoretical works in the plotted graphs. Covariances matrices plots were included and briefly discussed in this chapter.

Finally, the conclusion of this work is reported in Chapter 6. Also includes the future challenges and research directions.

CHAPTER 2: LITERATURE REVIEW

In this chapter, a review of previous studies and researches that is pertinent to this study was illustrated. More details about nuclear medicine and radiopharmaceuticals had been presented in this chapter. Main concepts of Positron Emission Tomography (PET) and Single Photon Emission Computed Tomography (SPECT) were discussed. Information about the proposed ^{55}Co, ^{61}Cu and ^{186}Re radioisotopes and their significance in the nuclear medicine were included in this chapter.

2.1 Nuclear Medicine

Nuclear medicine is a medical specialty that harnesses the power of radioactivity and high-tech equipment to help diagnosis and treat diseases in a unique way. In particular, nuclear medicine not only the study the function of organs, but also offer the potential to diagnose disease at an earlier stages than other diagnostic tests. Unlike other uses of radiation medicine such as X-ray which come from machines outside the body, instead radiation is injected, swallowed or inhaled to get inside the body. Nuclear medicine can be divided in to two branches imaging tests (diagnosis) and radionuclide therapy. However, Positron Emission Tomography (PET) and Single Photon Emission Computed Tomography (SPECT) are the two most common imaging modalities in nuclear medicine.

2.1.1 Positron Emission Tomography (PET) and Single Photon Emission Computed Tomography (SPECT)

PET and SPECT are non-invasive techniques used to create images for internal organs or tissues in the body, these images were constructed through detecting the gamma rays originally produced from radioactive material already administrated to the body. An intense array of scintillation crystals composite from solid crystals such as thallium-doped sodium iodide (NaI[Tl]), bismuth germante BGO ($Bi_4Ge_3O_{12}$), cerium-doped lutetium

oxyorthosilicate LSO (Lu_2SiO_5[Ce]) or cerium-doped gadolinium oxyorthosilicate GSO (Gd_2SiO_5[Ce]) were used for gamma detection in PET (Melcher, 2000). In order to enhance received photons signals, these scintillators were attached with photomultiplier tubes to magnify the electronic signals created by interaction between scintillator and the received photons, this electronic signal need to be processed later for image reconstruction.

However, the photons source in PET imaging is the two 511 keV gammas created from positron-electron annihilation, while the gamma rays used in SPECT are prompt gamma associated with radioisotope decay, some common isotopes used in SPECT scans ^{99m}Tc, ^{123,125}I, ^{111}In, ^{67}Ga, ^{177}Lu, ^{201}Ti and ^{117m}Sn. As a result, PET images are better in quality than those images taken by SPECT (Jadvar & Parker, 2006; Rahmim & Zaidi, 2008). In order to maximize the images quality, medical equipment producers tend to fuse the PET scanner with Computed Tomography (CT scanner) to produce the PET/CT scanner shown in Figure 2.1 taken from (Siemens Healthcare, 2018) or to merge PET scanner with Magnetic Resonance Imaging (MRI) in one hybrid system PET/MRI (Mannheim et al., 2018). Figure 2.2 taken from (Metrohm, 2015) shows the principle of PET scan, where the isotope disintegration occurred inside the body and the produced 511 keV detected by the scanner and registered in the sinogram file. Later, this file will go to further step for image reconstruction.

Figure 2.1: PET/CT scanner machine.

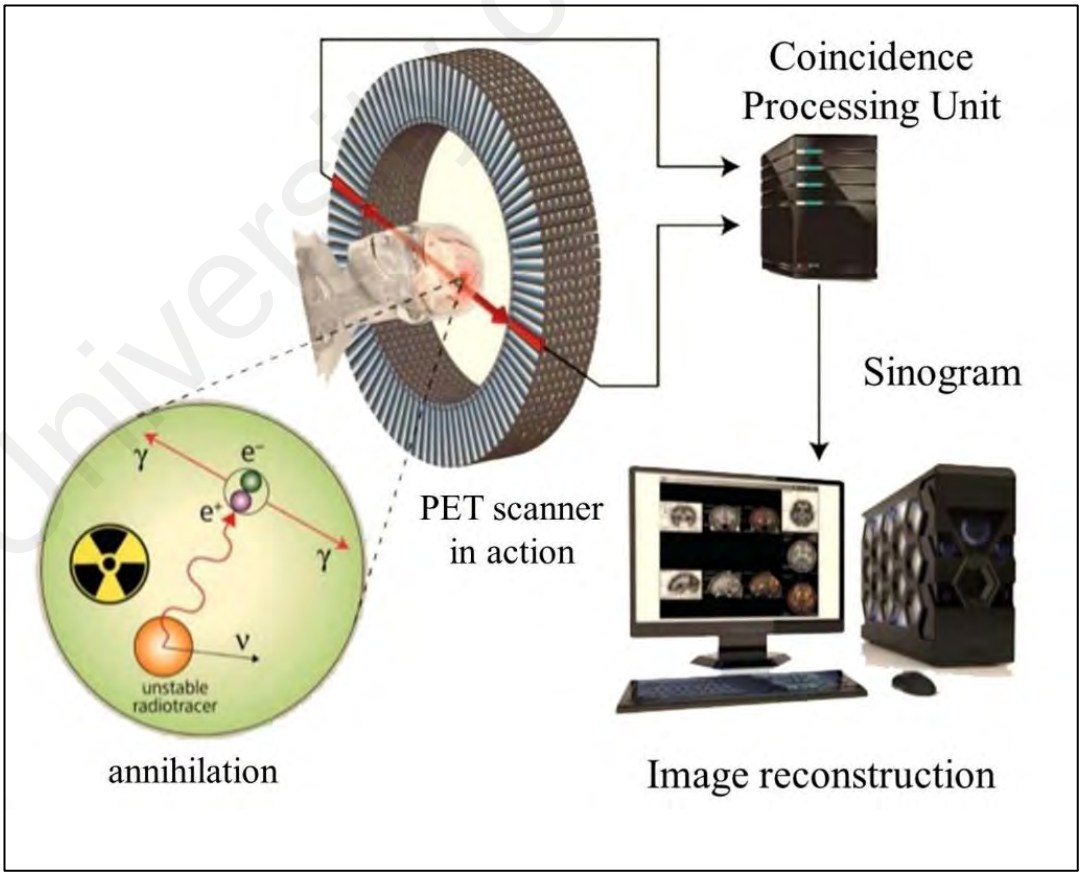

Figure 2.2: Principle of PET scan.

2.1.2 Radionuclide Therapy

In this therapeutic technique, an alpha or beta emitters were used to deliver a highly absorbed radiation dose to a targeted tumour and save the surrounding normal tissue from being affected. This selectivity property of therapeutic radionuclide made this kind of cancer treatment more preferable than using external beam radiotherapy. Since in many cases such as in bone metastases the whole body irradiation is impossible.

Many isotopes have been successfully used in the treatment of both benign and malignant tumours. ^{131}I, ^{32}P, ^{90}Sr, ^{90}Y and ^{99m}Tc are examples of currently used radionuclides. Certain physical and biochemical characteristics are required in the therapeutic radionuclide to consider it as suitable isotope for therapy. Mode of decay, physical half-life, daughter produced, radionuclide purity, energy released to the emitted particle and method of production are the physical characteristics to be considered in the choice of radionuclide. While the biochemical aspects include in vivo stability, tissue targeting, toxicity and retention of radioactivity in tumour (Yeong et al., 2014).

2.2 Radiopharmaceuticals

Radiopharmaceuticals, as the name propose, is a pharmaceutical formulae composite from radionuclide linked with molecular structure that determine the target organ/tissue. Since the radiolabelled molecules and their non-radioactive form are chemically identical, the organism cannot distinguish radiopharmaceuticals from their non-radioactive counterparts. Therefore, radiopharmaceuticals can be used to monitor the functional processes of the target organs/tissue by tracking radioactive molecules in vivo (Wadsak & Mitterhauser, 2010). In summary, radiopharmaceuticals are probes that sending information about physiological processes at molecular level to the outside detecting machine, and they are mainly composed from and radionuclide linked to molecular

structure (vehicle molecule). Figure 2.3 illustrates the concept of radiopharmaceutical and its components.

Vehicle molecule need to provide a high level of selectivity and specificity at the targets. Moreover, the radionuclide selection has to take the following consideration into account, radiopharmacological issues, physical properties of the radioisotope, radionuclide availability and radiochemical issues. Table 2.1 shows some of the currently used radionuclide for PET imaging; decay data were taken from National Nuclear Data Centre (nudat 2.7, 2018). Although the recently used PET radioisotopes such as ^{11}C, ^{13}N, ^{15}O, ^{18}F and ^{38}K have very high level of positron intensity, their physical half-lives are short. For instance, on site cyclotron required for ^{15}O production to pump the produced amounts directly to the scan room. For ^{11}C, ^{13}N, ^{38}K and ^{18}F half-lives are short for radiopharmaceutical preparation and delivery to the imaging place. Moreover, these short half-lives limit the physiological and biochemical processes can be tracked (Jadvar & Parker, 2006).

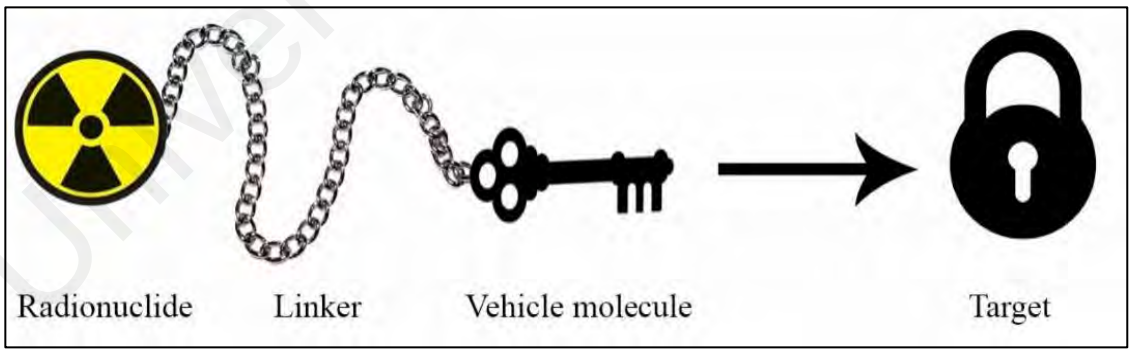

Figure 2.3: Radiopharmaceutical concept and its components.

Table 2.1: Examples of recently used radionuclides for PET imaging.

Radioisotope	Half-life	Production method	(β^+) intensity	Target organ/tissue	Reference
^{11}C	20.36 m	$^{14}N(p,\alpha)^{11}C$	99.7% (Kelley et al., 2012)	brain tumours and lung carcinoma	(Grassi et al., 2012)
^{13}N	9.96 m	$^{16}O(p,\alpha)^{13}N$	100% (Ajzenberg-Selove, 1991)	Cardiac imaging	(Wadsak & Mitterhauser, 2010)
^{15}O	122 s	$^{14}N(d,n)^{15}O$	99.9% (Ajzenberg-Selove, 1991)	Cerebral Blood flow	(Wadsak & Mitterhauser, 2010)
^{18}F	188 m	$^{18}O(p,n)^{18}F$	100% (Tilley et al., 1995)	Whole body	(Wadsak & Mitterhauser, 2010)
^{82}Rb	1.25 m	$^{82}Sr/^{82}Rb$ generator	100% (Tuli, 2003)	Myocardial blood flow	(Wadsak & Mitterhauser, 2010)
^{62}Cu	9.67 m	$^{62}Zn/^{62}Cu$ generator	100% (Nichols et al., 2012)	Imaging for hypoxia and perfusion in pulmonary lesions.	(Zhang et al., 2013)
^{68}Ga	67.7	$^{68}Ge/^{68}Ga$ generator	100% (McCutchan, 2012)	Evaluation of neuroendocrine tumours	(Wadsak & Mitterhauser, 2010)

2.3 Nuclear Reactions

As stated before, appropriate radioisotope is necessary for nuclear medicine to get the best results either in imaging or therapy, at the same time, isotopes to be used in nuclear medicine are short lived radioactive isotopes and they are not exist naturally. Thus, these radionuclides need to be produced different ways such as reactors, accelerators and generators.

Nuclear reaction defined as a change of atomic nucleus characteristics or identity caused by bombarding it with an energetic particle. The bombarding particle may be a neutron, a proton, an alpha particle, a heavy ion, or a gamma photons. In general, nuclear

reactions can be classified by the incident beam, bombarding energy, or target. In the case of incident beam classification, there are various type of projectiles charged-particle induced reaction such as protons (p), deuterons (d), alpha (α) or heavy-ion induced reaction such as ^{12}C, ^{16}O. Incident beam could also be neutrons, electron-induced reactions or photo-nuclear reactions such as gamma rays (Bertulani, 2007).

However, nuclear reaction follows several conservation laws, these laws play essential role in restricting the possible processes from take place when a given projectile bombard a target, these conservation laws are baryonic number, charge, energy and linear momentum, total angular momentum, isospin and parity. At any case, the incident particles must have the sufficient amount of energy to interact with the target nuclei, nuclear reaction equation written as incident channel and exit channel as follows $a + A \rightarrow b + B$ another more convenient form to describe nuclear reaction is A(a,b)B where *a, A* are the projectile and target *b, B* scattered particle (ejectile) and final nucleus, respectively. In line with reaction energy, every nuclear reaction the Q-value is calculated to describe the reaction energy, and therefore reaction type. The Q-value is given by (incident channel particles masses – exit channel particles masses) $*C^2$ as shown in Equation 2.1

$$Q = (m_a + m_A - m_b - m_B)C^2 \tag{2.1}$$

Where $m_a, m_A, m_b \; and \; m_B$ are the rest masses of projectile, target, ejectile, final nucleus, respectively, and C is the speed of light. A positive Q-value reaction exemplify exothermic reaction, and hence portion of energy is released. On the contrary, reactions with negative Q-value is endothermic and energy is required to initiate the reaction. Moreover, it is often possible to get the same exit channel starting from different combinations of target and incident projectile.

2.3.1 Nuclear Reaction Models

Due to nuclear reactions variety and complexity, numerus models and mechanisms were proposed to describe nuclear reactions. However, no single model can successfully describe all aspects of nuclear reactions, and therefore different reactions give useful information help to understand nucleus details. Table 2.2 shows some of nuclear reaction types and information obtained from each type (Aubrecht, 2003)

Table 2.2: Information obtained from some of nuclear reaction types.

Reaction	What is learned
Nucleon – nucleon scattering	Fundamental nuclear force.
Elastic scattering of nuclei	Nuclear size and interaction potential.
Inelastic scattering to excited states	Energy level location and quantum numbers.
Inelastic scattering to the continuum	Vibrational modes.
Transfer and knockout reactions	Details of shell model.
Fission reactions	Properties of Liquid Drop Model.
Fusion reactions	Astrophysical processes.
Compounds nucleus formation	Statistical properties of the nucleus.
Multi-fragmentation	Nuclear matter phases, Collective models.

According to Wigner (1995) the so called Compound nucleus model describes the nuclear reaction as a sequence of two events. In the first event, the projectile and the target nuclei merged together to form the compound nucleus. Although, this compound nucleus is not stable, but it has many of the stable nuclei properties such as well-defined energy levels. The second event is the decay of the compound nucleus into new pair of nuclei differ from initial. If the outgoing nuclei are similar to the nuclei formed the compound nucleus then there is no reaction took place and the process is scattering only. The probability of compound nucleus depends mainly on the energy of the colliding pairs, if

the energy of the colliding pairs is very close to any of the energy levels of the compound nucleus then the probability is very small. On the other hand, if the energy of the colliding pairs is perfect coincidence with any of the energy levels of the compound nucleus then the probability is very large.

In 1950, a forward peaking was observed in experiments done by Holt & Young (1950) and Burrows et al. (1950) in 8 MeV deuterons induced reactions which could not explain the compound nucleus model, therefore models describing Direct Reaction mechanism were proposed. First theoretical descriptions of direct nuclear reactions were based on simple plane wave approximation, distorted wave approximation, coupled channel formalism, later optical model and many other models were introduced. Figure 2.4 illustrates for the typical processes of protons-nucleus interactions.

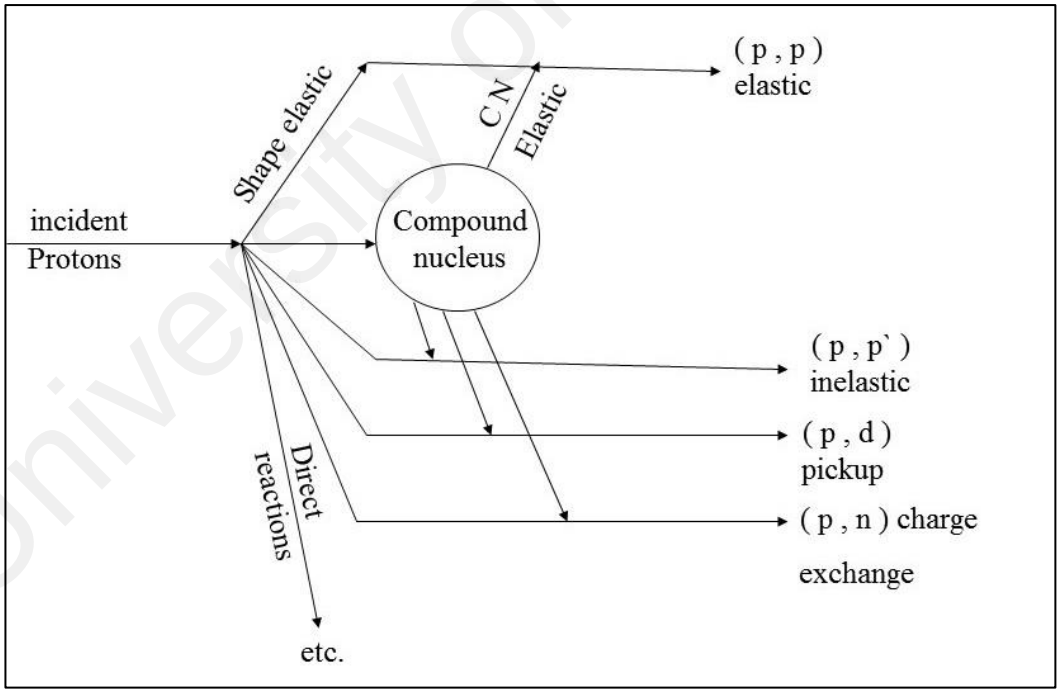

Figure 2.4: Illustration for the typical processes of protons-nucleus interactions taken from (Hodgson, 1971).

However, to ease the dealing with complex mathematical equations and to simplify the multi-particle quantum mechanics, these models in addition to many other models were combined together in computational codes for nuclear reaction modelling such as

EMPIRE and TALYS, these codes offer good options to apply more than one model for describing the nuclear reaction in wide energy range as well as different projectiles.

EMPIRE-3.2.2 and TALYS-1.8 were used for comparison purposes and discussed in later chapter in this thesis.

2.3.2 Cross-Sections

Reaction cross-section is the effective area that quantifies the intrinsic likelihood of particular event will be produced when an incident beam strikes a target object. Cross-section denoted by Latin lower case letter sigma "σ" and has the dimension of area. In nuclear reaction cross-section, because of extremely small nuclear dimensions in order of femtometer (1fm = 10^{-15} m) it is difficult to describe cross-sections in fm. Thus, the more applicable unit barn and mille barn (mb),1 barn = $1x10^{-28}$ m^2, is usually used (Cottingham & Greenwood, 2001). Cross-section is measured experimentally by the ratio shown in the Equation 2.2

$$\sigma = \frac{\text{number of reaction particles emitted}}{(\text{no. of beam particles per unit area})(\text{no. of target nuclei within the beam})} \qquad)2.2)$$

However, nuclear reactors and accelerators/reactors are used to produce isotopes for medical applications. Isotopes produced in reactors are generally neutron rich radionuclides and mostly decay by beta (β^-) emission. Isotopes produced by cyclotrons, on the other hand, are mainly neutron inadequate and decay by positron (β^+) emission or electron capture (EC) (Qaim, 2017). Since the study focuses on charged particles induced reactions, isotopes production via reactor routes is not included in this evaluation work.

2.3.3 Stacked Foils Technique

Most of the nuclear physicists perform their experiments to get the excitation function via irradiating thin layers with accelerated charged ion beam. In order to measure the cross-sections at different energies using mono-energetic ion beam, a series of thin foils -thicknesses in order of μm- made from target material were arranged together in stack. However, monitor reaction is used to monitor the beam energy and flux in the target foils. In order to measure energy of the beam passing the stacks, another set of foils composed from element with well measured excitation function need to be placed in front of the stack and inserted at different depths between target foils, monitor foils should be differ from target material (Daraban et al., 2008; Ditrói et al., 1995).

A third set of foils also required, degraders are used to gradually reduce the projectiles energy along the stack and to catch the reaction recoils. The catcher should be selected from low Z-material so doesn't decrease gamma attenuation during activity measurements, usually Al foils were used as catcher. Moreover, catcher or degrader foils should not produce radioisotopes same to those produced by the target in the stack. To collect the outgoing charged ions, Faraday cup also connected to the experiment.

Figure 2.5 shows a schematic diagram of the stacked foil arrangements. In addition to monitor foil, "The Stopping and Range of Ions in Matter" SRIM code also utilized in many of the recent experiments. SRIM calculate theoretically tables of stopping powers, ranges and straggling distributions for any ion at any energy in any target (Ziegler, 2004).

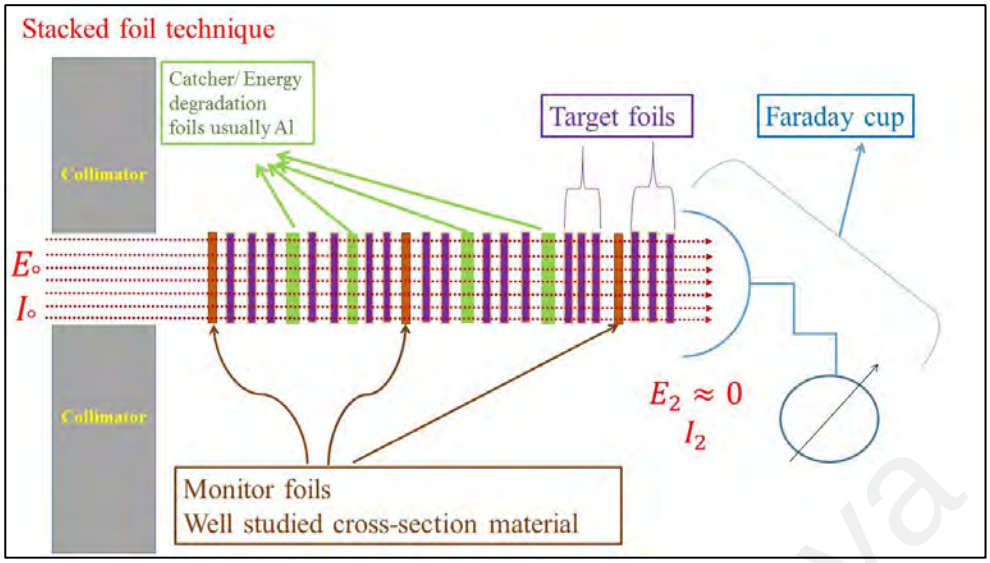

Figure 2.5: Schematic diagram the stacked foil arrangements.

2.3.4 Activation Formula

Furthermore, after bombardment the stack left for cooling, this cooling time remove the short lived isotopes from the stack foils before gamma measurement. Cross-section at the *i*th sample then calculated using the well-known activation formula shown in Equation 2.3 (Ghosh et al., 2017; Khandaker et al., 2010)

$$\sigma(E_i) = \frac{\lambda \times C(E_i)}{\varepsilon(E_\gamma) \times I_\gamma \times \rho \times t \times \varphi(1 - e^{-\lambda t_m})(e^{-\lambda t_c})(1 - e^{-\lambda t_i})} \tag{2.3}$$

Where λ is the decay constant (s^{-1}), $C(E_i)$ is the net count under the photo peak at the *i*th sample, $\varepsilon(E_\gamma)$ is the detection efficiency of the detector, I_γ is the γ-ray intensity, ρ is atomic density of the target (atoms/cm^3), t is the target thickness (cm), φ is the ion beam flux ($cm^{-2}s^{-1}$), t_m, t_c, t_i are the measurement time, cooling time and irradiation time, respectively, measured in seconds.

It is self-evident that the cross-section accuracy generally lean on the accuracy of different nuclear data such as isotope half-life, gamma intensity and monitor reaction cross-section. In addition to the accuracy of experiment equipment such as detector efficiency, beam energy accuracy and foils thicknesses.

2.4 Literature Review for ^{55}Co to be used in Nuclear Medicine

As stated in the preceding sections, the relatively short-lived positron emitters ^{11}C ($T_{1/2}$=20.3 min), ^{13}N ($T_{1/2}$=10.0 min), ^{15}O ($T_{1/2}$=2.0 min) and ^{18}F ($T_{1/2}$=110 min) are commonly used in PET technique. However, the drawback of these conventional PET radionuclides is that they are very short-lived, and therefore, the user has to be near to production facilities such as cyclotron. Moreover, for any targeting molecules having distribution times of several hours to days, conventional PET radionuclides are not always usable and alternative positron emitting radionuclides with matching half-lives and suitable labelling properties are thus necessary. In fact, the longest-lived radionuclides are suitable to be transported and used up to day(s) after their production, although it is noted that the fraction of radioactive impurities and/or daughter nuclides may grow as the desired radionuclide decays. The relatively long-lived radionuclide ^{55}Co ($T_{1/2}$=17.53 h) investigated here, is a promising candidate for PET imaging procedures, especially in diagnosing slower metabolic processes. It also plays a greater role as a Label for bleomycin in diagnostic nuclear medicine (Heinle et al., 1952; Sharma et al., 1986), and more recently, in some cardiac and cerebral studies (Spellerberg et al., 1998). Several authors (Jansen et al., 1994; Stevens et al., 1999) successfully applied ^{55}Co radioisotope as a PET imaging agent in the studies of ischemic stroke, and suggested its effective clinical use is limited up to 48 hours after the production due to the co-produced ^{56}Co ($T_{1/2}$=78.8 d, $I_{\beta+}$=19%) contaminant. Maziere et al. (1983) also used ^{55}Co nuclide for quantification of cerebrospinal fluid kinetics in different areas of the brain using PET imaging. ^{55}Co radioisotope was also applied as a potential renal imaging agent thru dynamic PET imaging of renal function of animal by Goethals et al. (2000).

2.5 Literature Review for ^{61}Cu to be used in Nuclear Medicine

Following the development of sophisticated technology together with various imaging procedures, the necessity on the development of new radio tracers show a great demand.

In the category of promising radionuclides, the ^{61}Cu ($T_{1/2} = 3.339\ h, E_{mean}(\beta^+) = 523\ keV, I_{total}(\beta^+) = 61.0\%$) offers appropriate radioactive properties to be used in Positron Emission Tomography (PET) and molecular imaging (Jalilian et al., 2009), and already been used for labelling of PET radio-pharmaceuticals such as (^{61}Cu-ATSM) Cu-diacetyl-bis(N4-methylthiosemicarbazone) and (^{61}Cu-ATPS) [^{61}Cu]-2-acetylpyridine thiosemicarbazone (McCarthy et al., 1999). The relatively long half-life of ^{61}Cu compared to the conventional PET radionuclides such as ^{18}F($T_{1/2}$=110 min), ^{15}O($T_{1/2}$=2 min), ^{13}N($T_{1/2}$=10 min) and ^{11}C($T_{1/2}$=20 min) allows producers to finalize chemical separation, radiolabelling without losing much of ^{61}Cu activity and gives chance to image slower metabolic processes in the body (Rowshanfarzad et al., 2006). Jalilian et al. (2006) showed interesting results in cancer treatment procedures, since various types of human cancers tend to accumulate copper which lead to DNA damage through reactive oxygen species (ROS) formation. In general, copper can form stable compounds with various organic molecules, which provides necessary biological affinity and therapeutic activity sufficient for targeting particular sites in the body (Krajčiová et al., 2014). Unlike other transition elements whose breaking their complexes up causes accumulation and toxicity in the tissue, copper atoms leaked from its compounds are removed quickly from normoxic cells (Laforest et al., 2005; Szymanski et al., 2012). ^{61}Cu decays to the stable ^{61}Ni via an EC/β^+ process (b_{EC} = 39%; $b_{\beta+}$ = 61%) which makes this isotope superior to ^{64}Cu in PET imaging due to the emission of low intensity β^+ particles ($E_{mean}(\beta^+) = 278\ keV, I_{total}(\beta^+) = 17.6\%$) by the later isotope (Jalilian et al., 2009). According to Williams et al. (2005), better quality images could be obtained by using ^{61}Cu than with ^{64}Cu, while the radiation dose is acceptable when compared to the widely used tracer ^{18}FDG.

2.6 Literature Review for ^{186}Re to be used in Nuclear Medicine

As a result of the similarity in electron configuration of technetium (Tc) and its neighbouring element rhenium (Re) in the periodic table, both the Tc and Re compounds have the similar chemical properties such as lipophilicity, ionic mobility, dipole moment and formal charge. Thus, the widely used Tc can be replaced by Re in some radiopharmaceuticals (Deutsch et al., 1986). The isotope ^{186}Re has a 3.7183 days half-life and decays by emitting beta particles with end point energy of 1069.5 keV ($I(\beta^-)_{total}$ =92.59%) which followed by emission of gamma photons with energy of 137.157 keV (Iγ=9.47%) and populate to the stable nucleus ^{186}Os and by EC (7.47%) to ^{186}W (Baglin, 2003b). Due to the emission of relatively high energetic beta particles E_{max} =1069.5 keV, ^{186}Re can be used as active material in radiopharmaceuticals to treat various types of tumours, and also recommended for routine clinical usage (Tebib et al., 2004). For example, HEDP[HEDP=(1-hydroxyethylidene) diphosphonate] (Deutsch et al., 1986) labelled with ^{186}Re was used for long time as palliative therapy of bone metastases from prostatic cancer (Maxon et al., 1992) or breast cancer (Lam et al., 2004), and for more than one painful metastatic site (Kolesnikov-Gauthier et al., 2000). Furthermore, ^{186}Re-sulfide colloid can be used in intra-articular corticotherapy especially medium joints (Klett et al., 2007; Knut, 2015; Özcan, 2014). In order to avoid bleeding during surgical synovectomies, radiosynovectomy can be applied using ^{186}Re on patients who suffer from hemophilia for rheumatoid arthritis and shows interesting results in pain reduction in the infected joints (Özcan, 2014; Silva et al., 2004). Furthermore, its appropriate gamma energy and intensity allow to track inside the patient body using SPECT modality or gamma camera, therefore, a better evaluation of the dose that has been delivered to desired site can be done (Eary et al., 1990; Knapp Jr et al., 1998; Palmedo et al., 2001). One of the promising applications for ^{186}Re is the radio immunotherapy using monoclonal antibodies labelled with ^{186}Re, since such radiolabelled

antibodies succeed in suppressing tumour from growing up after been administered into mice with metastases liver of human colon cancerous cells (Kinuya et al., 2002). It also shows better results than ^{131}I because of it's β particles has longer path inside the tumor and, as a result, a higher dose can be delivered to the tumour (Kinuya et al., 2005). Although the half-life of ^{186}Re is short, it is long enough to load it on chemical carrier and transports it far away from production stations (Ogawa et al., 2007).

2.7 Overview for Mathematical Methods and Computational Programs

Several mathematical techniques and computer codes were used in the current study. KALMAN filter combined with Generalized Least Squares method were implemented in the Simultaneous Evaluation on KALMAN code (SOK) code and used in this work. SOK code was developed and written in FORTRAN language by Japan Atomic Energy Agency JAERI (Kawano et al., 2000). Spline functions are utilized for curve fitting by SOK code, and this code requires LINUX platform to run. However, Figure 2.6 shows the flowchart of calculation steps carried out in this study.

For covariance matrices plotting, the ZV-View program an web tool developed by IAEA was used (Zerkin, 2009). Two more nuclear reaction modelling codes were used in this study, are EMPIRE-3.2.2 (Herman et al., 2007) and TALYS-1.8 (Koning & Rochman, 2012).

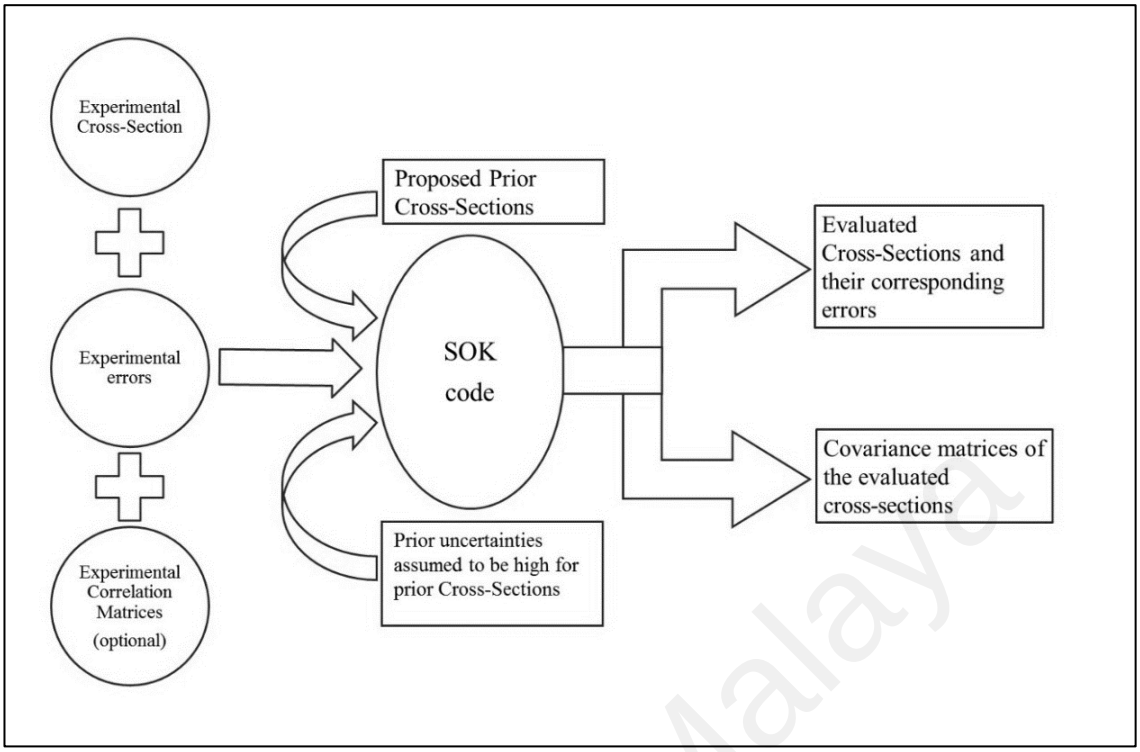

Figure 2.6: Flow chart of calculation procedure.

CHAPTER 3: ^{55}Co, ^{61}Cu AND ^{186}Re PRODUCTION CROSS-SECTION EVALUATION METHODOLOGY

In this chapter, experimental cross-section for ^{55}Co, ^{61}Cu and ^{186}Re production reactions were extracted from EXFOR library (EXFOR, 2018) and from original publications. Discussion, selection and de-selection for some experiments were done based on the explained reasons for each radioisotope.

3.1 Introduction

Nuclear data, especially cross-sections and decay data play an important role in the choice of a radionuclide for various applications. Decay profile such as decay energy, radiation type and half-life of a particular radionuclide determines the suitability of that radionuclide for possible applications in nuclear medicine. On the other hand, data of nuclear reaction cross-sections determine the possibility of producing a radionuclide in pure form or in no carrier added (NCA) form. Updated information of nuclear decay data can be obtained without significant deviation from established data bases such as the ENSDF library (Nichols & Tuli, 2007) and National Nuclear Data Centre NUDAT-2 data base (nudat2.7, 2018). But production cross-sections for a particular radionuclide measured by different authors and/or in laboratories mostly show considerable discrepancies.

In general, discrepancies among the different measurements may come due to various reasons: variations of monitor reactions, inappropriate cooling time, counting geometry and so on. However, it is possible to overcome the existing discrepancies among the data sets, if the experimental data could be evaluated precisely. Specifically, a more accurate form of nuclear reaction cross-sections can be obtained by evaluating reported cross-

sections considering all relevant parameters with respect to the updated ones, i.e., latest agreed values of standards.

3.2 Evaluation of Production Cross-Section for ^{55}Co

In this subsection, experiments lead to the production of Cobalt-55 ($T_{1/2}$=17.53 h, $E_{\beta+}\ (mean)$ =570 keV, $I_{\beta+}\ (total)$ =76%) will be considered for study in the energy range of 40 MeV down to the threshold energy of the ^{56}Fe(p,2n)^{55}Co nuclear reaction due to its significance as a potential PET imaging agent in medical applications.

3.2.1 ^{55}Co Production Route Selection

There are three common routes for the production of ^{55}Co, namely ^{56}Fe(p,2n)^{55}Co, ^{54}Fe(d,n)^{55}Co and ^{58}Ni(p,α)^{55}Co. Out of these, the ^{56}Fe(p,2n)^{55}Co reaction has the highest yield but the level of the ^{56}Co ($T_{1/2}$=78.8 d; $I_{\beta+}$=19.7%) impurity is about 2.6% (Jansen et al., 1994; Lagunas-Solar & Jungerman, 1979; Nieweg et al., 1981; Srivastava et al., 1993). However, according to (Jansen et al., 1995), contamination from ^{56}Co would be insignificant for the clinical use of ^{55}Co within the 48 hours of production. The ^{54}Fe(d,n)^{55}Co process leads to the highest purity product, provided highly enriched ^{54}Fe is used as a target material (Sharma et al., 1986; Zaman & Qaim, 1996) which is rather expensive. The need for high level enrichment of ^{54}Fe (5.8%) target, the non-availability of desired energies deuteron beams, and the possibility of considerable amount of neutron emission via deuteron break up process reflects limited use of ^{54}Fe(d,n)^{55}Co production route. The ^{58}Ni(p,α)^{55}Co production route finds limited application due to the high level (≅2%) of ^{57}Co ($T_{1/2}$=271.74 d) impurity (Maziere et al., 1983). Spellerberg et al. (1998) investigated the production of ^{55}Co from proton irradiations on highly enriched ^{58}Ni target, and reported a batch yield of 240 MBq (E_p=15→7 MeV) at EOB with 0.5% impurity from ^{57}Co (at EOB) which is relatively better than Maziere et al. (1983) reported

data. In fact, the reported batch yield by Spellerberg et al. (1998) is sufficient for applications in humans but the proton irradiations on enriched ^{58}Ni cannot be considered as the ideal process to produce ^{55}Co. This is because, ^{58}Ni(p,2p)^{57}Co reaction has large cross-sections and the half-life of ^{55}Co is very short compared to ^{57}Co half-life, therefore, the level of ^{57}Co impurity at the end of separation (EOS) would be invariably >0.5%. Moreover, it is not an easy process to separate ^{57}Co from the irradiated samples. However, based on the several favourable criterions: availability of low energy proton cyclotrons, ^{56}Fe (91.754%) target abundance, cost effectiveness and so on, ^{56}Fe(p,2n)^{55}Co reaction may be considered as the suitable one to produce ^{55}Co positron emitter and could apply to the patients within a moderate time of 48 hrs after the production with negligible impurity from ^{56}Co.

3.2.2 ^{56}Fe(p,2n)^{55}Co Experiments

It is to be pointed out that many earlier investigations (Al-Abyad et al., 2009; Cohen & Newman, 1955; Jansen et al., 1994; Jenkins & Wain, 1970; Kim et al., 2014; Lagunas-Solar & Jungerman, 1979; Michel et al., 1979; Nieweg et al., 1981; Read, 1968; Remsberg & Miller, 1963; Srivastava et al., 1993; Wenrong et al., 1993; Zhuravlev et al., 1984) are available in the literature leading to the production of ^{55}Co radioisotope by proton irradiations on natural and/or enriched ^{56}Fe targets due to its significance in nuclear medicine, testing of nuclear model calculations, integral data validation and some other applications. To obtain a more accurate form of production cross-sections, we evaluated pure experimental cross-sections of ^{55}Co radioisotope available in the EXFOR library (EXFOR, 2018) up to the energy range from 15 MeV the threshold energy to 40 MeV; relevant to its medical applications. Relevant details of this evaluation procedure are presented in the following sections.

A total of eight investigations (Cohen & Newman, 1955; Jenkins & Wain, 1970; Lagunas-Solar & Jungerman, 1979; Levkovskij, 1991a; Read, 1968; Remsberg & Miller, 1963; Wenrong et al., 1993; Zhuravlev et al., 1984); are available in the EXFOR library (EXFOR, 2018) for the production of ^{55}Co via the ^{56}Fe(p,2n)^{55}Co reaction. On the other hand, some other measured data (Al-Abyad et al., 2009; J. Barrandon et al., 1975; Daum, 1997; Kim et al., 2014; Michel et al., 1979; Williams & Fulmer, 1967) are also available for the ^{nat}Fe(p,x)^{55}Co reactions within our energy region of interest. Most of the reported data seems dedicated to measure the production cross-sections of ^{55}Co radioisotope by proton irradiations on natural and/or enriched ^{56}Fe targets but significant discrepancies are found among them, especially, in the absolute values of the reported cross-sections. Natural iron contains four stable isotopes: ^{54}Fe 5.85%, ^{56}Fe 91.75%, ^{57}Fe 2.12%, and ^{58}Fe 0.28%. The radionuclide ^{55}Co is produced mainly via the ^{56}Fe(p,2n)^{55}Co (E_{thr}=15.71 MeV) reaction when irradiated an iron target with natural isotopic composition. Considering the formation of ^{55}Co via the contribution of ^{57}Fe(p,3n)^{55}Co (E_{thr}=23.49 MeV) reaction from ≥25 MeV, the literature data for the ^{nat}Fe(p,x)^{55}Co reactions are corrected for ^{56}Fe(p,2n)^{55}Co reaction. All of the experimental data of ^{56}Fe(p,2n)^{55}Co reaction are presented in Figure 3.1 for a gross comparison.

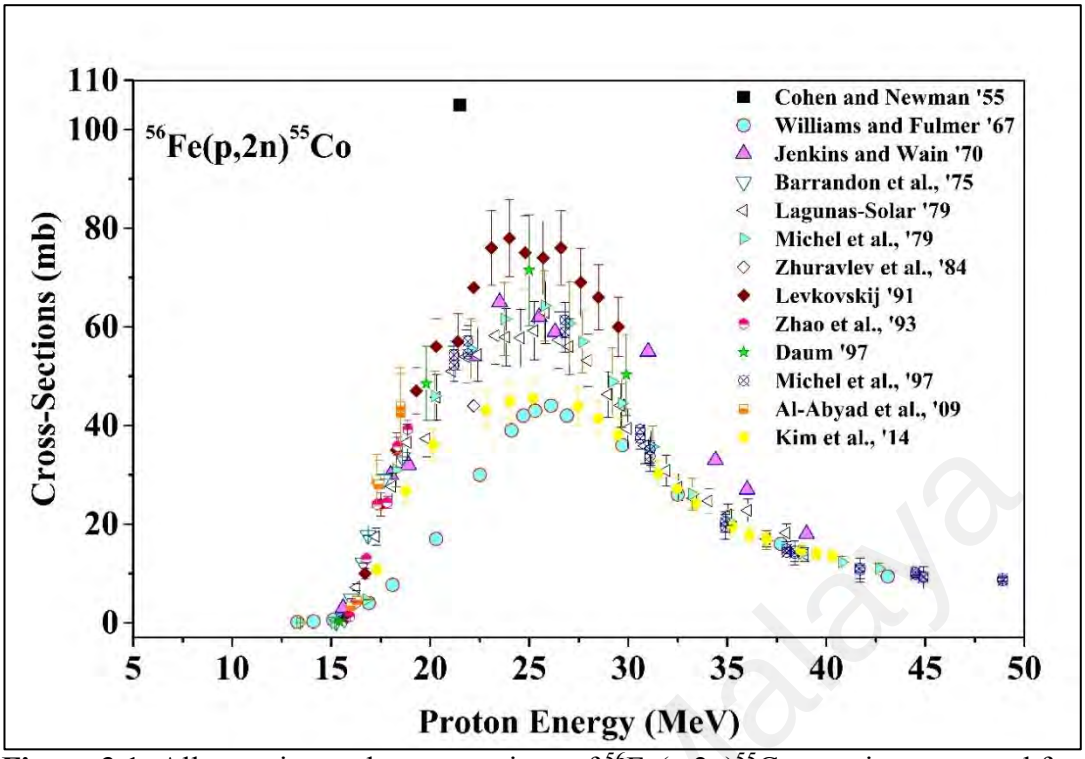

Figure 3.1: All experimental cross-sections of ^{56}Fe(p,2n)^{55}Co reaction extracted from the EXFOR data base for the production ^{55}Co without any correction.

Figure 3.1 shows a considerable discrepancy among the measured data. In general, discrepancies among the different measurements may come from the use of different monitor reactions. On the other hand, measurements of a particular radionuclide having insufficient cooling time (if the formation of nuclide is contributed to by any precursor decay) may also provide erroneous magnitudes. We tried to understand the reason and/or sources of discrepancies based on the given information in the original publications, and the acceptance or rejection of the reported data within the framework of this evaluation endeavour are presented in the following section.

3.2.2.1 Selection and Renormalization of the ^{56}Fe(p,2n)^{55}Co Cross-Sections

Jenkins and Wain (1970) reported an excitation function for the ^{56}Fe(p,2n)^{55}Co nuclear reaction in the energy range of 15.6-39.0 MeV by proton irradiation on separated ^{56}Fe target isotope. The beam current was measured by a Faraday cup connected to a beam current integrator with an accuracy of ±3%. Jenkins et al. claimed the accuracy of their measured data as compared to the ^{65}Cu(p,n)^{65}Zn reaction cross-section of 624 mb at 8.25

MeV, which showed for them good agreement with (McGowan et al., 1964). The latest data for the $^{nat}Cu(p,n)^{65}Zn$ reaction cross-section is 183.55mb at 8.25 MeV taken from IAEA data base (IAEA, 2007), and normalized for isotopic $^{65}Cu(p,n)^{65}Zn$ reaction cross-sections by considering the natural abundance of ^{65}Cu (30.83%). The decay data of ^{55}Co ($T_{1/2}$=18.2 h; $E\gamma$=480 keV (12%); $E\gamma$=930 keV (80%); $E\gamma$=1410 keV (13%)) radioisotope obtained from their original publication showed significant deviation from the latest data ($T_{1/2}$=17.53 h; $E\gamma$=477.2 keV (20.2%); $E\gamma$=931.1 keV (75%); $E\gamma$=1408.5 keV (16.9%)) taken from the NUDAT-2 data base (Junde, 2008). The reported data were, therefore, renormalized based on the latest gamma-ray intensity and the cross-section of the monitoring reaction.

$^{56}Fe(p,2n)^{55}Co$ reaction cross-sections was measured by Lagunas-Solar & Jungerman (1979) in the energy range of 15.6-38.9 MeV using a stacked-foil activation technique in conjunction with Ge (Li) detector gamma-ray spectrometry. The total number of incident protons striking the natural iron (^{56}Fe-91.66%) target was calculated from the total charge collected by a Faraday cup. Decay data of the ^{55}Co radioisotope ($T_{1/2}$=18.5 h; $E\gamma$=477 keV (16%); $E\gamma$=931 keV (73%); $E\gamma$=1408 keV (18%)) was collected from the original publication, and found a significant deviation from the latest ones ($T_{1/2}$=17.53 h; $E\gamma$=477.2 keV (20.2%); $E\gamma$=931.1 keV (75%); $E\gamma$=1408.5 keV (16.9%)) taken from the NUDAT-2 data base (Junde, 2008). About 4% contribution was reported by the authors in the formation of ^{55}Co nuclide through other reaction channels such as $^{57}Fe(p,3n)^{55}Co$ (E_{thrs}=23.5 MeV). The reported data was, therefore, corrected for $^{57}Fe(p,3n)$ contribution above the threshold energy of 25 MeV, and renormalized based on the latest decay data of gamma-ray intensity. However, we even found a significant up-gradation of decay data such as the half-life of ^{55}Co nuclide, it is quite hard to normalize the reported data based on the half-life of ^{55}Co because it depends on detailed experimental parameters and/or conditions.

Cross-sections of $^{56}Fe(p,2n)^{55}Co$ reaction in the energy range of 15.8-29.5 MeV was measured by Levkovskij (1991a) using the conventional stacked-foil activation technique by irradiating iron target with protons. Information about the decay data is not available in the original publication but "6th edition of Tables of Isotopes" (Lederer et al., 1967) was referred. $^{nat}Mo(p,x)^{96}Tc$ reaction from the simultaneously irradiated natural molybdenum was used to monitor proton beam intensity, and reported larger cross-sections than any other measurements available in the literature. This high monitor reaction cross-section (250±10 mb at 30 MeV) used by them is probably the main reason of the larger cross-sections of $^{56}Fe(p,2n)^{55}Co$ reaction. The decay data of ^{55}Co ($T_{1/2}$=18.2 h; $E\gamma$=480 keV (12%); $E\gamma$=930 keV (80%); $E\gamma$=1410 keV (13%)) as referred in their original publication showed significant deviation from the latest data ($T_{1/2}$=17.53 h; $E\gamma$=477.2 keV (20.2%); $E\gamma$=931.1 keV (75%); $E\gamma$=1408.5 keV (16.9%)) taken from the NUDAT-2 data base (Junde, 2008). The reported data are, therefore, renormalized with respect to the monitor reaction cross-section and also for the latest gamma-ray intensity.

Wenrong et al. (1993) measured $^{56}Fe(p,2n)^{55}Co$ reaction cross-sections using the conventional stacked-foil activation technique in the energy range of 15.9-18.8 MeV by irradiating a natural iron target with protons. A Faraday cup was used to measure the beam current. The provided decay data of ^{55}Co ($T_{1/2}$=17.53 h; $E\gamma$=477.19 keV (20.2%); $E\gamma$=931.24 keV (75%)) radioisotope mentioned in their original publication showed no variation with the latest decay data of ^{55}Co ($T_{1/2}$=17.53 h; $E\gamma$=477.2 keV (20.2%); $E\gamma$=931.1 keV (75%)) taken from the NUDAT-2 data base (Junde, 2008). It is noted that no other channels such as $^{57}Fe(p,3n)^{55}Co$ made any contribution in the reported energy range. The reported data were only renormalized based on the latest target abundance (^{56}Fe-91.754%).

Al-Abyad et al. (2009) used the conventional stacked foil technique to measure the cross-section of $^{56}Fe(p,2n)^{55}Co$ reaction from the threshold energy up to 18.5 MeV. A charge integrator and the $^{nat}Cu(p,x)^{62}Zn$, $^{nat}Cu(p,x)^{65}Zn$ and $^{nat}Ti(p,x)^{48}V$ monitor reactions were used to determine the proton beam current delivered on the natural iron target. The authors used the decay data for the ^{55}Co ($T_{1/2}$=17.5 h; $E\gamma$=477.2 keV (20.2%); $E\gamma$=931.1 keV (75%)) from (Lederer & Shirley, 1978) and (Firestone, 1998) works, which shows no difference from the latest decay data of ^{55}Co ($T_{1/2}$=17.53 h; $E\gamma$=477.2 keV (20.2%); $E\gamma$=931.1 keV (75%)) taken from NUDAT-2 data base (Junde, 2008). Note that no other channels such as $^{57}Fe(p,3n)^{55}Co$ made any contribution in the reported energy range. The reported data were only renormalized based on the latest target abundance (^{56}Fe-91.754%).

Wenrong et al. (1993) measured $^{nat}Fe(p,x)^{55}Co$ reaction cross-sections using the conventional stacked-foil activation technique in the energy range of 17.31-40.3 MeV by irradiating a natural iron target with protons. The beam intensity was monitored by the IAEA recommended $^{nat}Cu(p,x)^{62}Zn$ monitor reactions (IAEA, 2007). The provided decay data of ^{55}Co ($T_{1/2}$=17.53 h; $E\gamma$=477.2 keV (20.2%); $E\gamma$=931.1 keV (75%); $E\gamma$=1408.5 keV (16.9%)) radioisotope was collected from the original publication, and no variation has been found with the latest decay data of ^{55}Co ($T_{1/2}$=17.53 h; $E\gamma$=477.2 keV (20.2%); $E\gamma$=931.1 keV (75%); $E\gamma$=1408.5 keV (16.9%)) taken from the NUDAT-2 data base (Junde, 2008). The reported data for the $^{nat}Fe(p,x)^{55}Co$ reactions are corrected for $^{56}Fe(p,2n)^{55}Co$ reaction up to the proton energy of 25 MeV to avoid any contribution from other target isotopes such as $^{57}Fe(p,3n)^{55}Co$ (E_{thrs}=23.5 MeV). Figure 3.2 shows the selected experimental data for the present evaluation, while Figure 3.3 shows the selected data set after renormalization and correction and Table 3.1 summarize the selected experiments considered for study.

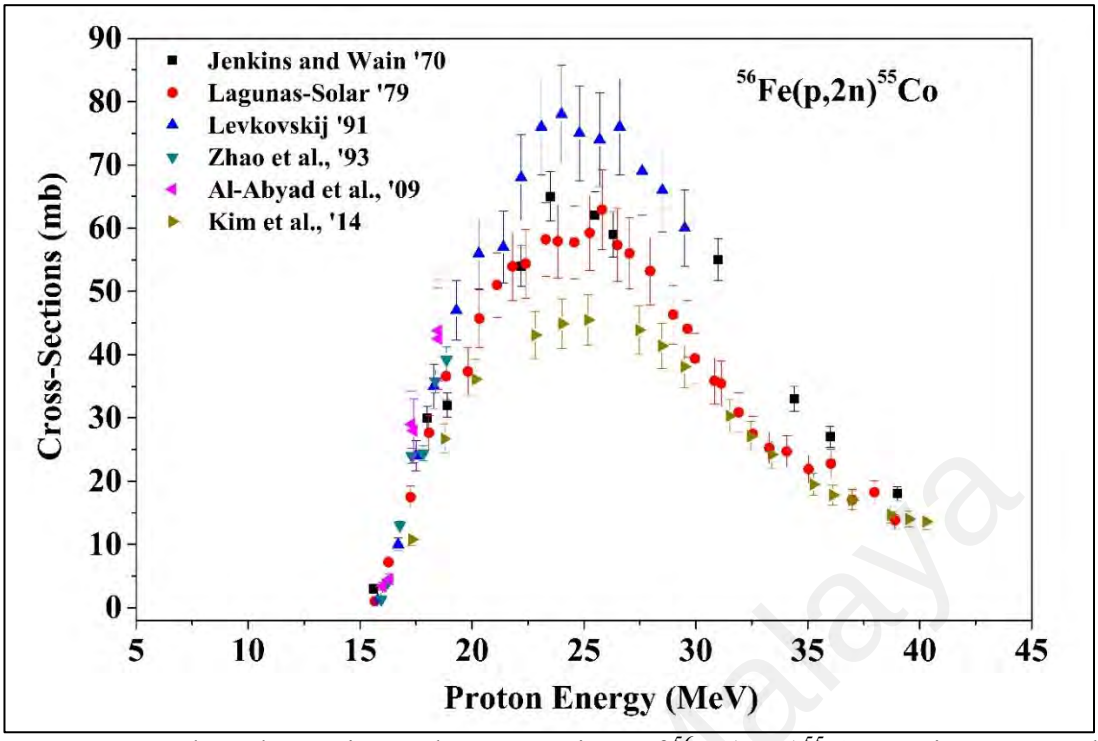

Figure 3.2: Selected experimental cross-sections of ^{56}Fe(p,2n)^{55}Co reaction extracted from the EXFOR data base before renormalization.

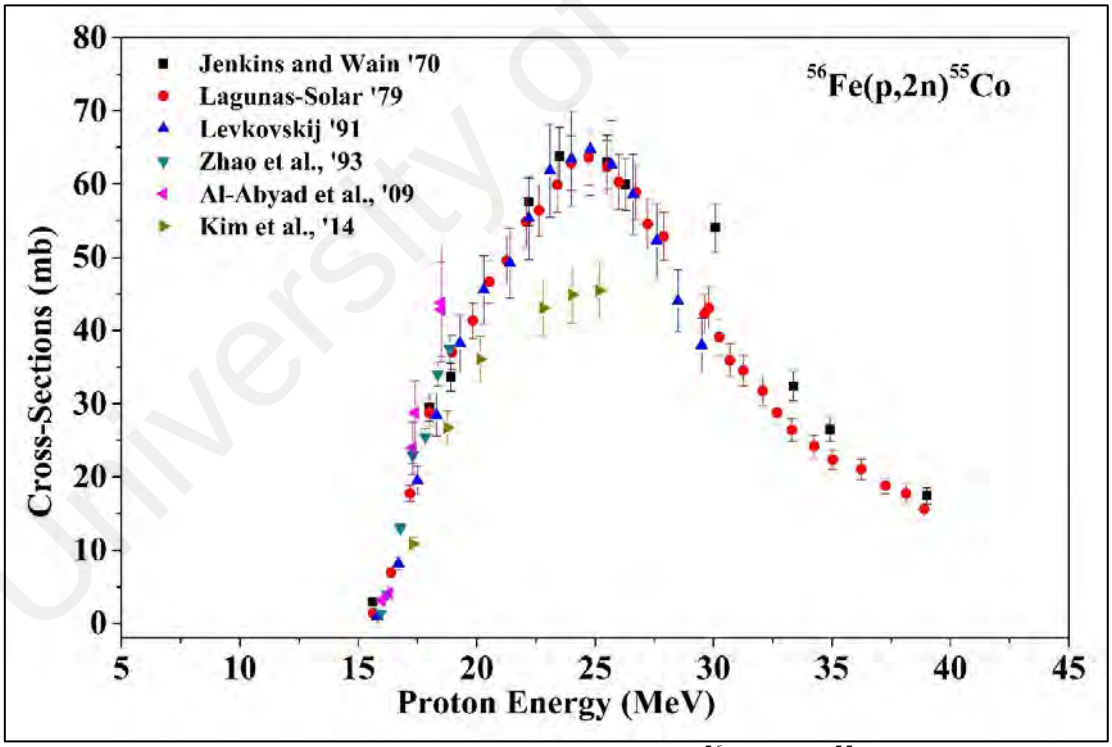

Figure 3.3: Selected experimental cross-sections of ^{56}Fe(p,2n)^{55}Co reaction extracted from the EXFOR data base after renormalization.

Table 3.1: A brief description on various correction factors used in the current ^{55}Co evaluation.

Authors	**Fe56 abundance in sample used by authors (%)**	**Fe56 abundance adopted in this evaluation (Tuli, 2005) (%)**	**Gamma intensity adopted by authors (%)**	**Gamma intensity adopted in this evaluation (Junde, 2008) (%)**	**Monitor cross-sections used by the authors (mb)**	**Monitor cross-sections adopted in this evaluations (mb)**	**Total correction factor**	**Systematic errors given by authors (%)**	**Systematic errors used in this evaluations (%)**	**Statistical errors used in this evaluations (%)**	**Correction for ^{57}Fe(p,3n) contribution**
Jenkins (1970)	(100)[a]	91.754	12 (480 keV); 80 (930 keV); 13 (1410 keV)	20.2±17 (477.2 keV) 75±4 (931.1 keV)	^{65}Cu(p,n)^{65}Zn 624 at 8.25 MeV [b]	^{nat}Cu(p,x)^{65}Zn 183.55 mb at 8.25 MeV (IAEA, 2007)	0.3419	BC=3 TT=1.5 CS<6 *Err(E)=3*	3.35	6	no contribution
Lagunas-Solar (1979)	91.66 Natural target		16 at 477 keV; 73 at 931 keV	16.9±8 (1408.5 keV)	Absolute (Faraday Cup used)	-	0.7923	BC=5 TT=1 DE=3 CS=2 *DD=4* *TOT=10* *Err(E)=1*	5.91	2	Corrected by 4%

Table 3.1, continued.

Authors	Fe56 abundance in sample used by authors (%)	Fe56 abundance adopted in this evaluation (Tuli, 2005) (%)	Gamma intensity adopted by authors (%)	Gamma intensity adopted in this evaluation (Junde, 2008) (%)	Monitor cross-sections used by the authors (mb)	Monitor cross-sections adopted in this evaluations (mb)	Total correction factor	Systematic errors given by authors (%)	Systematic errors used in this evaluations (%)	Statistical errors used in this evaluations (%)	Correction for ^{57}Fe(p,3n) contribution
Levkovskij (1991)	91.68 [c] Natural target	91.754	12 at 480 keV; 80 at 930 keV [c]; 13 at 1410 keV	20.2±17 at 477.2 keV 75±4 (931.1 keV)	^{nat}Mo(p,x)^{96}Tc 250±10 at 30 MeV (Levkovskij, 1991a)	^{nat}Mo(p,x)^{96}Tc 195.3 at 30 MeV (Takács et al., 2002)	0.8326	TOT=10	4.0 [e]	10	Corrected
Zhao (1993)	91.72[d] Natural target		20.2 at 477.19keV ; 75.0 at 931.24 keV	16.9±8 (1408.5 keV)	Absolute (Faraday Cup used)	-	0.9996	BC=2; TT=3; DE=2.5; CS=1.5; *Err(E)=N/A*	4.38	1.5	no contribution
Al-Abyad et al., (2009)	91.75		20.2 at 477.2 keV; 75 at 931.3 keV		Absolute (Beam current integrator) and ^{nat}Cu(p,x)^{6265}Zn, ^{nat}Ti(p,x)^{48}V	-	1.0	BC=10.0; TOT=15.0;	10.0	11.18	No contribution

Table 3.1, continued.

Authors	^{56}Fe abundance in sample used by authors (%)	^{56}Fe abundance adopted in this evaluation (Tuli, 2005) (%)	Gamma intensity adopted by authors (%)	Gamma intensity adopted in this evaluation (Junde, 2008) (%)	Monitor cross-sections used by the authors (mb)	Monitor cross-sections adopted in this evaluations (mb)	Total correction factor	Systematic errors given by authors (%)	Systematic errors used in this evaluations (%)	Statistical errors used in this evaluations (%)	Correction for ^{57}Fe(p,3n) contribution
Kim et al., (2014)	91.754	91.754	20.2 at 477.2 keV; 75 at 931.1keV	20.2±17 at 477.2 keV; 75±4 at 931.1 keV; 16.9±8 at 1408.5 keV	^{nat}Cu(p,x)^{62}Zn from the IAEA updated in 2007 (IAEA, 2007)	-	1.0	BI=7; DE= 5; CS=3 – 5; Gamma ray abundance=2; TOT= 9.5 – 10.5	9.0	3 - 5	No contribution

Several acronyms that indicated in Table 3.1 are described as follows:

BC=Beam current, BI= Beam intensity,

TT=Target thickness, DD=Decay data,

CS=Counting, DE=Detector efficiency,

Err(E)=Energy error. Italicized information was not applied in the current fitting.

Some considerations related to the experiment listed Table 3.1 were described in the following notes

a. “Separated” Fe-56 sample used, 100% assumed.

b. (Jenkins & Wain, 1970) didn't use $^{65}Cu(p,n)^{65}Zn$ as monitor reaction. They just claimed the accuracy of their measured data as compared to the $^{65}Cu(p,n)^{65}Zn$ reaction cross-section of 624 mb at 8.25 MeV. The abundance of ^{65}Cu mentioned in Lederer (1967) was as 30.9 %. Therefore, the cross-sections of 624mb at 8.25 MeV mentioned by Jenkins & Wain (1970) for $^{65}Cu(p,n)^{65}Zn$ reaction is corrected by the current value of ^{65}Cu (30.83 %) as 622.58 mb.

c. Isotopic abundance information is not given in the article, but Lederer et al. (1967) was cited.

d. Value is not given in the article, but (Browne et al., 1986) is cited for half-lives, gamma-ray energies and branching ratios.

e. (Levkovskij, 1991a) reported a total of 10% error in their measurement but not mentioned specifically the contribution of systematic part and statistical part. The given experimental uncertainty is treated as statistical uncertainty. In order to construct the experimental correlation matrix, we have considered a constant 4% systematic uncertainty for this data.

3.2.2.2 Exclusion of the $^{56}Fe(p,2n)^{55}Co$ Cross-Sections from this Evaluation

Cohen & Newman (1955) reported $^{56}Fe(p,2n)^{55}Co$ reaction cross-section at 21.5 MeV proton energy, and showed a large deviation from any other measurements. Activity of ^{55}Co was measured by using a scintillation counter whereas the efficiency of the spectrometer was measured by determining absolute disintegration rate of beta counting, with a phosphorous-32 standard for the Geiger counter calibration. It should be noted that old activation cross-sections by beta-decay detection may give this deviated results

compared to the recent measurements in general, and therefore, this data has not been considered in this evaluation procedure.

Read (1968) measured $^{56}Fe(p,2n)^{55}Co$ reaction cross-section (0.71±0.06 mb at 370 MeV) by using Berkeley 184-inch Cyclotron, and Remsberg & Miller (1963) irradiated enriched ^{56}Fe (99.7%) target by 380 MeV proton from Nevis Synchrocyclotron and reported $^{56}Fe(p,2n)^{55}Co$ reaction cross-section as 0.77±0.08 mb at 370 MeV proton energy. As we were motivated to evaluate ^{55}Co radionuclide formation cross-section at low energy leading to medical applications, we therefore, exclude these high energy region data from this evaluation procedure.

Michel et al. (1979) measured the $^{56}Fe(p,2n)^{55}Co$ reaction cross-section by irradiating the proton on natural iron target in the energy range from 13.4 MeV to 44.5 MeV. A conventional stacked foil activation technique combined with GeLi gamma-ray spectrometry was used to determine the reported cross-section. Since the source of errors was not mentioned in the original publication, it was not possible to construct the relevant correlation matrix, and therefore the data were deselected from the current evaluation.

Zhuravlev et al. (1984) analysed neutron spectra from proton-induced reaction in ^{56}Fe nucleus, and reported $^{56}Fe(p,2n)^{55}Co$ cross-section at 22.2 MeV proton energy by using the time-of-flight technique. The reported data showed a significant discrepancy from other measurements perhaps due to difference in the measurement technique and, we have neglected this data to perform an accurate evaluation of $^{56}Fe(p,2n)^{55}Co$ reaction cross-section.

The $^{nat}Fe(p,x)^{55}Co$ cross-sections was reported by Daum (1997) in the energy range of 16-30 MeV by irradiating a high purity iron foil using an external beam line of Compact Cyclotron at Forschungszentrum, Karlsruhe, Germany. Information on target purity,

irradiation time, cooling time, details uncertainty etc. is not available in the EXFOR database, thus the reported cross-sections is not used in the current evaluation.

Williams & Fulmer (1967) measured ^{nat}Fe(p,x)^{55}Co cross-sections by proton irradiation on metallic foils of natural iron in the energy region of 13.3-60.3 MeV. The decay data of ^{55}Co ($T_{1/2}$=18 h; $E\gamma$=477 keV (24%); $E\gamma$=1410 keV (24%)) as referred in their report showed significant deviation from the latest data ($T_{1/2}$=17.53 h; $E\gamma$=477.2 keV (20.2%); $E\gamma$=1408.5 keV (16.9%)) taken from the NUDAT-2 data base (Junde, 2008). A probable error of 30% of the cross-sections was stated without any further specification, therefore the data are neglected from the present evaluation.

^{nat}Fe(p,x)^{55}Co cross-sections was reported by Lagunas-Solar & Jungerman (1979) in the energy range of 15.25-18.58 MeV using a stacked-foil activation technique together with Ge (Li) detector gamma-ray spectrometry. A high purity metallic foil was irradiated by an external beam line of 20 MeV cyclotron at CEA, Saclay, France but no information on the target abundance, beam current monitoring is reported in the publication. Since the reported cross-section is below the threshold of other contributing reaction channels such as ^{57}Fe(p,3n)^{55}Co, they are only contributed by the ^{56}Fe target isotope via the ^{56}Fe(p,2n)^{55}Co reaction. Decay data of the ^{55}Co radioisotope ($T_{1/2}$=18.2 h; $E\gamma$=931.1 keV) was collected from the EXFOR database (Otuka et al., 2014) but information about gamma-ray intensity, cross-section uncertainty is absent, thus their data are excluded from this evaluation.

3.3 Evaluation of Production Cross-Section for ^{61}Cu

In this part, production cross-sections of ^{61}Cu ($T_{1/2} = 3.339\ h, E_{mean}(\beta^+) = 523\ keV, I_{total}(\beta^+) = 61.0\%$) a promising radionuclide for PET imaging applications, were evaluated for the light-charged-particle-induced reactions on Co, Ni, Zn targets. The

various production routes of ^{61}Cu were compared, and recommended excitation functions were derived using a well-defined statistical procedure explained in the following section.

3.3.1 ^{61}Cu Production Routes Selection

A number of studies were conducted for the measurement of ^{61}Cu production cross-sections via ^{nat}Cu(n,x)^{61}Cu (Kim et al., 1999; Michel et al., 2015) and ^{63}Cu(n,3n)^{61}Cu (Qaim et al., 1980; T.S.Soewarsono, 1992; Uwamino et al., 1992; Vrzalová et al., 2013; Y.Uno, 1996) reactions by the use of nuclear reactor, but such processes provide ^{61}Cu in carrier added form with low specific activity. On the other hand, production of ^{61}Cu has also been reported in many studies (Ansari et al., 2004; Budzanowski et al., 1967; Gadioli et al., 1984; Jastrzebski et al., 1986; Levkovskij, 1991a; Michel & Brinkmann, 1980; Singh et al., 1993; Skulski et al., 1992; Sterns, 1962; Szelecsényi et al., 2002; Yoshio & Yukio, 1976; Zhukova et al., 1972) via light-charged particles-induced reactions on various targets Co, Zn, Ni by using cyclotrons or accelerators. In such studies, excitation functions for the residual radionuclides of ^{59}Co(α,2n), ^{58,60}Ni(α,d;x) and ^{nat}Zn(p,x) nuclear processes were measured, physical yields were deduced, and finally optimum parameters towards the NCA production of ^{61}Cu were determined.

However, among the various studied nuclear processes, ^{59}Co(α,2n)^{61}Cu, ^{58}Ni(α,p)^{61}Cu, ^{60}Ni(d,n)^{61}Cu and ^{64}Zn(p,α)^{61}Cu reactions were selected for this study because of their consistency with the available facilities, and can be performed using in a low energy accelerator/cyclotron. However, a close observation on such cross-sections found in EXFOR database for the reactions that produce ^{61}Cu show a considerable degree of discrepancy even within the same excitation energy. But, it is possible to evaluate/correct the reported data by using the updated value of some relevant parameters such as gamma-ray intensity, monitor cross-sections, target abundance etc. that are generally available in the original publications. To obtain a more accurate form of production cross-sections,

we evaluated the experimental cross-sections of ^{61}Cu radioisotope available in the EXFOR library (EXFOR, 2018) up to the energy range from threshold to 55 MeV; relevant to its medical applications. The experimental data were first renormalized, in case of any discrepancy found between experimental data and the standard values. Relevant details of this evaluation procedure are presented in the following sections.

As mentioned in the preceding section, ^{61}Cu can be produced via neutrons or charged-particles induced reactions. Because of complexity in installations, operation etc., use of nuclear reactors are no longer preferable to produce the desired isotope for medical applications, especially for β^+ emitters. Conversely, the light-charged particles such as protons, deuterons, helion and alphas can be used as projectiles to induce nuclear reactions on different targets for the production of ^{61}Cu radionuclide. However, such reactions may also produce some other unwanted Cu contaminants such as ^{57,58,59,60,62,66}Cu together with the desired products. Because of their relatively short half-lives, most of these isotopes have no effect on the production of desired radionuclide, the cooling time guarantees decaying of these isotopes and wipe them out from products (Ditrói et al., 1997). Furthermore, it is possible to remove other non-isotopic impurities and/or elements by chemical separation process. But, the only radioactive isotope that makes a considerable contamination is ^{64}Cu due to its relatively long half-life ($T_{1/2}$=12.7 h) when compared to ^{61}Cu half-life ($T_{1/2}$=3.339 h). Fortunately, the producers can avoid ^{64}Cu contaminant by using a lower energy window than the ^{64}Cu threshold energy. Table 3.2 illustrates the relevant information for the production of ^{61}Cu via different routes. The Threshold energies in Table 3.2 are obtained from the Q-value calculator maintained by the Brookhaven National Laboratory (NNDC, 2018).

Table 3.2: A summary of literature for the production of ^{61}Cu isotope.

Target material	Isotopic abundance (%)	Projectile	Production reaction	Q-value (MeV)	Threshold energy (MeV)	Energy window (MeV)	Maximum reported cross-section for ^{61}Cu (mb)	Threshold of ^{64}Cu contaminant (MeV)	References
^{58}Ni	68.0	α	(α,p)	-3.11	3.32	10-20	881	-	(Takács et al., 1996)
^{60}Ni	26.2	p	(p,γ)	4.80	0.00	15-30	46.9	-	(Al Saleh et al., 2007)
		d	(d,n)	2.58	0.00	5-15	366[a]	-	(Zweit et al., 1991)
		α	(α,p2n)	-15.01	16.02	40-50	367	-	(Singh et al., 2005)
^{64}Zn	49.2	p	(p,α)	0.84	0.00	5-25	122	-	(Barrandon et al., 1975)
		d	(d,αn)	-2.12	2.18	10-30	95.6	^{64}Cu at 2.09 MeV	(Bissem et al., 1980)
^{66}Zn	27.7	p	(p,α2n)	-18.19	18.47	35-60	158	^{64}Cu at 11.29 MeV	(Szelecsényi, Kovács et al., 2005)

Table 3.2, continued.

Target material	Isotopic abundance (%)	Projectile	Production reaction	Q-value (MeV)	Threshold energy (MeV)	Energy window (MeV)	Maximum reported cross-section for ^{61}Cu (mb)	Threshold of ^{64}Cu contaminant (MeV)	References
^{59}Co	100	^{3}He	(^{3}He,n)	6.61	0.00	10-30	9.6	-	(Fenyvesi et al., 2004)
		α	(α,2n)	-13.96	14.91	20-40	590	-	(Skulski et al., 1992)

[a]The maximum reported is 500 mb but the data set containing this value excluded as explained later

Figures 3.4, 3.5 and 3.6 illustrate all experimental cross-sections available in EXFOR library for the production of ^{61}Cu via light-charged-particle-induced reactions on ^{58,60}Ni, ^{59}Co, ^{64,66}Zn, ^{nat}Ni and ^{nat}Zn targets. The presented data in Figures 3.4, 3.5 and 3.6 were normalized to 100% isotopic abundance for the ^{58,60}Ni, ^{59}Co, ^{64,66}Zn target nuclides. The suitable reactions for the NCA production of ^{61}Cu were chosen based on the information available at Table 3.2 and Figures 3.4, 3.5 and 3.6. It is also important to consider the price of target materials for the cost effective production of desired nuclide, thus an approximate cost of target materials has been obtained from Good Fellow Corporation catalogues. It shows that the prices of Co, Ni and Zn targets (purity 99.9%) per 100 gm (~150 µm particle size) are listed as 345, 210 and 181 USD, respectively. Since the target materials are not expensive and they show relatively large cross-sections for ^{61}Cu in the low energy region, thus it is worth to produce ^{61}Cu by using these target materials for application purposes.

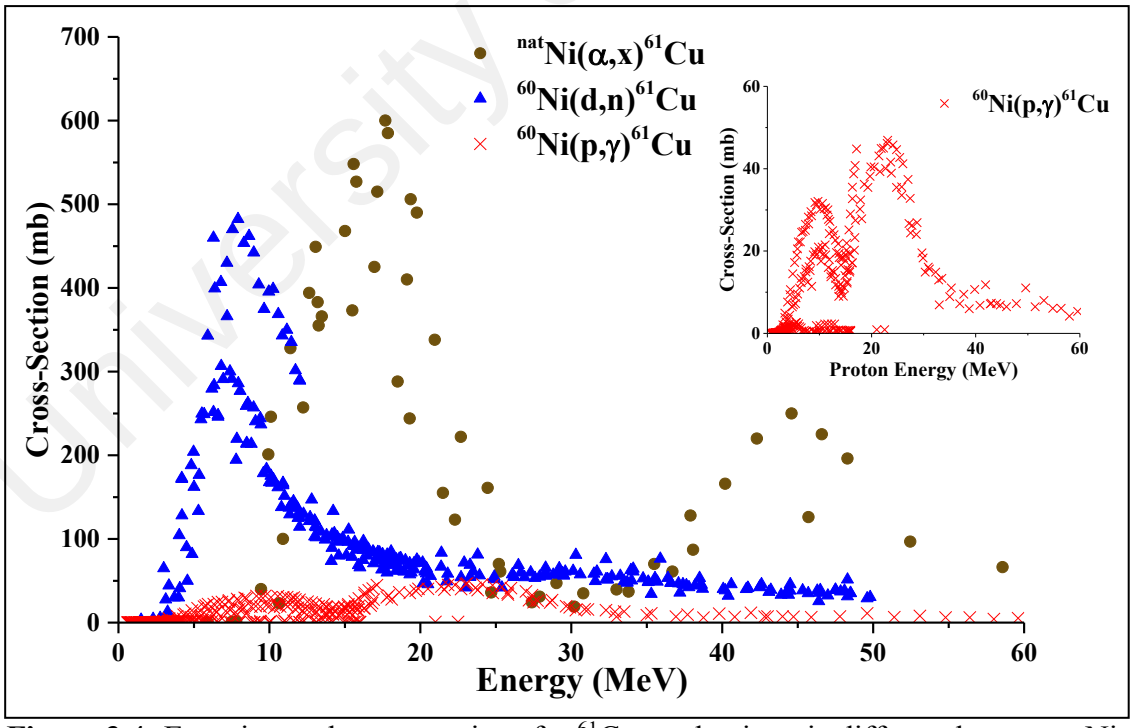

Figure 3.4: Experimental cross-sections for ^{61}Cu production via different beams on Ni target.

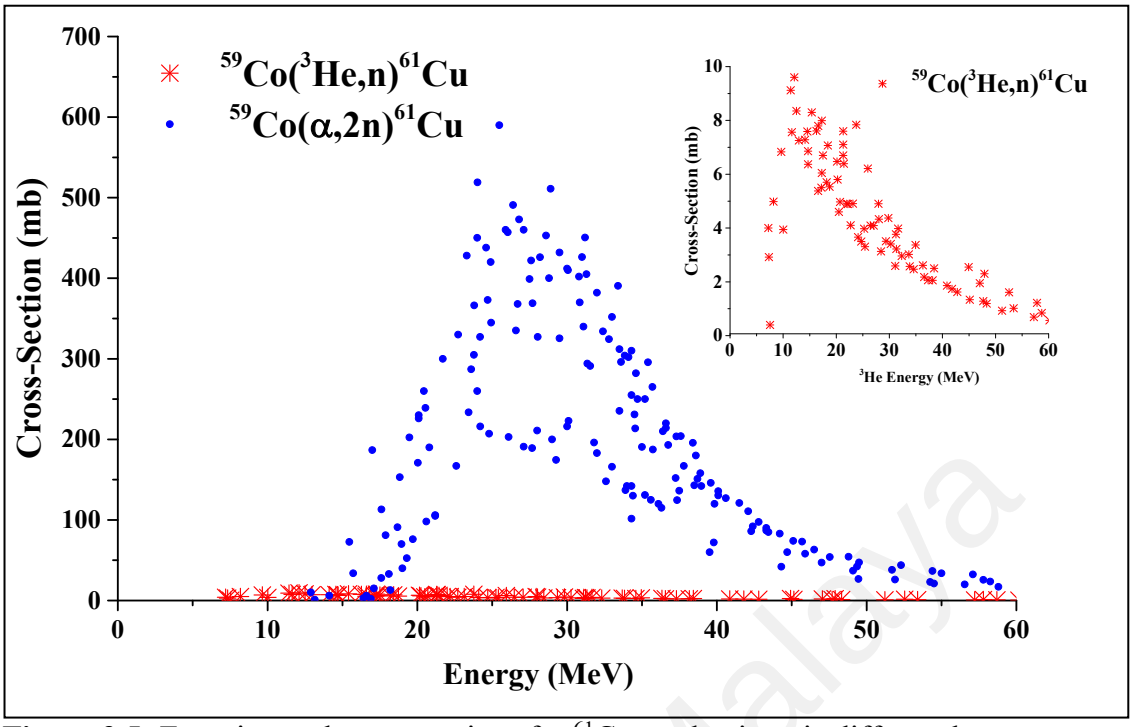

Figure 3.5: Experimental cross-sections for ^{61}Cu production via different beams on ^{59}Co target.

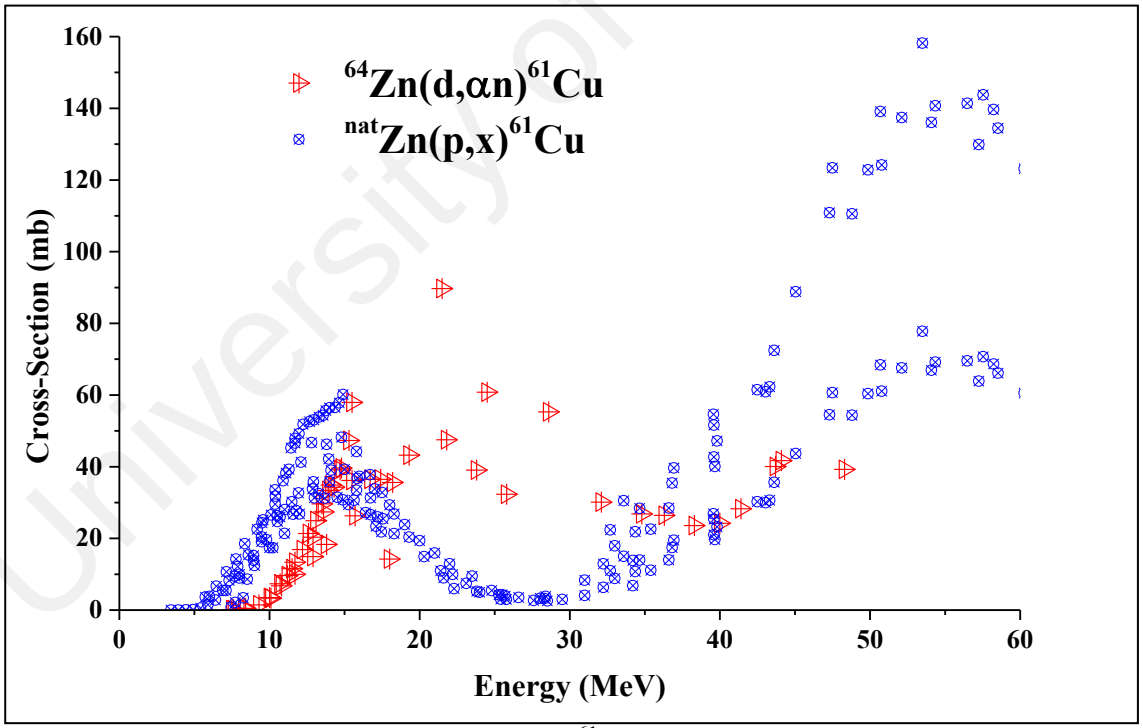

Figure 3.6: Experimental cross-sections for ^{61}Cu production via different beams on Zn target.

3.3.2 Production of ^{61}Cu via ^{3}He- and α-Induced Reactions on ^{59}Co

A survey of literature reveal that several authors (Fenyvesi et al., 2004; Jastrzebski et al., 1986; Michel & Galas, 1983; Nagame et al., 1988; Pichard et al., 2011; Szelecsényi et al., 2004; Yoshio & Yukio, 1976) studied the possibility of ^{61}Cu production via the use of ^{59}Co(^{3}He,n)^{61}Cu reaction. However, due to the lower cross-sections of ~10 mb in the peak energy region and non-availability of expensive ^{3}He beam, this route is not efficient enough to produce ^{61}Cu in big amounts. Therefore, this reaction has been excluded from this evaluation study.

On the other hand, despite of huge efforts were done to obtain the most accurate form of excitation function for the ^{59}Co(α,2n)^{61}Cu reaction (Ansari et al., 2004; Budzanowski et al., 1967; Gadioli et al., 1984; Jastrzebski et al., 1986; Levkovskij, 1991b; Michel & Brinkmann, 1980; Singh et al., 1993; Skulski et al., 1992; Sterns, 1962; Szelecsényi et al., 2002; Yoshio & Yukio, 1976; Zhukova et al., 1972), clear discrepancies is found among the reported data (See in Figure 3.7). Unfortunately, not all published works are well documented, especially the absence of detail experimental uncertainties which serve as an essential input of SOK code for data evaluation. As for example, some old studies conducted by Budzanowski et al. (1967), Sterns (1962) and Yoshio & Yukio (1976) reported no experimental errors, such data are excluded from this evaluation. Jastrzebski et al. (1986) used the stacked foil activation technique to measure ^{59}Co(α,2n)^{61}Cu cross-sections in the energy range 18.8 - 20.1 MeV via in-beam γ-ray measurements and radioactivity measurements. To be consistent in the evaluation, the reported cross-sections determined by radioactivity measurements using high resolution Ge(Li) detector has been considered for this evaluation. Other authors, (Ansari et al., 2004; Gadioli et al., 1984; Levkovskij, 1991b; Michel & Brinkmann, 1980; Singh et al., 1993; Skulski et al., 1992; Szelecsényi et al., 2002; Zhukova et al., 1972) measured the production cross-sections of ^{61}Cu through irradiating ^{59}Co by α-particle in the energy range

14.1 – 170.3 MeV, in those data were picked up for this evaluation but only up to an energy of 65.0 MeV that can easily been produced in medical cyclotrons. Moreover, selection of this energy range ensures the opening of no other channel except the $^{59}Co(\alpha,2n)^{61}Cu$ reaction for ^{61}Cu production (Szelecsényi et al., 2002). Almost in all of the selected experiments, faraday cup was used for beam monitoring, thus no correction is made due to monitor process using faraday cup technique. Beside the use of faraday cup (Ansari et al., 2004; Gadioli et al., 1984; Levkovskij, 1991b; Michel & Brinkmann, 1980; Singh et al., 1993), different monitoring reactions were included for determining the beam intensity as shown in Detailed information about monitor cross-sections is absent from the original publications. However, only three authors reported the intensity of the gamma line used in ^{61}Cu identification, and the data were updated using the decay data for the ^{61}Cu 282.95keV gamma line intensity of 12.2% taken from NUDAT2.7 library (Zuber & Singh, 2015). Moreover, correction for the target abundance is not required since ^{59}Co is mono-isotopic target. Table 3.3 Summarizes the selected studies for the evaluation of $^{59}Co(\alpha,2n)^{61}Cu$ reaction cross-sections.

Table 3.3: Experimental data of available studies on $^{59}Co(\alpha,2n)^{61}Cu$ reaction.

Authors	Alpha energy range (MeV)	Gamma intensity	Method followed	Monitor	Total correction factor	Uncertainties given by authors (%)	Overall Uncertainty (%)	Detector used
Zhukova et al. (1972)	16.4 - 36.3	No information	Stacked foil technique	No information	None	20-60	20-60	Ge(Li) & Scintillation counter
Michel & Brinkmann (1980)	170.3 - 26.0	13.0% at 282.9 keV	Stacked foil technique	Faraday cup; $^{27}Al(a,4p3n)^{24}Na$; $^{27}Al(a,4p5n)^{22}Na$	1.06	Monitor=10	10	No information
Gadioli et al. (1984)	85.0 - 13.2	No information	Stacked foil technique	Faraday cup; $^{27}Al(a,x)^{24}Na$ 39.3 mb at 85 MeV; Recommended by IAEA 39.3 mb a 85 MeV	1.0	No information	4.3- 9.1	Ge(Li)
Jastrzebski et al. (1986)	81.8 - 20.1	No information	Stacked foil technique	Faraday cup; $^{27}Al(a,x)^{22}Na$	1.0	Current integration=5; Target thickness=5; Efficiency=5.	8.7	Ge(Li)
(Levkovskij, 1991b)	20.1 - 45.9	No information	Powder activation compressed and packed in Al foils	Faraday cup; $^{nat}Mo(a,xn)^{97}Ru$ reaction	None	10	10	No information

Table 3.3, continued.

Authors	Alpha energy Range (MeV)	Gamma intensity	Method followed	Monitor	Total correction factor	Uncertainties given by authors (%)	Overall Uncertainty (%)	Detector Used
Skulski et al. (1992)	14.1 - 25.5	No information	Stacked foil technique	Faraday cup	1.0	No information	No information	Ge(Li)
Singh et al. (1993)	18.7 - 47.5	No information	Stacked foil technique	$^{65}Cu(a,2n)^{67}Ga$ 300keV I=19.0%	1.0	Overall error=15; Detector efficiency= 2-5; Target thickness= 1-2; Photopeak area =2-5; St. dev.=10; Spectroscopic data=3.9.	15	HPGe & Ge(Li)
Szelecsényi et al. (2002)	17.6 - 57.8	12.5% at 283keV	Stacked foil technique	Faraday cup	1.02	Combined error= 10-14; Atoms uniformity=5; Nuclear data=3; Beam intensity=7; Detector efficiency=5; Stat. uncertainty=5; Recoil effect=3.	10-14	HPGe

Table 3.3, continued.

Authors	**Alpha energy Range (MeV)**	**Gamma intensity**	**Method followed**	**Monitor**	**Total correction factor**	**Uncertainties given by authors (%)**	**Overall Uncertainty (%)**	**Detector Used**
Ansari et al. (2004)	16.99 - 49.5	13.2% at 283keV	Stacked foil technique	Faraday cup; $^{63}Cu(a,2n)^{67}Ga$ reaction. But no information on cross-sections	1.08	Monitor reaction= 4; Statistical error=1; Dead time=10; Target thickness=1; Detector eff.=1; Over all=5.	5	Ge(Li)

After all the possible corrections of the experimental data have been done, relevant input files were prepared for used in SOK code to find the best curve that fit all experimental data using the least square concept. Note that this code reduces the errors associated with experimental data using the KALMAN filter and least squares method, the complete evaluation procedure described in Chapter 4. Figure 3.8 represents the selected data for evaluation after correction.

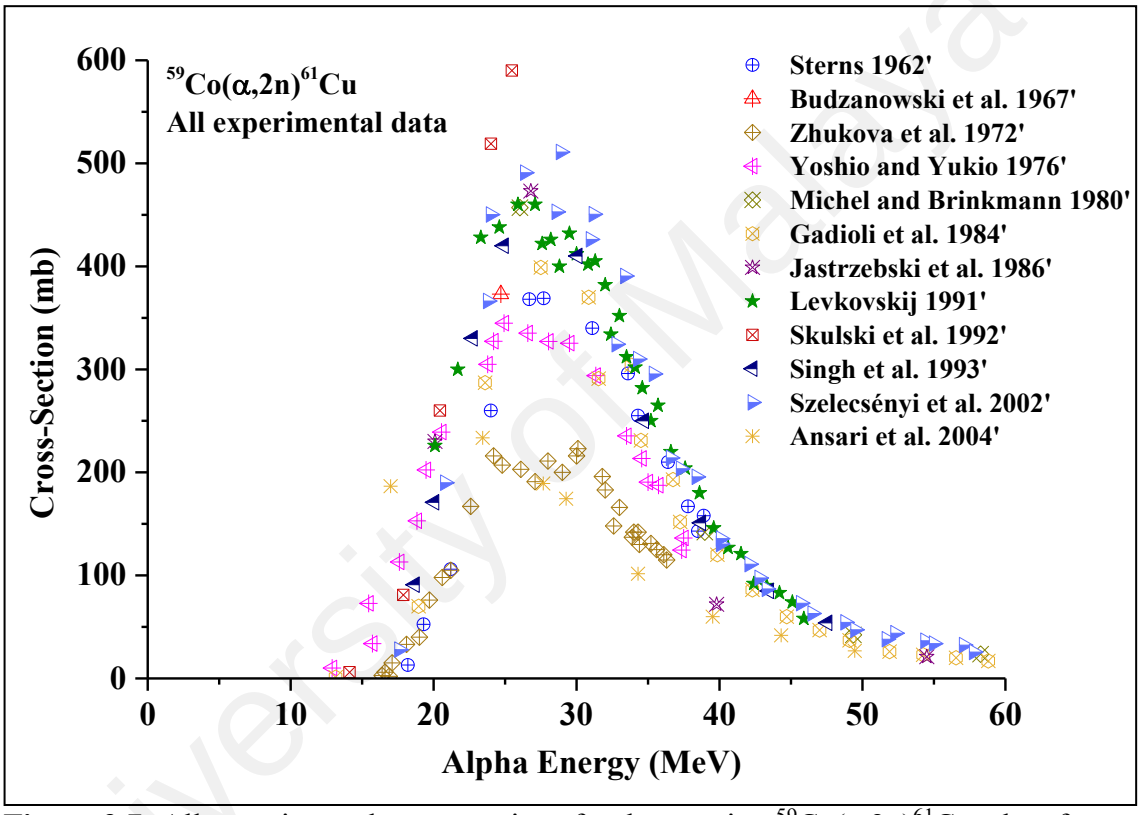

Figure 3.7: All experimental cross-sections for the reaction ^{59}Co(α,2n)^{61}Cu taken from EXFOR library without any correction.

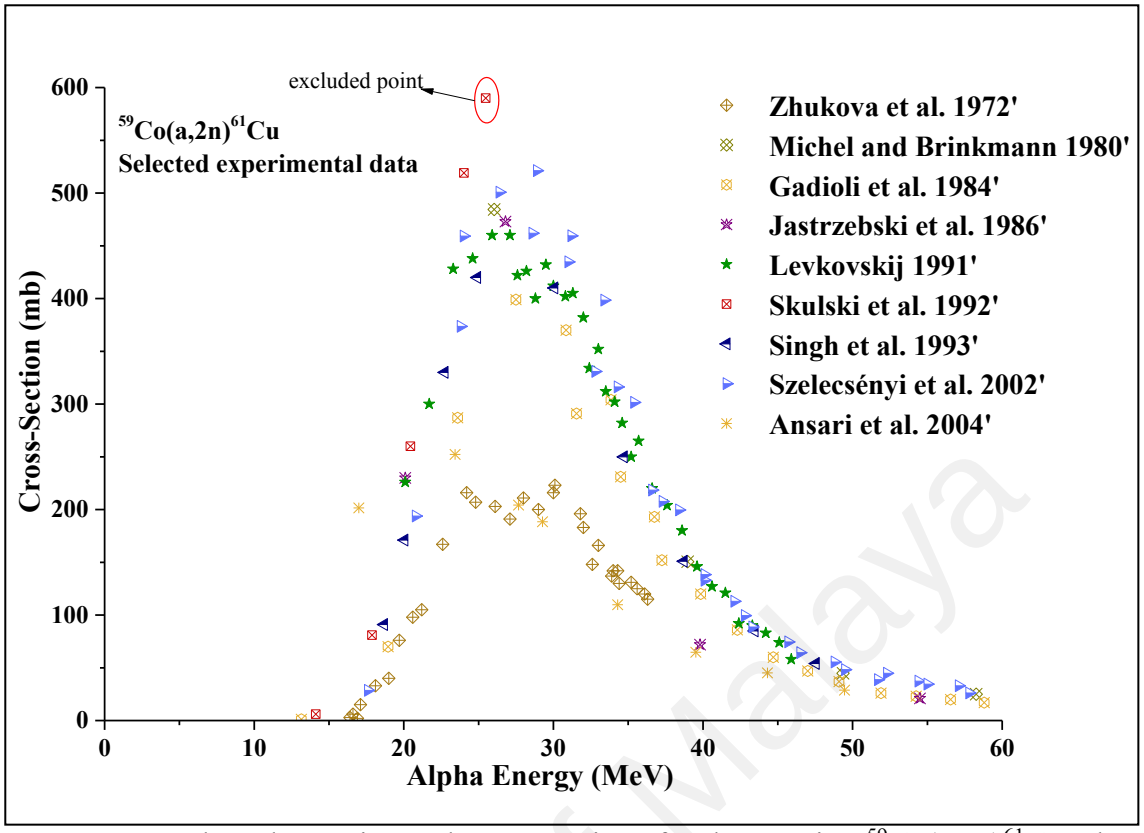

Figure 3.8: Selected experimental cross-sections for the reaction ^{59}Co(α,2n)^{61}Cu taken from EXFOR library after correction.

3.3.3 Production of ^{61}Cu via α-Induced Reactions on ^{58}Ni and ^{60}Ni

^{61}Cu can also be produced via alpha particle induced reactions on natural or enriched nickel (Ni) targets. Naturally occurring nickel is mainly composed of two stable isotopes ^{58}Ni (68.077%) and ^{60}Ni (26.223%). According to the EXFOR library, a total of ten earlier investigations were carried out for the production of ^{61}Cu through alpha induced reactions on enriched or natural Ni targets (Antropov et al., 1985; Hisakazu et al., 1978; Levkovskij, 1991b; McGowan et al., 1964; Michel et al., 1983; Paul et al., 1995; Singh et al., 2005; Takács et al., 1996; Vlieks et al., 1974; Yadav et al., 2008). Among those studies, McGowan et al. (1964), Vlieks et al. (1974) and Levkovskij (1991b) used the ^{58}Ni enriched target and the remaining authors used the natural target. Figure 3.9 shows all experimental cross-sections listed on EXFOR database for the ^{58}Ni(α,p)^{61}Cu and ^{60}Ni(α,p2n)^{61}Cu reactions. Note that, ^{58}Ni(α,p)^{61}Cu reaction is the only contributing channel in the energy range of 3.0 – 24.0 MeV (Takács et al., 1996).

It is clearly observed in Figure 3.4 that the maximum cross-section for the $^{60}Ni(\alpha,p2n)^{61}Cu$ is lower than the $^{58}Ni(\alpha,p)^{61}Cu$ reaction, and $^{60}Ni(\alpha,p2n)^{61}Cu$ data lies in the high energy region. Because of the higher abundance of ^{58}Ni target and lower threshold energy of $^{58}Ni(\alpha,p)^{61}Cu$ reaction, we have considered that production of ^{61}Cu via $^{58}Ni(\alpha,p)^{61}Cu$ reaction is more practical than the $^{60}Ni(\alpha,p2n)^{61}Cu$. Under these circumstances, higher yield of ^{61}Cu with lower beam energy could be obtained, thus, for the purpose of present evaluation, we only considered the data reported in the low energy region. Except McGowan et al. (1964) and Vlieks et al. (1974), in most of the studies, the activity of the produced radionuclide was determined by gamma-ray spectrometry.

Despite the fact that McGowan et al. (1964) and Vlieks et al. (1974) have utilized beta counting technique with NaI scintillation counters in product identification , but their reported cross-sections lie in line with the recently measured data.

Paul et al. (1995) studied the excitation function for the $^{nat}Ni(\alpha,x)^{61}Cu$ reaction in the high energy region (>25 MeV), which is outside of our present interest. Information on uncertainty is absent in the reported data by Hisakazu et al. (1978), but the cross-section uncertainty is an essential input in SOK code for data evaluation. Antropov et al. (1985) reported two extremely high cross-sections (not shown in Figure 3.9) of 1500 mb and 2200 mb at the energies of 13.0 and 16.5 MeV, respectively. Hence, these two scattered data points together with the Paul et al. (1995) data were excluded from this evaluation study. Although the threshold energy of $^{60}Ni(\alpha,p2n)^{61}Cu$ reaction is theoretically 16.0 MeV, but in practice the formation of ^{61}Cu via this reaction starts from 24.0 MeV (See in Figure 3.9). Table 3.4 represents the literature data relevant to ^{61}Cu production, while Figure 3.10 shows the selected data considered for evaluation.

Table 3.4: All experimental data for $^{58}Ni(\alpha,p)^{61}Cu$ and $^{nat}Ni(\alpha,x)^{61}Cu$ reactions available in EXFOR library.

Author	**Alpha energy (MeV)**	**Target Abundance (%)**	**Gamma Intensity Used by authors**	**Total correction factor**	**Detector**	**Monitor reaction**	**Uncertainties given by authors (%)**
McGowan et al. (1964)	4 -11	^{58}Ni 98.4	No information	1.0	NaI scintillation counters	No information	Detector efficiency= 6; Thick-target positron yields=6; Positron per decay =15; Absolute accuracy=16; Stopping power=8; Total error=20.
Vlieks et al. (1974)	5.5-11	^{58}Ni 98.89	No information	1.0	NaI(Tl)	No information	Target thickness= 20; Detector efficiency=5; Statistical error =2.
Hisakazu et al. (1978)	40	Natural	12% at 284keV	0.98	Ge(Li)	Faraday cup	Target uniformity= 3.
Michel et al. (1983)	16.0-170.9	Natural	No information	1.0	Ge(Li)	Faraday cup $Al(a,x)^{22,24}Na$	No information.
Antropov et al. (1985)	13.0-25.0	Natural	No information	1.0	No information	No information	Error total =4.0-10.0.

Table 3.4, continued.

Author	Alpha energy (MeV)	Target abundance (%)	Gamma intensity used by authors	Total correction factor	Detector	Monitor reaction	Uncertainties given by authors (%)
Levkovskij (1991b)	7-46	^{58}Ni	No information	1.0	No information	No information	10.
Paul et al. (1995)	75, 105	Natural	No information	1.0	Ge	Faraday cup; ^{197}Au(a,an)^{196}Au	Total 15.
Takács et al. (1996)	2.4-24.7	Natural	No information	1.0	HpGe	Faraday cup; ^{nat}Ti(a,x)^{51}Cr ^{nat}Cu(a,x)^{66}Ga	Beam intensity= 4 at 2.4-16 MeV; =15 at 16-24.7 MeV; Beam current =8; Detector efficiency= 5-8; Nuclear data =3; Total= 10-20.

Table 3.4, continued.

Author	Alpha energy (MeV)	Target Abundance (%)	Gamma Intensity Used by authors	Total correction factor	Detector	Monitor reaction	Uncertainties given by authors (%)
Singh et al. (2005)	23.5 -49	Natural	11.3% at 283keV	0.92	HPGe	Faraday cup $^{27}Al(\alpha, \alpha 2pn)^{24}Na$	Systematic =15; Counting statistics=1–4; Detection efficiency=3–4; Target thickness= 1–2; Beam current = 5–6; Total error= 7-9.
Yadav et al. (2008)	8.0-40.0	Natural	12.5% at 283.0 keV	1.02	HpGe	*	Fitting= 3; Solid angel effect= 2; Target thickness= 1; Beam current=3; Beam intensity=2; Total error= 15.

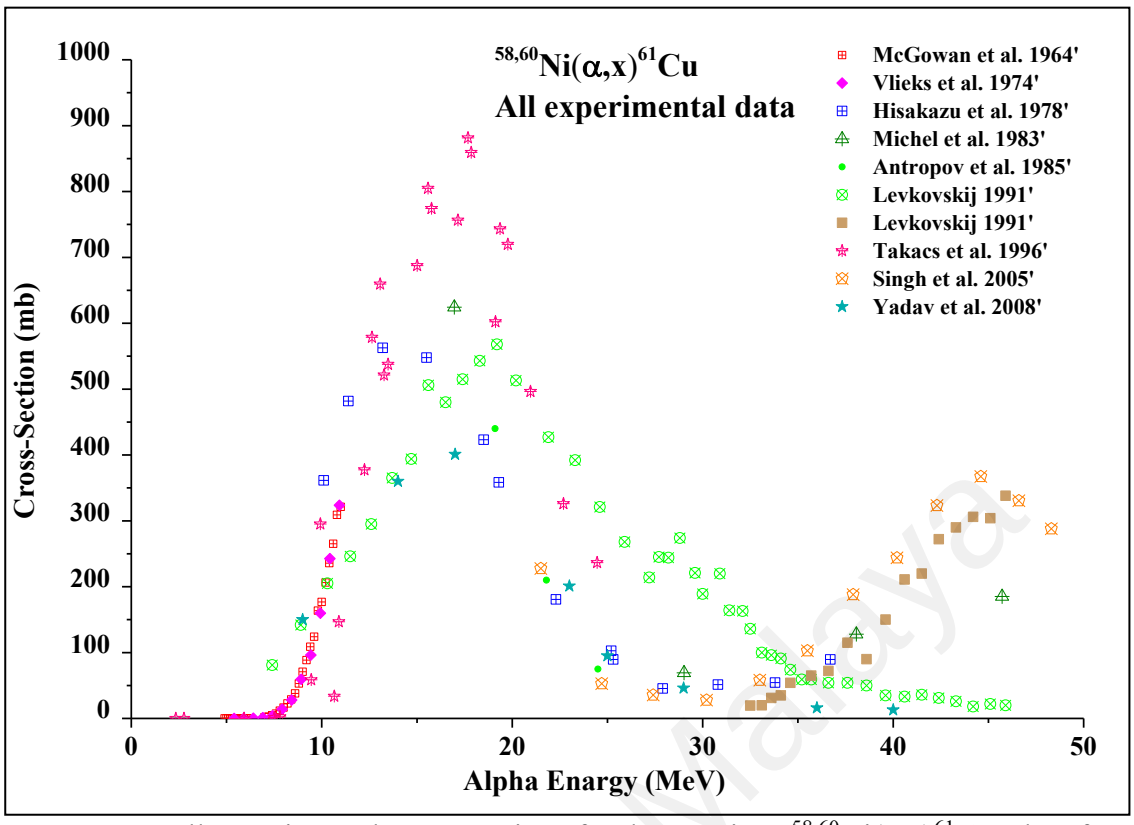

Figure 3.9: All experimental cross-sections for the reactions ^{58,60}Ni(α,x)^{61}Cu taken from EXFOR library without any correction.

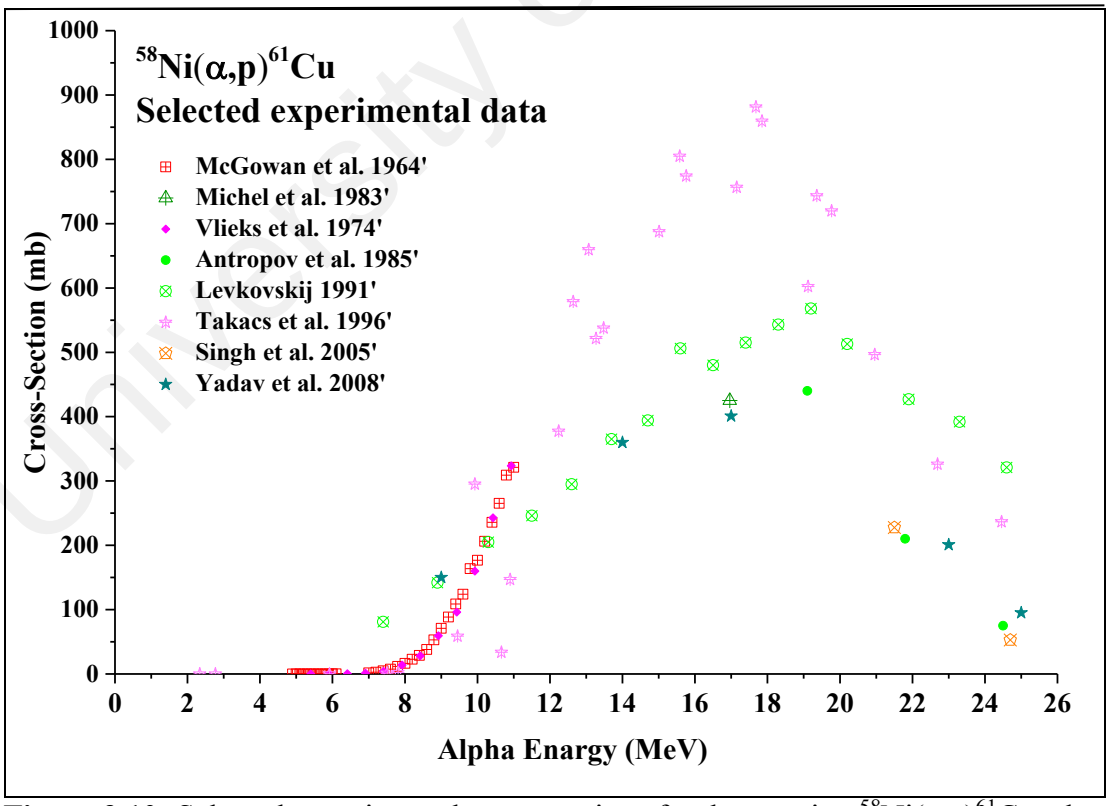

Figure 3.10: Selected experimental cross-sections for the reaction ^{58}Ni(α,p)^{61}Cu taken from EXFOR library without any correction.

3.3.4 Production of ^{61}Cu via Deuteron Induced Reaction on ^{60}Ni

So far ten experiments were done to study the ^{61}Cu production by deuteron irradiation on natural nickel target as listed in EXFOR library. (Avrigeanu et al., 2016; Coetzee Paul & Peisach, 1972; Cogneau et al., 1967; Hermanne et al., 2013; Hermanne et al., 2007; Ochiai, 2007; Takács et al., 2001; Takács et al., 2007; Usman et al., 2016; Zweit et al., 1991). Although most of the authors used nickel target with natural isotopic composition, but eventually only the ^{60}Ni(d,n)^{61}Cu reaction contributed to the formation of ^{61}Cu because the interaction of deuteron with the most abundant ^{58}Ni target isotope cannot lead to the formation of ^{61}Cu.

All experimentalists used gamma-ray spectrometry, while Budzanowski et al. (1963) reported only one cross-section for ^{60}Ni(d,n)^{61}Cu reaction determined via beta counting technique with CsI(Tl) scintillation detector. Furthermore, Cogneau et al. (1967) also adopted the beta counting technique for product activity measurement, both of the authors Budzanowski et al. (1963) and Cogneau et al. (1967) reported clearly higher cross-sections than all other data available in the literature. Note that all other authors used conventional stacked-foil activation technique combined with gamma-ray spectrometry and performed the study relatively in recent time, thus to be consistent in the current evaluation, old activation data obtained via beta counting technique are excluded from this evaluation.

Table 3.5 summarizes some relevant parameters used in those experiments as reported in their original publications. Figure 3.11 shows all experimental cross-sections of ^{60}Ni(d,n)^{61}Cu reactions as they were listed in EXFOR (2018) library. All authors adopted almost the same ^{60}Ni isotopic abundance of 26.2% which is similar to the latest ^{60}Ni abundance listed on NUDAT library. However, some deviation was found between monitor reaction cross-section used by the authors (Hermanne et al., 2007; Takács et al.,

1997; Takács et al., 2001; Takács et al., 2007; Usman et al., 2016; Zweit et al., 1991) with the latest recommended cross-sections provided by IAEA (2017), thus the data were corrected accordingly. Similarly fine adjustments were made to the cross-sections based on the latest 656.0 keV gamma line intensity of I(γ)=10.8% (Zuber & Singh, 2015) when required before performing the evaluation. Figure 3.12 represents the selected data after correction where the circled data point reported by Zweit et al. shows very higher value compared to other authors, thus this data point has been dropped out from this evaluation study. Furthermore, following the procedure available in the next chapter, the correlation matrices for the selected experiments were constructed using the sources of uncertainties that are reported in the original publications (See in Table 3.5). Note that the correlation matrices used as the input of SOK code to calculate the covariance matrix (Khandaker et al., 2017)

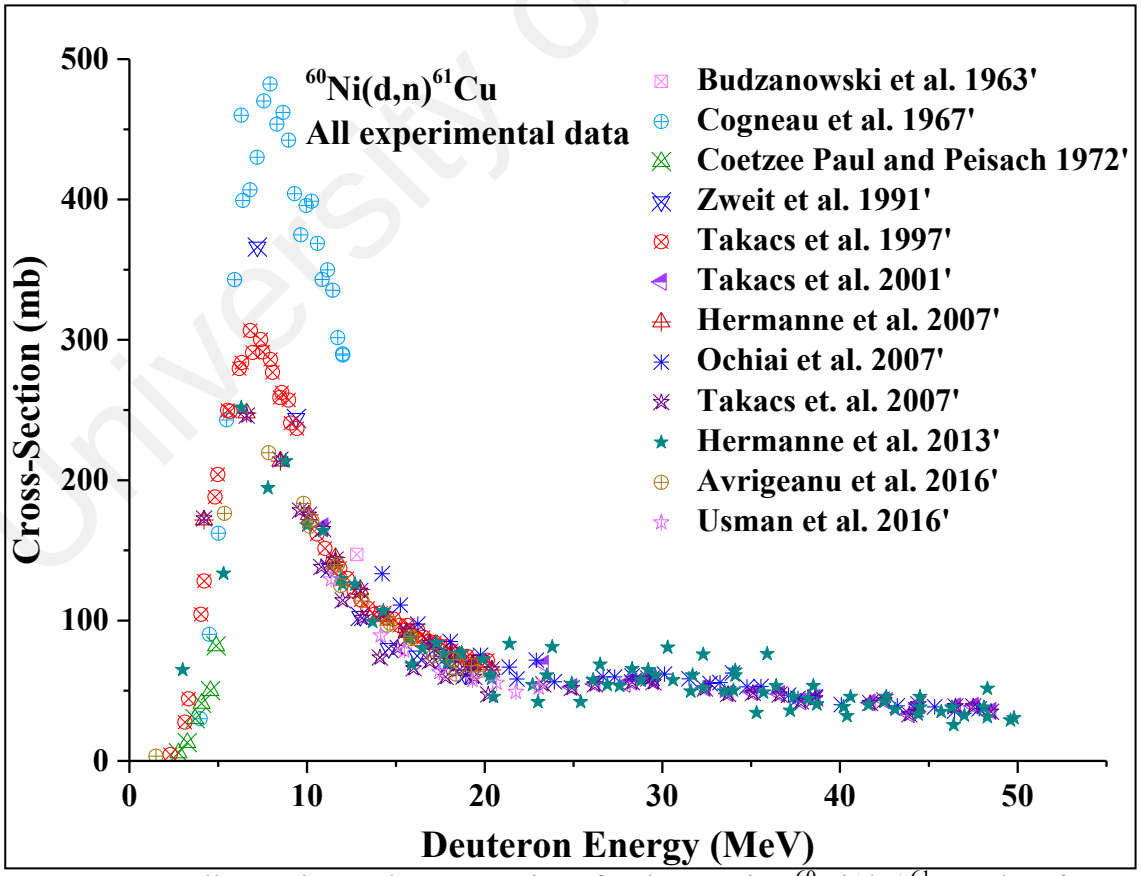

Figure 3.11: All experimental cross-sections for the reaction ^{60}Ni(d,n)^{61}Cu taken from EXFOR library without any correction.

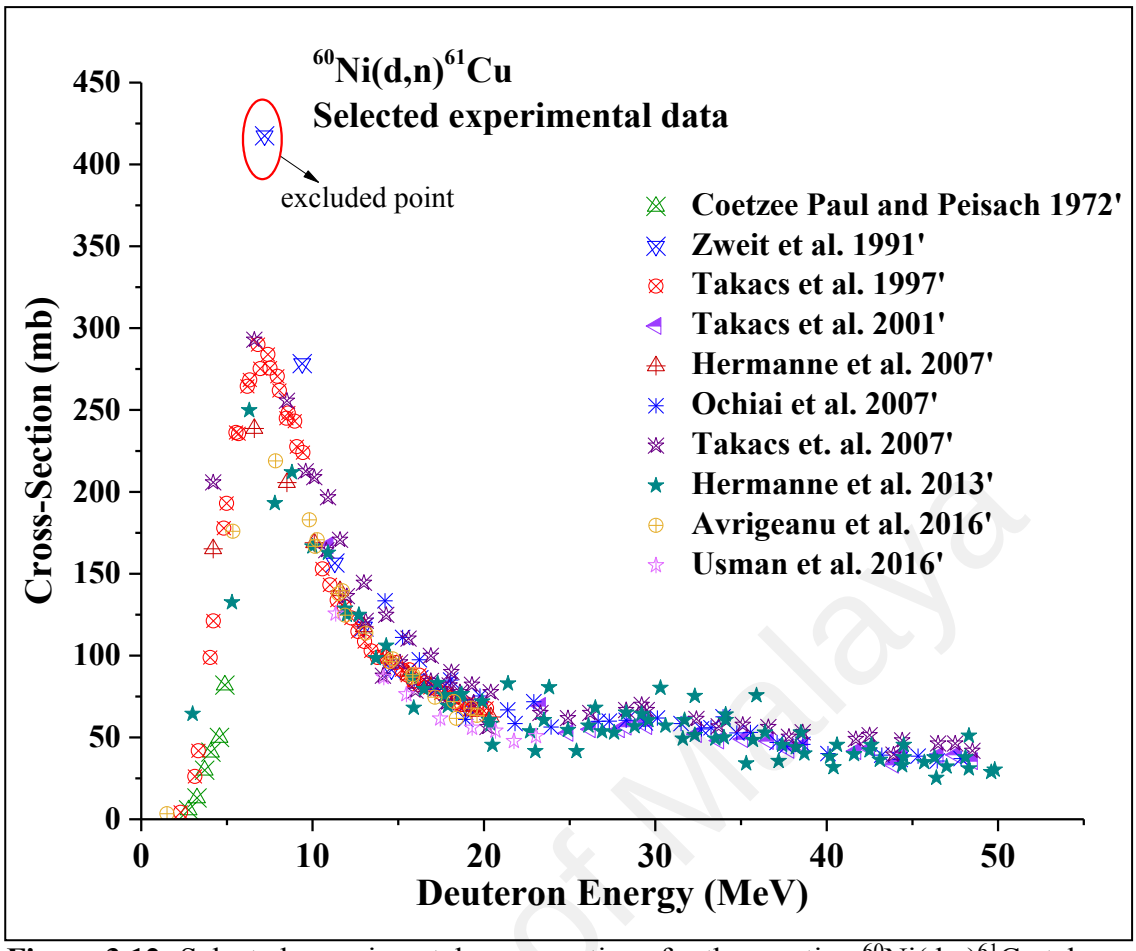

Figure 3.12: Selected experimental cross-sections for the reaction $^{60}Ni(d,n)^{61}Cu$ taken from EXFOR library after correction.

Table 3.5: Summary of several parameters for $^{nat,60}Ni(d,n)^{61}Cu$ experiments.

Author	**Deuteron energy (MeV)**	**Target abundance (%)**	**Gamma intensity used by authors**	**Monitoring process**	**IAEA recommended monitor reaction cross-section**	**Total correction factor**	**Uncertainties (%)**
Budzanowski et al. (1963)	12.8	^{60}Ni, 100 enriched	No gamma, used beta counting technique	Faraday cup	-	No information	No information
Cogneau et al. (1967)	2.0-12.0	Natural	No gamma, used beta counting technique	No information	-	No information	Total error=20
Coetzee Paul & Peisach (1972)	2.7-5.0	Natural	No information	Faraday cup	-	1.0	Target thickness=2.5; Beam current=1.5; Calibration=1; Gamma-ray intensity=20; Detector efficiency=3.

Table 3.5, continued.

Author	**Deuteron energy (MeV)**	**Target abundance (%)**	**Gamma intensity used by authors**	**Monitoring process**	**IAEA recommended monitor reaction cross-section**	**Total correction factor**	**Uncertainties (%)**
Zweit et al. (1991)	19.0-7.0	^{60}Ni=26.42	No information	^{27}Al (d,αp)^{24}Na 34.1 mb at 18.3 MeV (Martens & Schweimer, 1970)	^{27}Al (d,αp)^{24}Na 37.01 mb at 18.3 MeV	1.27	Beam current=5-10; Thicknesses=2; Cross-section measurements=11-17; Statistical uncertainties=10
Takács et al. (1997)	20.2-2.3	^{60}Ni=26.1	Eγ=656.0keV; Iγ=10.7%	Faraday cup; ^{27}Al(d,x)^{24}Na 54 mb at 21 MeV (Takács et al., 1997)	^{27}Al (d,αp)^{24}Na 51.8 mb at 21.0 MeV	0.95	Systematic error= 12; Faraday cup, monitor reaction= 10.

Table 3.5, continued.

Author	Deuteron energy (MeV)	Target abundance (%)	Gamma intensity used by authors	Monitoring process	IAEA recommended monitor reaction cross-section	Total correction factor	Uncertainties (%)
Takács et al. (2001)	50-10.9	^{60}Ni =26.1	Eγ=656keV; Iγ=10.66%	Faraday cup; ^{27}Al(d,x)^{24}Na 50.8 mb at 21 MeV (Takács et al., 2001)	^{27}Al (d,αp)^{24}Na 51.8 mb at 21.0 MeV	1.00	Total uncertainty=10; Number of target atoms=3; Decay data=3; Beam intensity=5-8; efficiency calibration 3-6; Statistical uncertainty= 1-5.
Hermanne et al. (2007)	20.5-4.2	^{60}Ni=26.22	Eγ=656.0keV; Iγ=10.8%	Faraday cup ^{nat}Ti(d,x)^{48}V 296 mb at 20.5 MeV (Tarkanyi et al., 2001)	^{nat}Ti(d,x)^{48}V 285.1 mb at 20.5 MeV	0.96	Decay data=1-5; Statistical error=15; Detecting efficiency=5; Beam intensity=5; Target uniformity=8; Total uncertainty=10-20.
Ochiai (2007)	14.2-49.0	^{60}Ni=26.22	No information	No information		1.0	Total error=10-20.

Table 3.5, continued.

Author	Deuteron energy (MeV)	Target Abundance (%)	Gamma intensity used by authors	Monitoring process	IAEA recommended monitor reaction cross-section	Total correction factor	Uncertainties (%)
Takács et al. (2007)	50-4.2	Natural	Eγ=656.0keV; Iγ=10.77%	Faraday cup; $^{24}Na(d,x)^{24}Na$ 22.8 mb at 48.5 MeV; $^{27}Al(d,x)^{22}Na$ 27.6 mb at 48.5 MeV; $^{nat}Ti(d,x)^{48}V$ 50.6 mb at 48.5 MeV (Tarkanyi et al., 2001)	$^{24}Na(d,x)^{24}Na$ 23.37 mb at 48.5 MeV; $^{27}Al(d,x)^{22}Na$ 29.64 mb at 48.5 MeV; $^{nat}Ti(d,x)^{48}V$ 54.9 mb at 48.5 MeV	1.21	Target uniformities=5; Gamma intensity=4-6; Detection efficiency=3-7; Counting uncertainty=1-9; Target abundance=1-5; Total error=8-15.
Hermanne et al. (2013)	50.0-3.0	$^{60}Ni = 26.1$	Eγ=656.0keV; Iγ=10.77%	$^{27}Al(d,x)^{22,24}Na$ and $^{nat}Ti(d,x)^{48}V$ (Hermanne et al., 2013) [a]	No information	0.99	Surface density of target nuclei=5; Beam flux= 6; Detector efficiency= 3–8; Statistical uncertainty=3–8; Decay data= 1–5; Overall uncertainty= 12.

Table 3.5, continued.

Author	Deuteron energy (MeV)	Target Abundance (%)	Gamma intensity used by authors	Monitoring process	IAEA recommended monitor reaction cross-section	Total correction factor	Uncertainties (%)
Avrigeanu et al. (2016)	20.0-1.5	^{60}Ni =26.22	Eγ=656.0keV; Iγ=10.77%	Faraday cup		1.0	Beam energy=1; Efficiency=2; Beam current= 5; Foil thickness=2.
Usman et al. (2016)	23.7-9.5	^{60}Ni =26.22	Eγ=656.0keV; Iγ=10.8%	Faraday cup; ^{nat}Ti(d,x)^{48}V 217.54 mb at 23.88 MeV (Usman et al., 2016)	^{nat}Ti(d,x)^{48}V 214 mb at 23.88 MeV	0.98	Target thickness=1; Beam energy=1; Beam intensity=5; Detector efficiency= 4; Gama ray intensity= 18.5; Statistical uncertainty=4.9.

[a]Monitor reactions listed in the original publication in terms of beam current no cross-section listed

3.3.5 Production of ^{61}Cu via Proton Induced Reaction on ^{64}Zn

Zinc target shows higher ^{61}Cu production cross-sections than those obtained by Ni target when irradiated with proton beam as illustrated in Figure 3.6. Figure 3.13 shows experimental cross-sections for ^{nat}Zn(p,x)^{61}Cu reaction available in the EXFOR database (Asad et al., 2014; Barrandon et al., 1975; Cohen et al., 1954; Gyürky et al., 2014; Hermanne et al., 1999; Levkovskij, 1991b; Szelecsényi, Kovács, et al., 2005; Uddin et al., 2007; Aleksandrov, 1990) in the energy range of 0.0 - 60.0 MeV. ^{64}Zn (49.2%), ^{66}Zn (27.7%) and ^{68}Zn (18.5%) are mainly the three contributing isotopes for ^{61}Cu production in the mentioned energy range. But, the production of ^{64}Cu via the competing ^{66}Zn(p,α2n)^{64}Cu reaction could be considered as contaminant for ^{61}Cu product, and this could avoid by limiting the energy range up to 25.0 MeV (Szelecsényi et al., 2005; Tárkányi et al., 2005).

^{64}Cu contaminant can also be produced via other contributing ^{68}Zn(p,αn)^{64}Cu reaction, but this process produces a low cross-sections of 1-13 mb (Hilgers et al., 2003) following the relatively lower abundance of ^{68}Zn (18.5%) target isotope (nudat2.7, 2018), and again this can be ignored by limiting the incident beam energy of maximum 25.0 MeV. Under this circumstances, the available literature data for ^{61}Cu production are compiled only in the energy range of 0-25 MeV for this evaluation.

Furthermore, some authors such as Cohen et al. (1954) used beta-particle detection technique in products identification without any information on uncertainties, while Karol & Miller (1968), Aleksandrov (1990) and Hermanne et al. (1999) conducted measurements in the high energy range (> 25 MeV), these data were excluded from this evaluation. Table 3.6 summarizes all literature data together with the relevant information on each experiment. Almost in all of the selected studies for this evaluation, the authors utilized a similar procedure together with the gamma-ray spectrometry for ^{61}Cu

identification. Thus, necessary corrections were done for the monitor cross-sections, gamma-ray intensity and target abundance, wherever required. Correction for monitor reactions was performed using the latest cross-section found on IAEA database (IAEA, 2017), and latest gamma-ray intensity of 12.2% (Zuber & Singh, 2015) was used for correction of branching ratio. Correlation matrices were built using the given uncertainties in each experiment, except in Szelecsényi, Kovács, et al. (2005) work since the source of uncertainties was not reported in their work, 5% systematic uncertainty and 10% statistical uncertainty were assumed. Figure 3.14 illustrates the selected $^{64}Zn(p,\alpha)^{61}Cu$ data after necessary correction, and ready to be used as input for SOK for this evaluation. The plotted cross-sections in Figure 3.14 were renormalized to 100% abundance of ^{64}Zn target isotope.

Table 3.6: Summary of relevant experimental information for $^{nat,64}Zn(p,x)^{61}Cu$ reactions needed for this evaluation.

Year	Isotopic abundance	Proton energy range (MeV)	Gamma intensity	Monitor Reaction	Detector used	Total Correction factor	Uncertainty (%)	notes
Cohen et al. (1954)	Enriched target	7.1 -23.5	*	*	Beta detection		*	Excluded
Karol & Miller (1968)	No information	370	*	*	*		*	Excluded
Barrandon et al. (1975)	Natural	5-20	282.9 keV	$^{65}Cu(p,n)^{65}Zn$ 700 mb at 10 MeV; Recommended by IAEA 716.6 at 10 MeV	Ge(Li)	1.02	19	Selected
Aleksandrov (1990)	No information	660	No information	No information	No information		No information	Excluded
Levkovskij (1991b)	100 enriched ^{64}Zn	7-30	No information	$^{nat}Mo(p,x)^{96}Tc$ 250 mb at 30 MeV; Recommended by IAEA $^{nat}Mo(p,x)^{96}Tc$ 192.8 mb at 30 MeV	No information	0.96	total error=10	Selected

Table 3.6, continued.

Year	Isotopic abundance (%)	Proton energy range (MeV)	Gamma intensity used by authors	Monitor Reaction	Detector used	Total Correction factor	Uncertainty (%)	notes
Hermanne et al. (1999)	^{68}Zn enriched ^{64}Zn =0.65	34-32	No information	Faraday cup	HPGe		No information	Excluded
Szelecsényi, Kovács, et al. (2005)	48.8	9.0 -100.0	12.5% at 283 keV	No information	HPGe	1.01	systematic=5; statistical=10.	Selected
Uddin et al. (2007)	48.6	4.0 - 40.0	12.2% at 282.95 keV	^{nat}Cu(p,xn)^{62}Zn 12.1 mb at 40.0 MeV used by authors; 13.1mb at 40.0 MeV given at IAEA	HPGe	0.99	Statistical=10.0, monitor flux= 7, calibration efficiency= 4; total uncertainty=13.	Selected
Asad et al. (2014)	48.6	3.2 -18.0	12.20% at 282.95keV	^{63}Cu(p,n)^{63}Zn 82.4 mb at 18.0 MeV used by authors; 93.0 mb at 18 MeV given at IAEA; ^{65}Cu(p,n)^{65}Zn 34.2 mb at 18 MeV used by the authors; 34.1 mb at 18 MeV by IAEA	HPGe	1.11	Beam current=10-12; Detector efficiency=5; Foil thickness=4-7; Irradiation time=1-2; Total uncertain= 13-16.	Selected

Table 3.6, continued.

Year	Isotopic abundance (%)	Proton energy range (MeV)	Gamma intensity	Monitor Reaction	Detector used	Total Correction factor	Uncertainty (%)	notes
Gyürky et al. (2014)	Enriched ^{64}Zn =97.1	3-8	12.2% at 283 keV	No information	HPGe	1.0	Target thickness= 8; Detection efficiency= 5; charge collection= 3; decay data = 5; Counting stat. = 10.	Selected

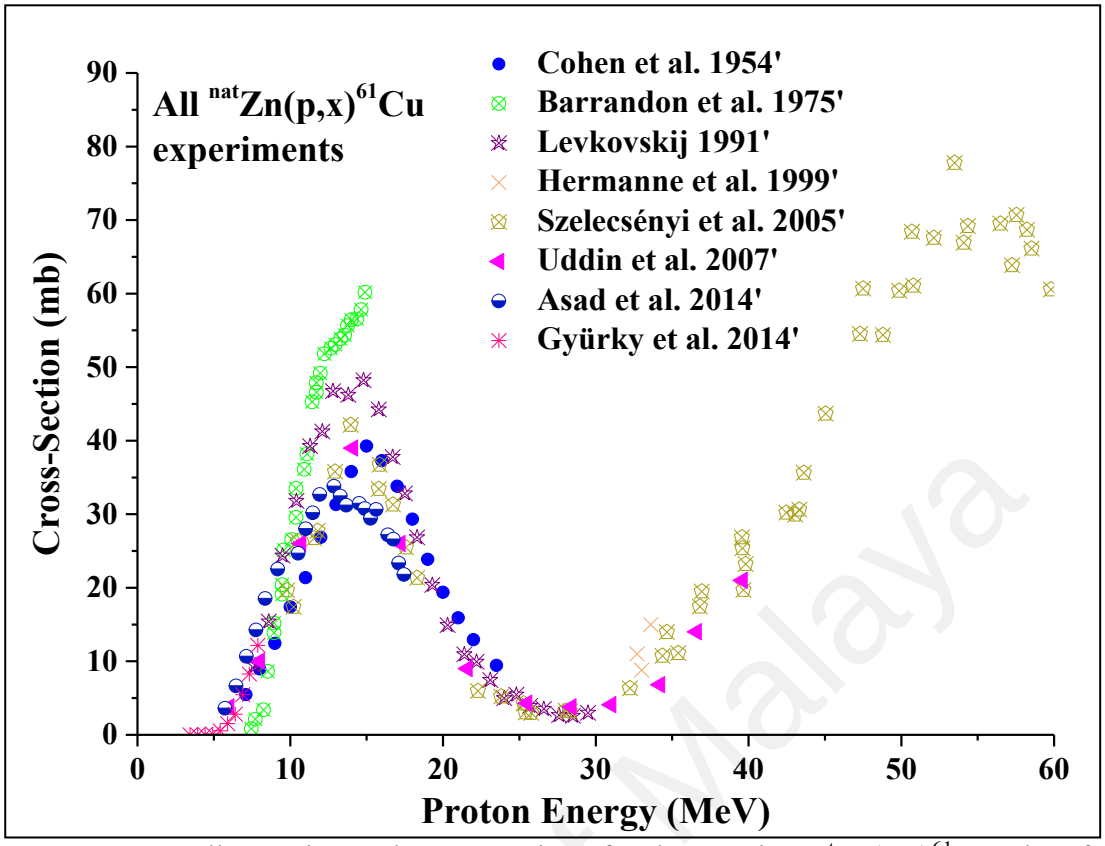

Figure 3.13: All experimental cross-sections for the reaction $^{nat}Zn(p,x)^{61}Cu$ taken from EXFOR library without any correction.

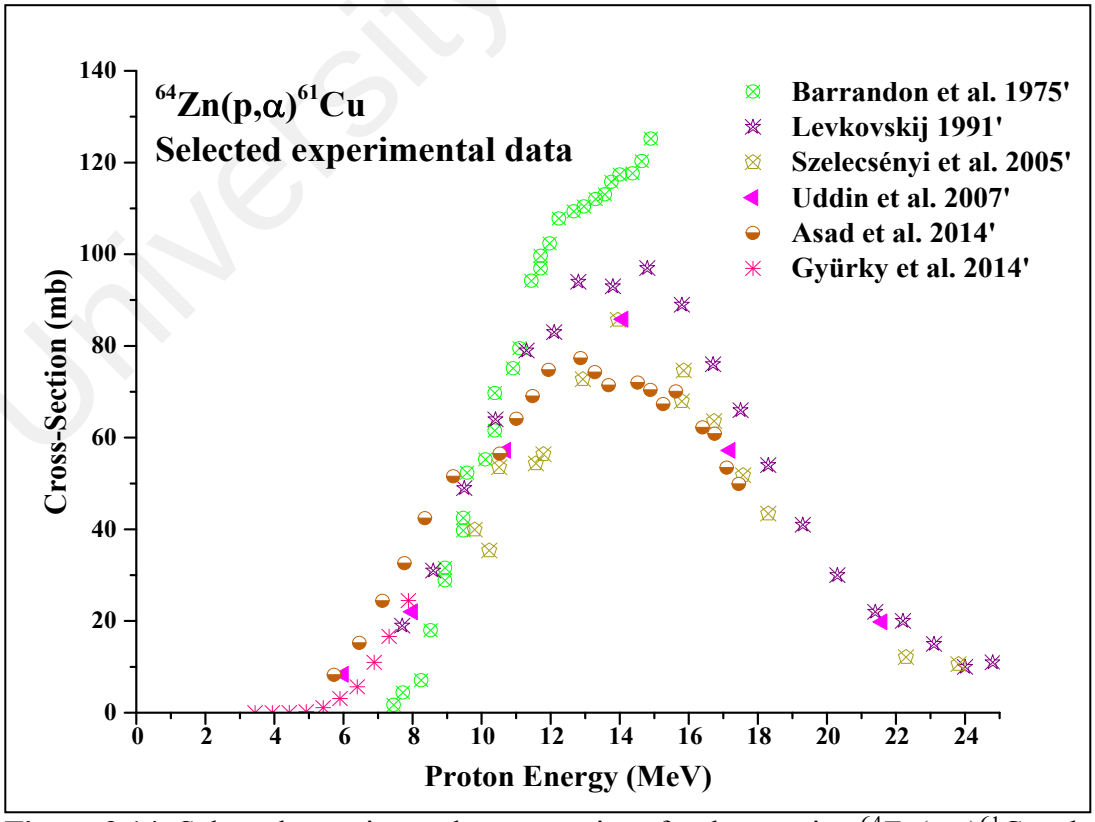

Figure 3.14: Selected experimental cross-sections for the reaction $^{64}Zn(p,\alpha)^{61}Cu$ taken from EXFOR library without any correction.

3.4 Evaluation of Production Cross-Section for ^{186}Re

^{186}Re ($T_{1/2}$=89.24 h, $E(\beta^-)_{total} = 346.7$ keV, $I(\beta^-)_{total} = 92.59\%$), an intense beta-emitter shows great potential to be used as an active material in therapeutic radiopharmaceuticals due to its suitable physio-chemical properties. ^{186}Re can be produced in several ways, however charged-particle induced reactions show to be promising towards no carrier added production. In this part, production cross-sections of ^{186}Re were evaluated following the light-charged particle induced reactions on tungsten.

3.4.1 ^{186}Re Production Routes Selection

Number of processes can be used for the production of ^{186}Re; the dominant one is the neutron activation on different materials via the use of nuclear reactor. Several nuclear reactions such as ^{185}Re(n,γ)^{186}Re (Matters et al., 2016) and ^{187}Re(n,2n)^{186}Re (Druzhinin et al., 1967) can be identified as useful reactions but this route provides ^{186}Re in carrier added form with low specific activity. On the other hand, production of ^{186}Re has also been reported in some experiments like ^{186}W(^{3}He,x)^{186}Re and ^{186}W(α,x)^{186}Re (Scott et al., 1968), and spallation of ^{208}Pb (Enqvist et al., 2001), ^{197}Au (Rejmund et al., 2001) using ^{1}H as a high energy projectile. Besides this, ^{186}Re radioisotope can also be produced via charged particles induced reactions such as ^{186}W(p,n)^{186}Re and ^{186}W(d,2n)^{186}Re using cyclotrons. Moreover, unlike the nuclear reactor, cyclotrons can be easily installed in the periphery of hospitals and can also be operated easily towards the production of desired isotope with no carrier added (NCA) form (Nozaki & Hazue, 1995; Vera Ruiz & Lambrecht, 1998). However, an accurate knowledge of nuclear reaction cross-sections plays a crucial role for the NCA production of desired radionuclide by cyclotron.

A review of literature revealed that several works were carried out for the production of ^{186}Re via light charged-particles irradiations on a tungsten target (Alekseev & Lazarev, 2006; Bonardi et al., 2010; Guertin et al., 2014; Khandaker et al., 2017; Khandaker et al.,

2008; Lapi et al., 2007; Menapace et al., 2007; Moustapha et al., 2006; Shigeta et al., 1996; Szelecsényi et al., 1997; Tárkányi et al., 2006; Zhang et al., 2001; Zhang et al., 1999). In such studies, excitation functions for the residual radionuclides of $^{nat}W(p,d; x)$ nuclear processes were measured, physical yields were deduced towards the NCA production of ^{186}Re radionuclide. However, a close observation on such studies show a considerable degree of discrepancy even within the same excitation energy (See in Figure 3.15). But, it is possible to correct the reported data or reduce the discrepancy by using the updated value of some relevant parameters such as gamma-ray intensity, monitor cross-sections, target abundance etc. that are generally available in the original publications. On the other hand, corrections on time parameters such as half-lives are difficult due to lack of information related to the irradiation, cooling and measurement time (Khandaker et al., 2017). However, among the various studied reactions, although $^{186}W(d,2n)^{186}Re$ shows four times higher cross-sections than that of $^{186}W(p,n)^{186}Re$ (Ishioka et al., 2002), both of them are promising and selected for this evaluation study because of their consistency with the available facilities since no high energy proton, neutron or alpha beams are required (Zhang et al., 2001).

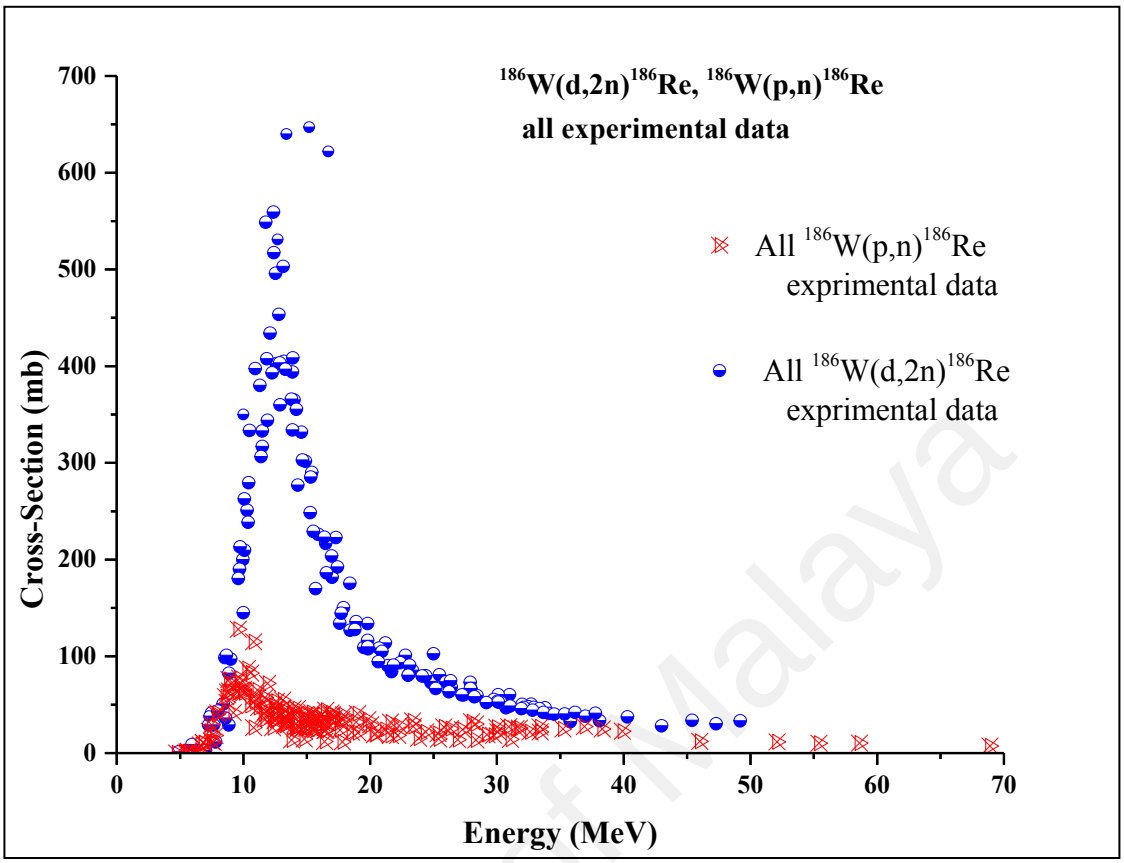

Figure 3.15: A general comparison of $^{186}W(d,2n)^{186}Re$ and $^{186}W(p,n)^{186}Re$ cross-sections available in the EXFOR database.

3.4.2 Selection and Renormalization of $^{nat}W(p,x)^{186}Re$ and $^{186}W(p,n)^{186}Re$ Reactions Cross-Sections

A total of ten experiments related to the ^{186}Re production via proton-induced reactions on natural and/or enriched tungsten target are available in the EXFOR (EXFOR, 2017) data base (Bonardi et al., 2011; Khandaker et al., 2008; Lapi et al., 2007; Miah et al., 2002; Shigeta et al., 1996; Tárkányi et al., 2007; Tárkányi et al., 2006; Titarenko et al., 2011; Treytl & Caretto, 1966; Zhang et al., 1999). To cope up with the objective of this evaluation work (that is, evaluation of production cross-sections of ^{186}Re for medical applications), we extracted the literature data within the energy range of 4 - 60 MeV. Figure 3.16 shows all experimental cross-sections of (p,x) reactions without any correction or any pre-treatment, where the reported cross-sections among the measurements show a large discrepancy in the peak region about a factor of 4.

Treytl & Caretto (1966) measured the excitation functions for the (p,n) reactions on several elements ^{45}Sc, ^{64}Ni, ^{103}Rh, ^{130}Te and ^{186}W by using protons with relatively high energy from 130 MeV to 420 MeV. This data is out of our energy region of interest, and hence was excluded from this evaluation.

Shigeta et al. (1996) reported ^{186}W(p,n)^{186}Re cross-sections by irradiating a pellet compressed from $^{186}WO_3$ powder (^{186}W enrichment level was 99.79%) with protons in the energy range of 5.4 MeV-20.0 MeV. They monitored the beam current by using a faraday cup, and also the average beam current was determined from the radioactivity produced in copper monitor foils. Shigeta et al. determined the ^{186}Re product through detection of the characteristic 137.2 keV gamma line ($I_\gamma = 9.3\%$) via a HPGe gamma-ray spectrometer, and their data are corrected using the latest intensity of $I_\gamma = 9.47\%$ for the 137.2 keV gamma line (Baglin, 2003b). Two cross-sections data points of Shigeta et al. work were excluded from this evaluation because of their unusual magnitudes compared to more recent works at the same energy. The data was finally renormalized for 100% enrichment of ^{186}W target.

Excitation function for the ^{nat}W(p,xn)^{186}Re reaction was measured by irradiating 22.5 MeV protons on natural tungsten via conventional stacked foil technique at Shanghai Institute of Nuclear Research by Zhang et al. (1999). The characteristic 137.2 keV ($I\gamma$=9.20%) gamma line (Reus & Wesymeier, 1983) was used in identification of ^{186}Re product. Their data are corrected using the latest decay data ($I_\gamma = 9.47\%$) taken from NuDat2.6 library (Baglin, 2003b). Zhang employed the ^{63}Cu(p,2n)^{62}Zn (61.3 mb at 22.4 MeV) as monitor reaction taken from (Grütter, 1982), which shows a big difference with the recommended cross-section available in the IAEA database. The monitor reaction ^{nat}Cu(p,x)^{62}Zn listed in the IAEA library has a cross-section of 71.9 mb at 22.4 MeV. Note that, this cross-section is only contributed by the ^{63}Cu(p,2n)^{62}Zn reaction because

of the other possible reaction $^{65}Cu(p,4n)^{62}Zn$ can only contributes above it's threshold energy of 31.6 MeV. Therefore, the IAEA reported $^{nat}Cu(p,x)^{62}Zn$ cross-sections were renormalized considering the natural abundance of 69.15% for ^{63}Cu, and thus the corrected cross-sections of the monitor reaction $^{63}Cu(p,2n)^{62}Zn$ becomes 104.0 mb at 22.4 MeV. This explains the lower cross-sections appeared in Zhang's work compared to the available literature data. According to Zhang et al., ^{186}Re produced exclusively from the $^{186}W(p,n)^{186}Re$ channel within their investigated energy range of 7.5-17.8 MeV. Thus, their data were renormalized by dividing the natural abundance of 28.43% for ^{186}W target.

Miah et al. (2002) reported cross-sections for $^{nat}W(p,x)^{186}Re$ reaction at four different energies in the range of 52.5-68.9 MeV by using a stacked foil activation technique. The beam current was monitored by Faraday cup technique, and the decay data of E_γ=137.2 keV (I_γ=9.2%) taken from (Reus & Wesymeier, 1983) work was used in calculation of cross-sections. Only two out of these four points lie within the energy region of our interest, and they were renormalized by using natural isotopic abundance of ^{186}W (28.43%) and the latest decay data of E_γ=137.2 keV ($I_\gamma = 9.47\%$) (Baglin, 2003b).

Tárkányi et al. (2006) measured the excitation functions of charged particles induced reactions on natural tungsten in an energy range from threshold to 34.0 MeV by using a stacked foil activation technique. Tárkányi et al. reported the data following two separate experiments performed by the cyclotron facility located at Hungary and Belgium with 18.0 MeV and 34.0 MeV proton beams, respectively. In both experiments, they used IAEA recommended $^{nat}Cu(p,x)^{62,63,65}Zn$ monitor reactions to determine the final beam intensity and also used a faraday cup to obtain the integrated charge. Tárkányi et al. used the 137.16 keV (I_γ=9.42%) gamma line in cross-section calculation which shows some deviation from the latest decay data of $I_\gamma = 9.47\%$ (Baglin, 2003a). The source of uncertainties are not reported in their original publication but based on a private

communication with the author, we have been informed that the uncertainty for counting statistics may varied between 1 and 7%, 5-8% for detector efficiency depending on the gamma energy, 1-3% for the target thickness, 7-10% for the beam intensity deduced from monitor reactions and 1-5% for decay data of the radionuclides of interest. Since the main characteristic 137.2 keV gamma line of ^{186}Re show a relatively low intensity 9.42%, thus the upper limits of uncertainties were used in correlation matrix construction. (Tárkányi et al. (2007) re-measured the excitation function of the ^{186}W(p,n)^{186}Re reaction in the energy range from threshold up to 30 MeV. A faraday cup together with the IAEA recommended ^{nat}Ti(p,x)^{48}V reaction (IAEA, 2007) was used to monitor the beam current, and the latest decay data of ^{186}Re taken from the NuDat2.6 (Baglin, 2003a) was used to calculate the cross-sections. Tárkányi et al. reported data was used in this evaluation without any correction except renormalized for 100% abundance of ^{186}W target isotope. Regarding uncertainties, we followed the same values/proportions adopted in their previous experiment (Tárkányi et al., 2006) to construct the correlation matrix.

Production cross-section of ^{186}Re was measured by Lapi et al.,(2007) by irradiating a high purity natural tungsten target with protons in the energy range from threshold to 17.6 MeV. The IAEA recommended ^{nat}Cu(p,n)^{65}Zn monitor reaction was used in determination of beam intensity together with 5% uncertainty. ^{186}Re was assessed via the use of E_γ=137.2 keV (I_γ=9.2 %(decay data which showed little difference from the latest decay data of E_γ=137.2 keV ($I_\gamma = 9.47$ %) (Baglin, 2003a). Therefore, we amended the results to the intensity, and also normalize the ^{186}W(p,n)^{186}Re data by dividing the natural abundance of ^{186}W (28.43%).

Khandaker et al. (2008) measured the excitation function for ^{186}Re radionuclide via proton activation on natural tungsten in the energy range from 6.6 MeV to 39.9 MeV. High purity tungsten foils with natural isotopic composition were used in their experiment

but the reported abundance of ^{186}W (28.6%) is slightly differ with the latest abundance of 28.43%. Meanwhile, ^{27}Al(p,x)^{24}Na (1.7 mb at 41.5 MeV) and ^{nat}Cu(p,x)^{62}Zn (11.8 mb at 42 MeV) monitor reactions (Tarkanyi et al., 2001) were employed for determining the beam flux. Monitor reaction cross-sections updated on the IAEA data base is 2.0 mb at 41.5 MeV for ^{24}Al(p,x)^{24}Na and 12.6 mb at 42.0 MeV for ^{nat}Cu(p,x)^{62}Zn (IAEA, 2017). Khandaker et al. used the decay data of E_γ=137.15 keV (I_γ=9.47%(for assessing ^{186}Re cross-sections which is identical to the latest decay data (Baglin, 2003a). Therefore, the reported cross-sections were renormalized using the updated monitor cross-sections and ^{186}W abundance.

Titarenko et al. (2011) reported three cross-section values for the ^{nat}W(p,n)^{186}Re reaction in the energy range of 40 MeV- 2.6GeV, where only one cross-section lies within our region of interest. The monitor reaction ^{27}Al(p,x)^{22}Na (43.5 mb at 44.6 MeV) (Titarenko et al., 2011) was used to determine the beam intensity, but it shows only a little difference with the IAEA recommended ones (43.8 mb at 44.5 MeV). We corrected the Titarenko et al. data using the monitor cross-section and then renormalized for ^{186}W(p,n)^{186}Re reaction. Since one point involved in this evaluation, the correlation matrix contains only one element and no other points are available to correlate with it.

Bonardi et al. (2011) measured excitation function of ^{nat}W(p,n)^{186}Re reaction via stacked foil activation technique in the energy range of 4.7-21.6 MeV. To calculate the ^{186}W(p,n)^{186}Re cross-sections, they adopted the decay data of E_γ=137.2 keV (I_γ=8.22%(taken from the table of isotopes (Firestone et al., 1998) which differs from the latest decay data of E_γ=137.2 keV (I_γ=9.47%((Baglin, 2003a). The reported ^{186}Re cross-sections were corrected using the monitor reaction cross-sections and the abundance of ^{186}W (Bonardi et al., 2011). Table 3.7 shows a summary of the ^{nat,186}W(p,n)^{186}Re experiments involved in this evaluation together with the information on corrections of different

factors. All of the uncertainties presented in Table 3.7 were used to construct the corresponding correlation matrices that were used as an input of the SOK code. Figure 3.17 shows the corrected experimental data ready to be used as input of SOK code.

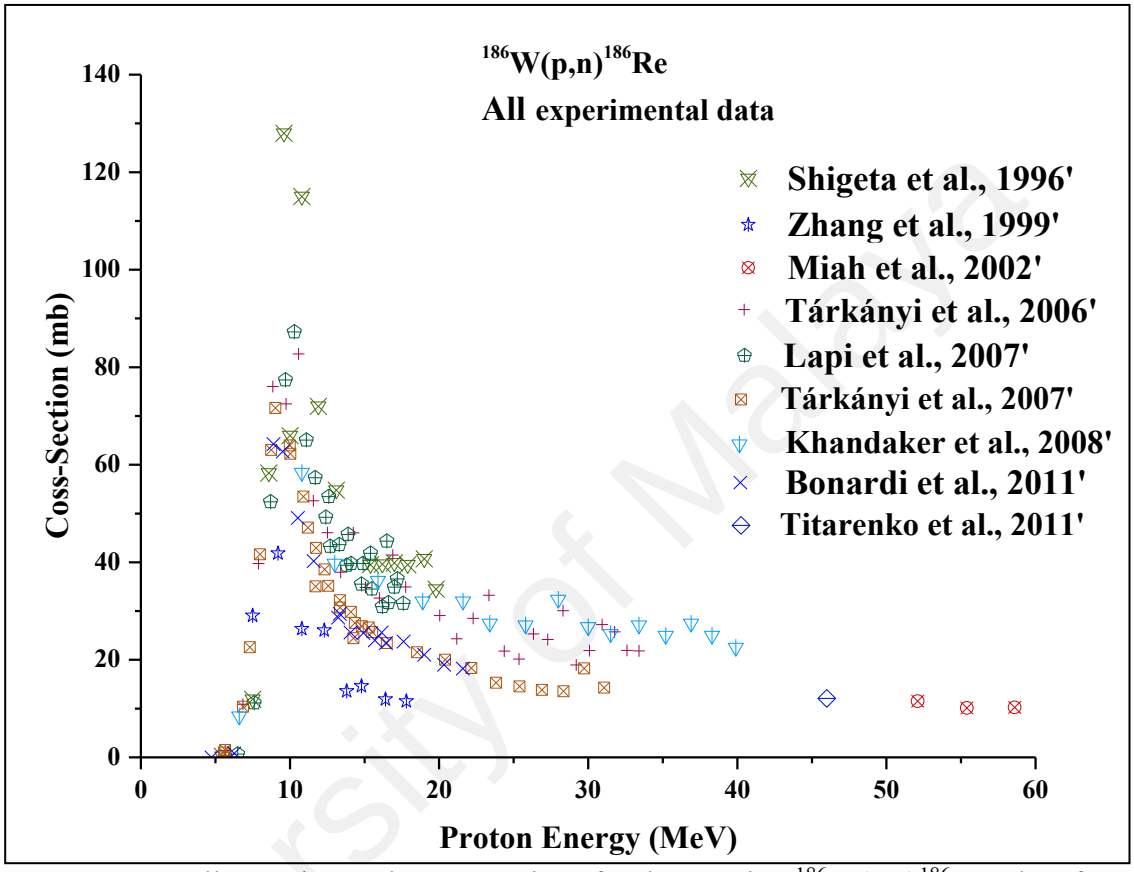

Figure 3.16: All experimental cross-sections for the reaction $^{186}W(p,n)^{186}Re$ taken from EXFOR library without any correction.

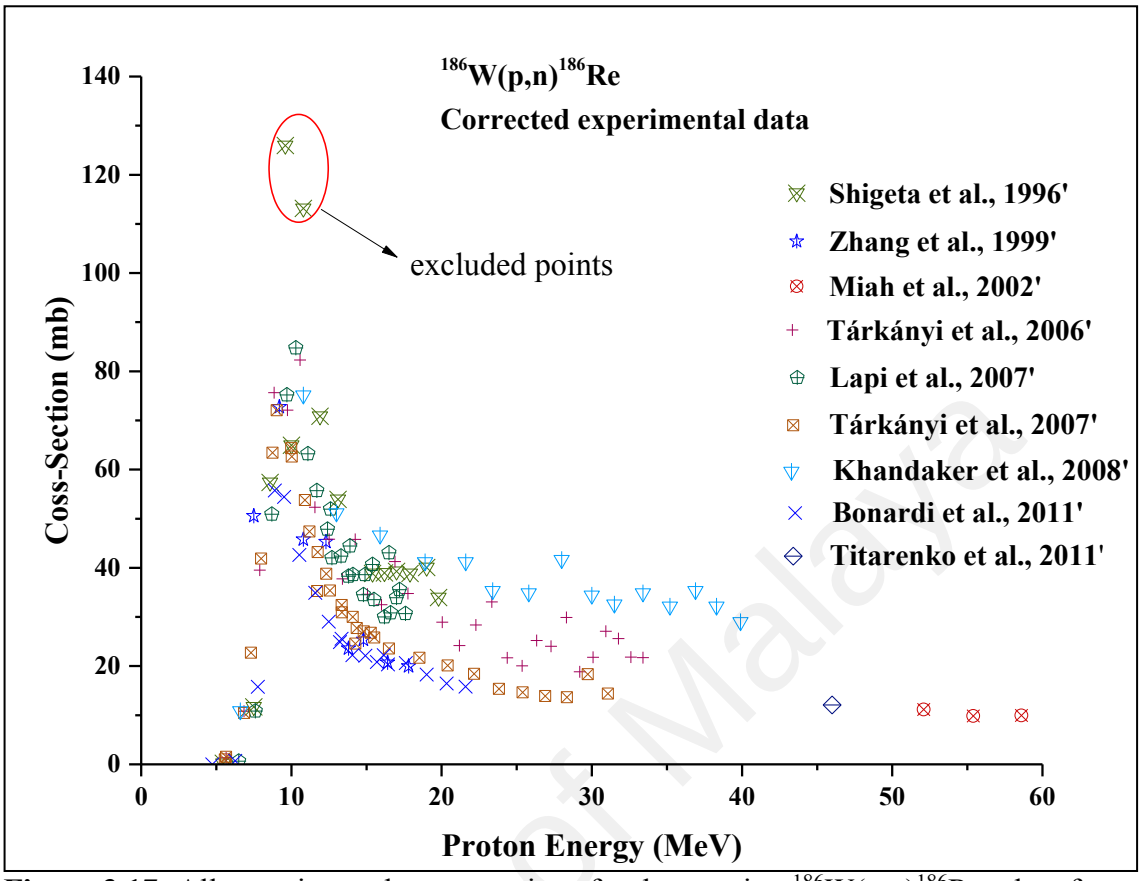

Figure 3.17: All experimental cross-sections for the reaction ^{186}W(p,n)^{186}Re taken from EXFOR library after correction.

Table 3.7: A brief information on the selected experiments for $^{nat,186}W(p,n)^{186}Re$ reactions used in this evaluation.

Authors	**Proton beam energy range MeV**	**Used ^{186}W target abundance used by authors (%)**	**^{186}W Abundance adopted in this evaluation (%)**	**Gamma intensity used by authors $I\gamma$**	**Gamma intensity adopted in this evaluation $I\gamma$**	**Monitor cross-section (mb)**	**Recommended monitor cross-section (IAEA, 2017)**	**Total correction factor**	**Detailed uncertainties given by authors (%)**	**Systematic uncertainty used in the evaluation (%)**	**Statistical uncertainty (%)**
Shigeta et al. (1996)	5.40-20.0	97.8 Enriched target	28.43 NUDAT 2.6 library	$I_\gamma = 9.3\%$ E_γ=137.2 keV	I_γ=9.47% E_γ=137.2keV NuDat2.6 (Baglin, 2003a)	Faraday cup		0.982	Counting efficiency=3, Target thickness=3.	4.2	8.0-24.5
Zhang et al. (1999)	7.5 -22.5	28.6		$I_\gamma = 9.2\%$ E_γ=137.2 keV		$^{63}Cu(p,2n)^{62}Zn$; 61.3 mb at 22.4 MeV	$^{63}Cu(p,2n)^{62}Zn$ 103.97 mb at 22.4 MeV	1.655	Detector efficiency=5, Statistical uncertainty=10.	5.0	10.0
Miah et al. (2002)	52.5 -68.9	28.6		$I_\gamma = 9.2\%$ E_γ=137.2 keV		Faraday cup		0.977	Gamma intensity=1.0, Self-absorption=1; Efficiency calibration=5; Proton fluence= 5.5; Mass of monitor foil= 1; Statistical uncertainty=2.	7.6	2.0

Table 3.7, continued.

Authors	**Proton beam energy range MeV**	**Used ^{186}W target abundance used by authors (%)**	**^{186}W Abundance adopted in this evaluation**	**Gamma intensity used by authors $I\gamma$**	**Gamma intensity adopted in this evaluation $I\gamma$**	**Monitor cross-section (mb)**	**Recommended monitor cross-section (IAEA, 2017)**	**Total correction factor**	**Detailed uncertainties given by authors (%)**	**Systematic uncertainty used in the evaluation (%)**	**Statistical uncertainty (%)**
Tárkányi et al. (2006)	5.6-34.0	28.6	28.43 NUDAT 2.6 library	$I_\gamma = 9.42\%$ E_γ=137.16 keV	I_γ=9.47% E_γ=137.2keV NuDat2.6 (Baglin, 2003a)	Faraday cup		1.001	Detector efficiency=1-7; Target thickness =1-3; Beam intensity=7-10; Nuclear data= 1-5; Statistical error= 1-7.	14.1	7.0
Tárkányi et al. (2007)	5.7 -25.4	28.6*		I_γ=9.47% E_γ=137.2 keV		Faraday cup		1.006	Detector efficiency=1-7; Target thickness=1-3; Beam intensity= 7-10; Nuclear data= 1-5; Statistical error=1-7.	14.1	7.0
Lapi et al. (2007)	1.4 -17.6	-		$I_\gamma = 9.2\%$ E_γ=137.2 keV		^{nat}Cu(p,n)^{65}Zn flux determination uncertainty <5% using this monitor	no monitor cross-section mentioned, Lapi used IAEA library data	0.971	Beam flux=5; Target thickness=5; Detector efficiency=5; Statistical error=3.	8.3	3.0

Table 3.7, continued.

Authors	Proton beam energy range MeV	Used ^{186}W target abundance used by authors (%)	^{186}W Abundance adopted in this evaluation (%)	Gamma intensity used by authors $I\gamma$	Gamma intensity adopted in this evaluation $I\gamma$	Monitor cross-section (mb)	Recommended monitor cross-section (IAEA, 2017)	Total correction factor	Detailed uncertainties given by authors (%)	Systematic uncertainty used in the evaluation (%)	Statistical uncertainty (%)
Khandaker et al. (2008)	6.6 - 39.9	28.6	28.43 NUDAT 2.6 library	I_γ=9.47% E=137.15 keV	I_γ=9.47% E_γ=137.2keV NuDat2.6 (Baglin, 2003a)	^{27}Al(p,x)^{24}Na (1.66 mb at 41.5 MeV) and ^{nat}Cu(p,x)^{62}Zn (11.8 mb at 42 MeV) (IAEA-TECDOC-1211)	^{27}Al(p,x)^{24}Na (2.0 mb at 41.5 MeV) and ^{nat}Cu(p,x)^{62}Zn (12.6 mb at 42 MeV)	1.294	Monitor flux= 7.0 ; Counting Efficiency=4.0; Efficiency calibration=1.5; Statistical= 0.5-10.0.	8.2	10.0
Titarenko, Batyaev, et al. (2011)	40 MeV - 2.6GeV	-		-		^{27}Al(p,x)^{22}Na; 43.47 mb at 44.6 MeV	^{27}Al(p,x)^{22}Na 43.76 mb at 44.6 MeV	1.007	Not required to this experiment	-	-
Bonardi et al. (2011)	4.7 -21.6	-		I_γ=8.22% E_γ=137.2 keV		Faraday cup		0.868	Calibrated point sources ^{152}Eu,^{133}Ba, ^{226}Ra= 2, 3, 1.5; Integrated charge 1-2; Target thickness= 2; Statistical error <0.01.	4.4	1.0

3.4.3 Selection and Renormalization of $^{nat}W(d,x)^{186}Re$ and $^{186}W(d,2n)^{186}Re$ Reaction Cross-Sections

A total of nine earlier works are available in the EXFOR database for the production of ^{186}Re via the deuteron induced reactions on tungsten target (Duchemin et al., 2015; Ishioka et al., 2002; Khandaker et al., 2017; Manenti et al., 2014; Nakao et al., 2006; Nassiff & Münzel, 1973; Pement & Wolke, 1966; Tárkányi et al., 2003; Zhenlan et al., 1981). Among all the studies, (Pement & Wolke, 1966) experiment was done by irradiating enriched (97.2%) tungsten oxide powder ($^{186}WO_3$) with deuteron. Since no information on error was mentioned in their work and beta counting technique was used in the assessment of ^{186}Re yield, thus this data is excluded from this evaluation. Note that some old activation experiments with beta counting technique sometimes showed erroneous results. In the remaining studies, (d,2n) is the only contributing channel for ^{186}Re production within our energy region of interest (Duchemin et al., 2015; Ishioka et al., 2002), thus $^{186}W(d,2n)^{186}Re$ cross-sections were extracted and renormalized for 100% abundance, when required, using the ^{186}W isotopic abundance adopted in this evaluation (28.43%) taken from the Berglund and Wieser (2009) work.

Several authors (Duchemin et al., 2015; Ishioka et al., 2002; Khandaker et al., 2017; Manenti et al., 2014; Nakao et al., 2006; Tárkányi et al., 2003) measured excitation functions for the $^{nat}W(d,x)^{186}Re$ reactions by deuteron irradiations on natural tungsten target via stacked-foil activation technique combined with gamma-ray spectrometry. All of the authors used the 137.2 keV gamma line to assess the radioactivity of ^{186}Re, but the intensity of this gamma line adopted by some of them show little differences from (See in Table 3.8) the latest decay data of (E_γ=137.2 keV, I_γ=9.47%) (Baglin, 2003a). Hence, the reported data were corrected using the updated intensity of 137.2 keV gamma-line. Moreover, Ishioka et al. (2002) data were corrected following the differences in their adopted monitor cross-sections $^{65}Cu(d,2n)^{65}Zn$ (31.8 mb at 35.0 MeV) (Fulmer &

Williams, 1970) with the recent data (45.2 mb at 35.0 MeV) available in the EXFOR database for the same reaction (Takács et al., 2001). Likewise, we corrected (Duchemin et al., 2015) results for $^{nat}Ti(d,x)^{48}V$ cross-section, where Duchemin et al. used 93.0 mb at 34.0 MeV (Tarkanyi et al., 2001) in their calculation which shows little difference with the latest value taken from the IAEA library as 92.5 mb at 34.0 MeV (IAEA, 2017). In Khandaker et al., (2017) experiment, the $^{27}Al(d,x)^{24}Al$ and $^{nat}Ti(d,x)^{48}V$ reactions were employed to monitor the deuteron beam intensity by adopting the latest cross-sections (32.0 mb at 37.5 MeV) and (78.0 mb at 38.0 MeV), respectively recommended by IAEA. On the other hand, Manenti et al., (2014) and Tárkányi et al., (2003) utilized faraday cup to monitor the deuteron beams intensities, therefore no scope to do any correction of their data. Several uncertainties were mentioned in their original publications related to $^{nat}W(d,x)^{186}Re$ cross-sections, these uncertainties were used to construct the corresponding correlation matrices. Uncertainties and other details including energy ranges, gamma-ray intensity, ^{186}W abundance etc. adopted by each author are listed in Table 3.8.

Nassiff & Münzel (1973), Zhenlan et al. (1981) irradiated isotopically enriched ^{186}Re target with 16.0 MeV deuteron beam, and measured excitation functions via the conventional stacked foil technique. Majority of experimental information are absent in Zhenlan et al. experiment, therefore the data are used without any correction. Nassiff and Münzel used $^{27}Al(d,\alpha p)^{24}Na$ reaction to determine the beam intensity, and adopted 26.8 mb at 17.2 MeV as the monitor cross-section taken from (Martens & Zyklotron-Laboratorium, 1969). However, it shows little difference with the IAEA recommended cross-sections of 25.4 mb at 17.2 MeV, and the data were corrected. Three scattered cross-section values appeared in Nassiff and Münzel's work were excluded from this evaluation. Figure 3.18 shows all experimental cross-sections of (d,2n) reaction without any correction and Figure 3.19 after correction; the red circled points are excluded from

Nassiff and Münzel work. More details about their experiment including uncertainties are listed in Table 3.8.

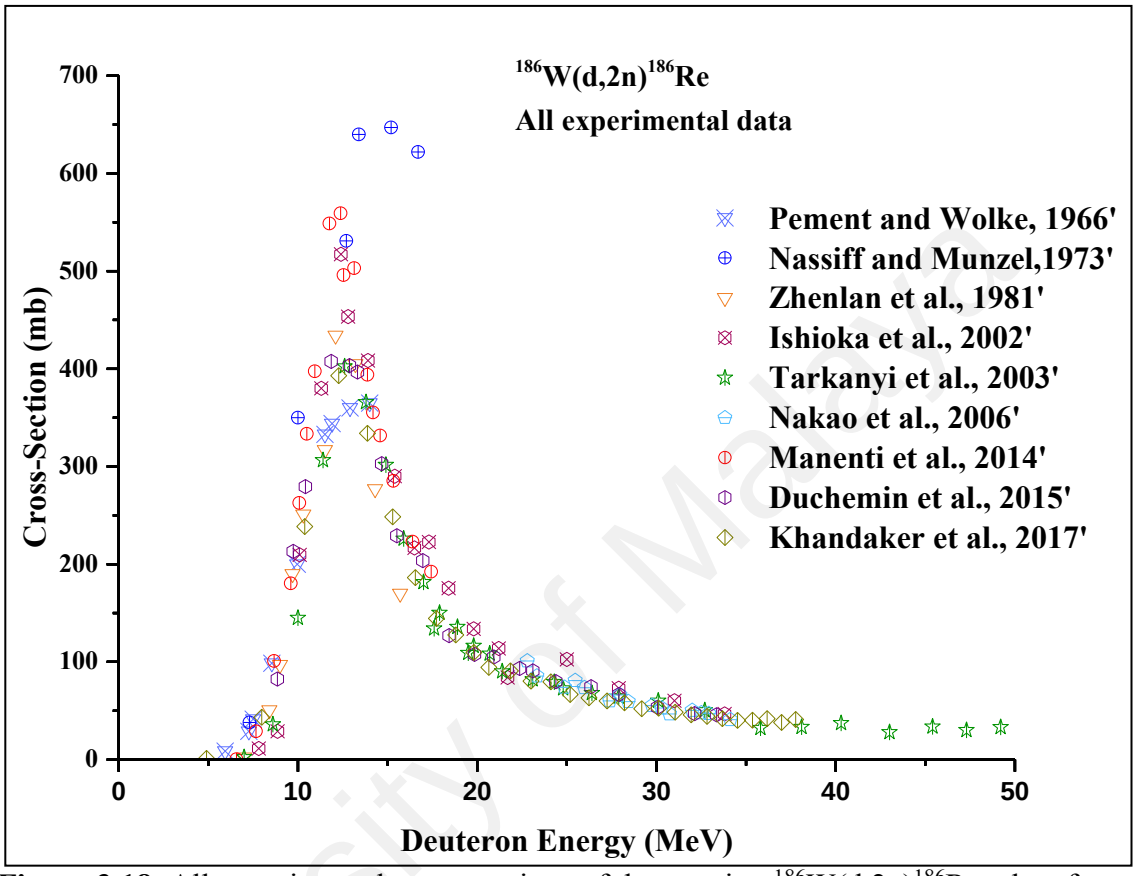

Figure 3.18: All experimental cross-sections of the reaction ^{186}W(d,2n)^{186}Re taken from the EXFOR library without any correction.

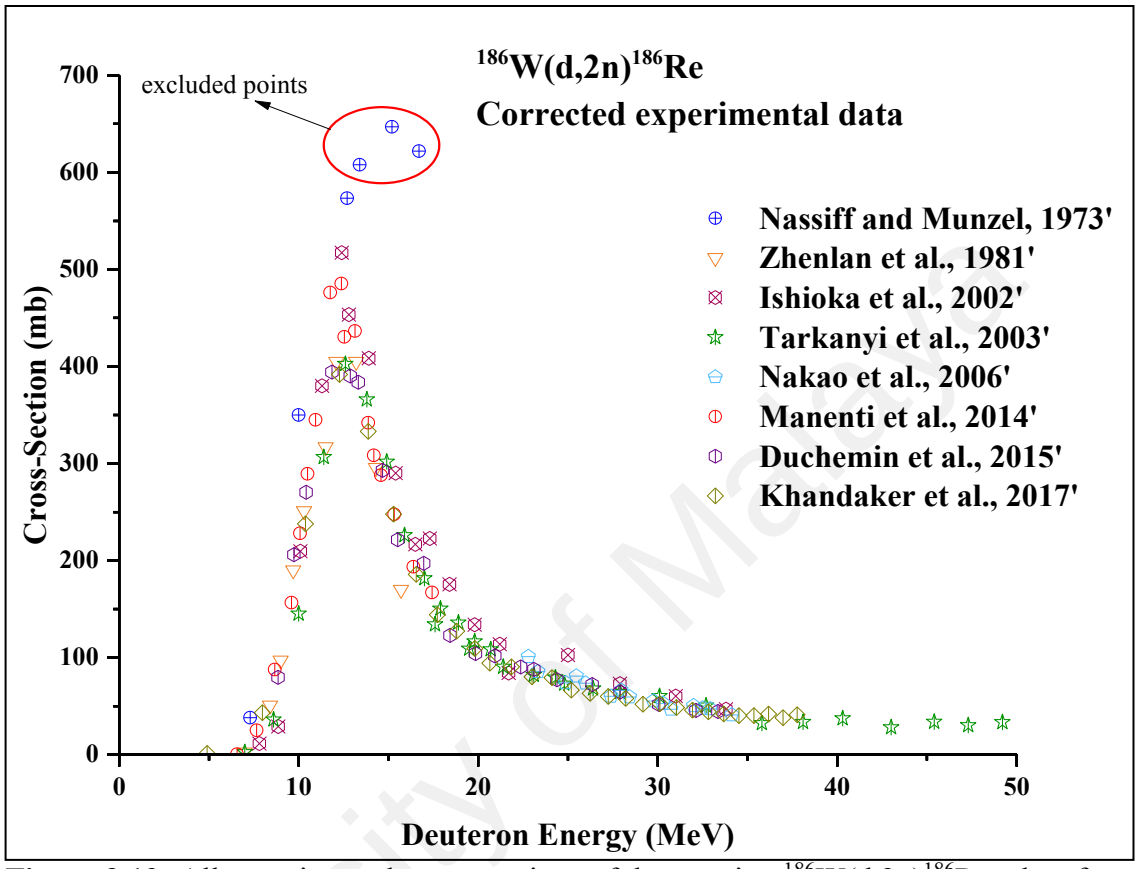

Figure 3.19: All experimental cross-sections of the reaction $^{186}W(d,2n)^{186}Re$ taken from the EXFOR library after correction.

Table 3.8: A brief information on the selected experiments for $^{nat,186}W(d,2n)^{186}Re$ reactions used in this evaluation.

Authors	**Deuteron beam energy range MeV**	**^{186}W Target abundance used by authors (%)**	**^{186}W Abundance adopted in this evaluation (%)**	**Gamma intensity used by authors $I\gamma$**	**Gamma intensity adopted in this evaluation $I\gamma$**	**Monitor cross-section (mb)**	**Recommended monitor cross-section**	**Total correction factor**	**Detailed uncertainties given by authors (%)**	**Systematic uncertainty used in the evaluation (%)**	**Statistical uncertainty (%)**
Nassiff & Münzel (1973)	7.3 - 16.2	^{186}W Enriched target	28.43 NUDAT 2.6 library	$I_\gamma = 9.2\%$ at E_γ=137.2 KeV (Schmorak, 1974)	I_γ=9.47% at E_γ=137.2 KeV NUDAT 2.6 (Baglin, 2003a)	Al(d,αp)24Na 26.82 mb at 17.2 MeV (Martens & Zyklotron-Laboratorium, 1969)	$^{27}Al(d,x)^{24}Na$ 25.43 mb at 17.2 MeV (IAEA, 2017)	0.921	Total error= 20.0; reported as total error; Assumed to be (10 systematic and 17.3 statistical)	10	17.3

Table 3.8, continued.

Authors	**Deuteron beam energy range MeV**	**^{186}W Target abundance used by authors (%)**	**^{186}W Abundance adopted in this evaluation (%)**	**Gamma intensity used by authors $I\gamma$**	**Gamma intensity adopted in this evaluation $I\gamma$**	**Monitor cross-section (mb)**	**Recommended monitor cross-section**	**Total correction factor**	**Detailed uncertainties given by authors (%)**	**Systematic uncertainty used in the evaluation (%)**	**Statistical uncertainty (%)**
Zhenlan et al. (1981)	7.0 - 15.7	^{186}W Enriched target used	28.43 NUDAT 2.6 library	-	I_γ=9.47% at E_γ=137.2 KeV NUDAT 2.6 (Baglin, 2003a)	-	-	-	Detector efficiency=4; Integration beam=5; Targets uniformity =2; Statistical uncertainty= 4.0-7.61.	6.7	4.0-7.6

Table 3.8, continued.

Authors	Deuteron beam energy range MeV	^{186}W Target abundance used by authors (%)	^{186}W Abundance adopted in this evaluation (%)	Gamma intensity used by authors $I\gamma$	Gamma intensity adopted in this evaluation $I\gamma$	Monitor cross-section (mb)	Recommended monitor cross-section	Total correction factor	Detailed uncertainties given by authors (%)	Systematic uncertainty used in the evaluation (%)	Statistical uncertainty (%)
Ishioka et al. (2002)	7.8 - 34.0	-	28.43 NUDAT 2.6 library		I_γ=9.47% at E_γ=137.2 KeV NUDAT 2.6 (Baglin, 2003a)	^{65}Cu(d,2n)^{65}Zn; 31.84 mb at 35 MeV (Fulmer & Williams, 1970)	^{65}Cu(d,2n)^{65}Zn; 45.2 mb at 35 MeV (Takács et al., 2001)	1.420	Counting efficiency=3; Target thickness=3; Statistical uncertainty= 22-49.	4.2	22.1 - 49.7

Table 3.8, continued.

Authors	Deuteron beam energy range MeV	^{186}W Target abundance used by authors (%)	^{186}W Abundance adopted in this evaluation (%)	Gamma intensity used by authors $I\gamma$	Gamma intensity adopted in this evaluation $I\gamma$	Monitor cross-section (mb)	Recommended monitor cross-section	Total correction factor	Detailed uncertainties given by authors (%)	Systematic uncertainty used in the evaluation (%)	Statistical uncertainty (%)
Tárkányi et al. (2003)	7.0 - 50.0	28.6	28.43 NUDAT 2.6 library	$I_\gamma = 9.42\%$ E_γ=137.16 keV (Tárkányi et al., 2003)	I_γ=9.47% at E_γ=137.2 KeV NUDAT 2.6 (Baglin, 2003a)	Faraday cup ^{nat}Al(d,x)^{22,24}Na ^{nat}Ti(d,x)^{48}V ^{nat}Fe(d,x)^{56}Co		1.001	Beam current=7; Number of target nuclei=5; Number of the produced nuclei =1–15	8.6	15.0
Nakao et al. (2006)	22.0 - 35.0	28.43		$I_\gamma = 9.2\%$ E_γ=137.2 keV[(a)]		^{nat}Cu(d,x)^{65}Zn; 44.92 mb at 35 MeV (Takács et al., 2001)	^{nat}Cu(d,x)^{65}Zn; 44.92 mb at 35 MeV (Takács et al., 2001)	0.972	Total error 10.0 - 20.0; Statistical ~13.3; From EXFOR	~14.9	~13.3

Table 3.8, continued.

Authors	**Deuteron beam energy range MeV**	**^{186}W Target abundance used by authors (%)**	**^{186}W Abundance adopted in this evaluation (%)**	**Gamma intensity used by authors $I\gamma$**	**Gamma intensity adopted in this evaluation $I\gamma$**	**Monitor cross-section (mb)**	**Recommended monitor cross-section**	**Total correction factor**	**Detailed uncertainties given by authors (%)**	**Systematic uncertainty used in the evaluation (%)**	**Statistical uncertainty (%)**
Manenti et al. (2014)	6.0 - 18.0	28.6	28.43 NUDAT 2.6 library	$I_\gamma = 8.22\%$ E_γ=137.15 keV (Firestone et al., 1998)	I_γ=9.47% at E_γ=137.2 KeV NUDAT 2.6 (Baglin, 2003a)	Faraday cup		0.873	Target thickness=2; Integrated charge= 2; Calibration sources= 2; Detector efficiency=1; Overall relative error = 4.5	3.6	4.5

Table 3.8, continued.

Authors	Deuteron beam energy range MeV	^{186}W Target abundance used by authors (%)	^{186}W Abundance adopted in this evaluation (%)	Gamma intensity used by authors $I\gamma$	Gamma intensity adopted in this evaluation $I\gamma$	Monitor cross-section (mb)	Recommended monitor cross-section	Total correction factor	Detailed uncertainties given by authors (%)	Systematic uncertainty used in the evaluation (%)	Statistical uncertainty (%)
C Duchemin et al. (2015)	8.0 - 43.0	28.6	28.43 NUDAT 2.6 library	I_γ = 9.2% E_γ=137.15 keV (C Duchemin et al., 2015)	I_γ=9.47% at E_γ=137.2 KeV NUDAT 2.6 (Baglin, 2003a)	^{nat}Ti(d,x)^{48}V; 93 mb at 34 MeV (Tarkanyi et al., 2001)	^{nat}Ti(d,x)^{48}V; 92.5 mb at 34 MeV (IAEA, 2017)	0.971	Target thickness=1 Measured activity 5-40 in W; Activity in ^{48}V=2	12.0[c] Taken from EXFOR	4.1
Mayeen Uddin; Khandaker et al. (2017)	4.9 - 37.8	28.6		I_γ = 9.47% E_γ=137.15 keV		^{nat}Ti(d,x)^{48}V 78 mb at 38 MeV; ^{27}Al(d,x)^{24}Na 32 mb at 37.5 MeV (Mayeen Uddin; Khandaker et al., 2017)	^{nat}Ti(d,x)^{48}V 78.3 mb at 38 MeV; ^{27}Al(d,x)^{24}Na; 31.8 mb at 37.5 MeV	0.997	Beam energy= 0.5; Target thickness =2.0; Counting statistics =0.23~23.27; Beam flux =5.0; Detector efficiency =4.0; Gamma Intensity =12.5;	13.3	27.3

CHAPTER 4: MATHEMATICAL FRAMEWORK

The mathematical techniques and methods employed to perform study were introduced in this chapter. Subsections included in this chapter are KALMAN filter, Least Squares approximation, Spline Fitting, a brief description for covariance matrices. The last section in this chapter discussed the EMPIRE and TALYS nuclear reaction model codes.

In other evaluation works, the Unified Monte Carlo approach (UMC) was used which basically amounts to apply Bayes Theorem along with the principle of Maximum Entropy, together with given prior and measured cross-sections and their covariance matrices as constants, to generate a posterior density function for the random variables that correspond to the evaluation (Smith, D., 2008).

4.1 KALMAN Filter

Simultaneous Evaluation of KALMAN (SOK) code is the main tool used in this work. SOK code comprise of several subroutines and functions written in FORTRAN language and compiled in LINUX Operating Systems (Kawano et al., 2000). Before running the code, several nuclear data need to be arranged into input files, these files should contain all experimental cross-sections in separated blocks, where each block represents the results of single experiment. Similarly, the uncertainties corresponded to these experimental cross-sections need to be included in separated blocks. Another set of input files contain one block of proposed cross-sections for the desired reaction covering the energy region of interest, large corresponding uncertainty (proposed) for this proposed cross-sections also required, and these files are mandatory to SOK code. An optional file can be prepared contains correlation matrices for experiments. This file helps the code to find a better uncertainty of estimated values.

KALMAN filter first proposed by Rudolf Emil Kalman (1930-2016) and named after him, common applications for this filter in our life include Global Positioning Systems (GPS), navigation systems, computer vision systems and signal processing (Li et al., 2015). It keeps track of the estimated state of the system and the variance or uncertainty of the estimate. The estimate is updated using a state transition model and measurements.

In the current study, SOK code employs the implemented KALMAN filter to get the closest estimation to the actual cross-section, this done by reducing the errors conjugated with its measurement. KALMAN filter is an iterative mathematical process that uses a set of equations and consecutive data input to estimate the true value of the object being measured, when the measured values contain unpredicted or random error, uncertainty or variation (Gibbs, 2011). This filter used when the variables of interest only can be measured indirectly or when measurements are available from various experiments with uncertainty exists.

In fact, this filter is an optimal estimator – regardless of all data follow the Gaussian or non-Gaussian distribution, it minimizes the mean square error of the estimated parameters. To perform this filtering three iterative steps need to be done again and again for the estimate to zoom in the actual correct value. Each time, KALMAN gain (*KG)* based on the measurement uncertainty E_M (See in Equation 4.1) need to be calculated. Secondly, calculation for the current estimation est_i given in Equation 4.2, and calculation of uncertainty in new estimation E_{est_i} given in Equation 4.3 calculate a new value compared to the estimate calculated in the second step. The estimated uncertainty and uncertainty of the measurement are required every time to calculate the KALMAN gain. Secondly, the KALMAN gain feeds in to the calculation of the current estimate. The adjustment to the previous estimate to come up with a new estimate depends on the gain and the measured data. The uncertainty in current estimate will be used in next

iteration loop to calculate new KALMAN gain (Shashank et al., 2013). Figure 4.1 summarise KALMAN filter in flow chart of single measured value. Following the repetition of these steps, the estimated error becomes smaller and the estimation itself becomes closer to the real value. As the iteration goes on, the estimated error becomes gradually smaller until the difference between two consecutive estimated errors becomes negligible. Regardless the pre-estimated value, quick convergence is guaranteed by setting up a high level of pre-estimated uncertainty (Bianchi & Tinnirello, 2003).

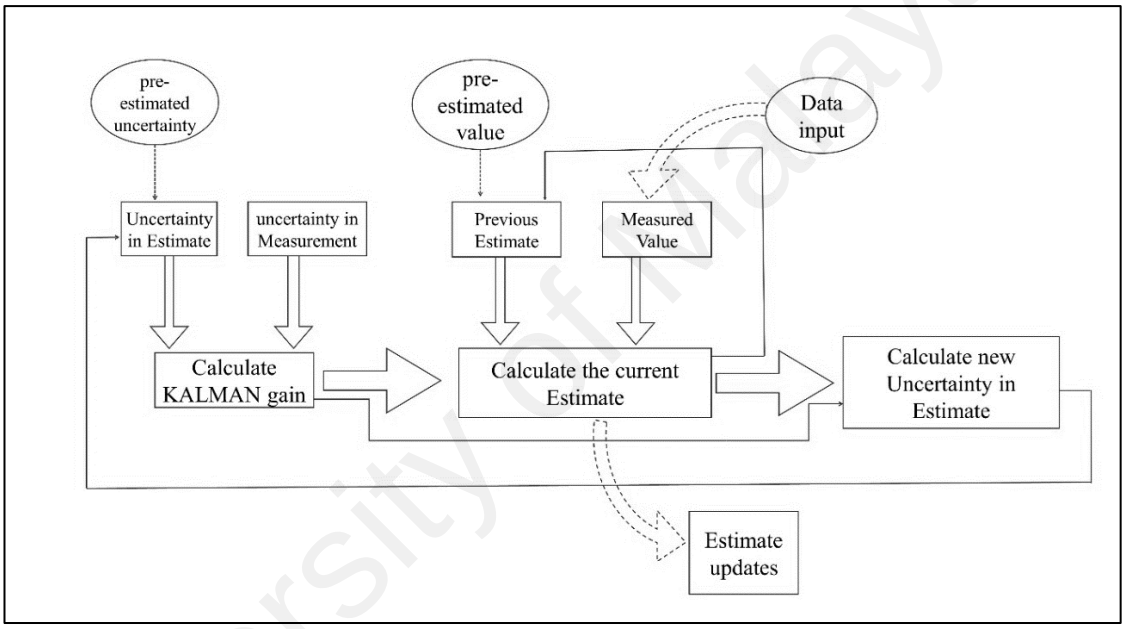

Figure 4.1: Flow chart for KALMAN filter calculation.

Equations 4.1, 4.2 and 4.3 represent KALMAN mathematical frame equations

$$KG = \frac{E_{est}}{E_{est} + E_M} \tag{4.1}$$

$$est_i = est_{i-1} + KG[M - est_{i-1}] \tag{4.2}$$

$$E_{est_i} = [1 - KG](E_{est_{i-1}}) \tag{4.3}$$

In Equations 4.1 and 4.2, KG stands for KALMAN Gain M represents the experimental measurement, est_i and E_{est} express the current estimate and the error in the current estimate, respectively. While est_{i-1} and E_{est_i} are the previous estimate and the error in the previous estimate, respectively. More details on KALMAN can be found

elsewhere (Gibbs, 2011; Zarchan & Musoff, 2013). It is important to mention that the accuracy of measurement plays the key role to secure the accuracy of the evaluated value. In principle, if the measurement is accurate enough then the KALMAN gain becomes close to unity and the new estimation becomes very close to the measured value. On the other hand, for an inaccurate measurement, the estimation of the measured value is stable since KALMAN gain is small and the updated estimation took only a little amount of delta part via the use of Equation 4.3.

4.2 Least Squares Approximations

Generalized Least Squares method (GLS) also included in SOK code. Unlike Ordinary Least Squares method (OLS), GLS is a method designed to solve the heteroscedasticity problem where the variances between values and the best fitted line are not constant. To do so, the experimental cross-sections were defined in the n-dimensional vector $\boldsymbol{y}$ Equation 4.4 and the evaluated cross-sections to be given in the matrix $\boldsymbol{x}$ Equation 4.5 with *m* elements. Note that n ≥ m+1 is required in order to find a unique least-squares solution.

$$\boldsymbol{y} = \begin{pmatrix} \sigma_{(\epsilon_1)} \\ \sigma_{(\epsilon_2)} \\ \vdots \\ \sigma_{(\epsilon_n)} \end{pmatrix} \tag{4.4}$$

$$\boldsymbol{x} = \begin{pmatrix} \boldsymbol{\sigma}_{(\boldsymbol{E_1})} \\ \boldsymbol{\sigma}_{(\boldsymbol{E_2})} \\ \vdots \\ \boldsymbol{\sigma}_{(\boldsymbol{E_m})} \end{pmatrix} \tag{4.5}$$

Where the relation between *x* and *y* given by the linear regression model in Equation 4.6:

$$\boldsymbol{y} = \boldsymbol{C}\boldsymbol{x} + \boldsymbol{e} \tag{4.6}$$

$$\boldsymbol{y} = \begin{pmatrix} \sigma_{(\epsilon_1)} \\ \sigma_{(\epsilon_2)} \\ \vdots \\ \sigma_{(\epsilon_n)} \end{pmatrix} = \begin{pmatrix} c_{11} & \cdots & c_{1m} \\ c_{21} & \cdots & c_{2m} \\ \vdots & & \vdots \\ c_{n1} & \cdots & c_{nm} \end{pmatrix} \begin{pmatrix} \boldsymbol{\sigma}_{(\boldsymbol{E_1})} \\ \boldsymbol{\sigma}_{(\boldsymbol{E_2})} \\ \vdots \\ \boldsymbol{\sigma}_{(\boldsymbol{E_m})} \end{pmatrix} + \begin{pmatrix} e_1 \\ e_2 \\ \vdots \\ e_n \end{pmatrix} \tag{4.7}$$

The vector $\boldsymbol{e}=\begin{pmatrix} e_1 \\ e_2 \\ \vdots \\ e_n \end{pmatrix}$ represents uncertainties, $\boldsymbol{C}=\begin{pmatrix} c_{11} & \cdots & c_{1m} \\ c_{21} & \cdots & c_{2m} \\ \vdots & & \vdots \\ c_{n1} & \cdots & c_{nm} \end{pmatrix}$ is the design matrix.

Generally, in this regression model the sum of the squares of the errors residuals can be defined as in Equation 4.8

$$\boldsymbol{S_r} = \sum_{i=1}^{n} \left(y_i - \sum_{j=0}^{m} x_j \, c_{ji} \right)^2 \tag{4.8}$$

To minimize this error, we need to derive $\boldsymbol{S_r}$ partially with respect to each of the coefficients and setting the resulting equation to zero (Equation 4.9)

$$\frac{\partial \boldsymbol{S_r}}{\partial c_{ij}} = 0 \tag{4.9}$$

The outcome of this process can be arranged in matrix as described in Equation 4.10

$$\left[[\boldsymbol{C}]^T [\boldsymbol{C}] \right] \{\boldsymbol{x}\} = \left\{ [\boldsymbol{C}]^t \{\boldsymbol{y}\} \right\} \tag{4.10}$$

From which the solution $\boldsymbol{x}$ given by Chapra & Canale (2015) and Leo (2012) (Equation 4.11)

$$\{\boldsymbol{x}\} = \left[[\boldsymbol{C}]^T [\boldsymbol{C}] \right]^{-1} \left\{ [\boldsymbol{C}]^t \{\boldsymbol{y}\} \right\} \tag{4.11}$$

Where the diagonal elements of the matrix $\left[[\boldsymbol{C}]^T [\boldsymbol{C}] \right]^{-1}$ are variances of $\boldsymbol{x}$'s, while the off-diagonal elements of $\left[[\boldsymbol{C}]^T [\boldsymbol{C}] \right]^{-1}$ are covariances of the *x*'s (Chapra & Canale, 2015; Draper & Smith, 2014; Leo, 2012).

And therefore, the covariance matrix given by Equation 4.12

$$\boldsymbol{V} = \begin{pmatrix} \sigma_1^2 & cov(x_1, x_2) & cov(x_1, x_3) \cdots \\ cov(x_2, x_1) & \sigma_2^2 & cov(x_2, x_3) \cdots \\ cov(x_3, x_1) & cov(x_3, x_2) & \sigma_3^2 \quad \cdots \\ \vdots & \vdots & \vdots \quad \ddots \end{pmatrix} \tag{4.12}$$

And its elements given by Equation 4.13 (Leo, 2012)

$$(V^{-1})_{i,j} = \frac{1}{2} * \frac{\partial^2 S}{\partial x_i \partial x_j} \tag{4.13}$$

In case of using the first order spline function, the elements of this design matrix $\boldsymbol{C}$ given by the rules c_{ij} Equation 4.14.

$$c_{ij} = \begin{cases} (\epsilon_i - E_{j-1})/(E_j - E_{j-1}); & E_{j-1} \leq \epsilon_i < E_j \\ (\epsilon_i - E_{j+1})/(E_j - E_{j+1}); & E_{j-1} \leq \epsilon_i < E_j \\ 0; & \text{Otherwise} \end{cases} \tag{4.14}$$

According to Kawano et al. (2000), least square solution $\hat{\boldsymbol{x}}$ in this case given by Equation 4.15

$$\hat{\boldsymbol{x}} = \boldsymbol{X C^t K^{-1} y} \tag{4.15}$$

Where $\boldsymbol{X}$ is the covariance of the evaluated cross-sections (Equation 4.16) and $\boldsymbol{K}$ is the covariance of the experimental data.

$$\boldsymbol{X} = (\boldsymbol{C^t K^{-1} C})^{-1} \tag{4.16}$$

4.3 Spline Interpolation Fitting

Since the experimental data are varied quickly in small intervals, fitting them with polynomial interpolation is useless. To avoid the over fitting problem associated with high order polynomial fitting, SOK code was designed to employ the spline functions for interpolation and fitting purposes. Splines gives more flexible curves for the data to be fitted. In principle, linear spline also called first-order spline connects points to be fitted

by straight lines between every two consecutive points, while the quadratic spline connects them by quadratic curves and gives smoother fitting curve.

4.3.1 Linear Spline Interpolation

Generally, the simplest spline type is the first-order splines and take the form of the straight lines connected together at interior knots. However, these line segments cover the data range need to be fitted and defined as a set of linear equations shown in (Equations 4.17-4.19 and 4.20)

$$f(x) = f(x_0) + m_0(x - x_0) \quad ; \; x_0 \le x \le x_1 \tag{4.17}$$

$$f(x) = f(x_1) + m_1(x - x_1) \quad ; \; x_1 \le x \le x_2 \tag{4.18}$$

$$\vdots$$

$$f(x) = f(x_{n-1}) + m_{n-1}(x - x_{n-1}) \; ; \; x_{n-1} \le x \le n \tag{4.19}$$

Where m_i is the slope of the straight line connecting the points:

$$m_i = \frac{f(x_{i+1}) - f(x_i)}{x_{i+1} - x_i} \tag{4.20}$$

For instance, consider the function f(x)=sin(x) where the function pass through x=[-3, -2, -1, 0, 1, 2, 3] (Figure 4.2). for such points [(-3,-0.14), (-2,-0.9), (-1,-0.8), (0,0), (1,0.8), (2,0.9), (3,0.14)], one can fit them using 1st order spline by defining straight lines connected together at the interior knots (Figure 4.3), and therefore for any x lies in fitted range an approximate value of the function at that x can be easily calculated by using the listed fitting equations. In order to get better fitting more knots are required, note that higher order of spline can fit data in better way as shown in the following subsection.

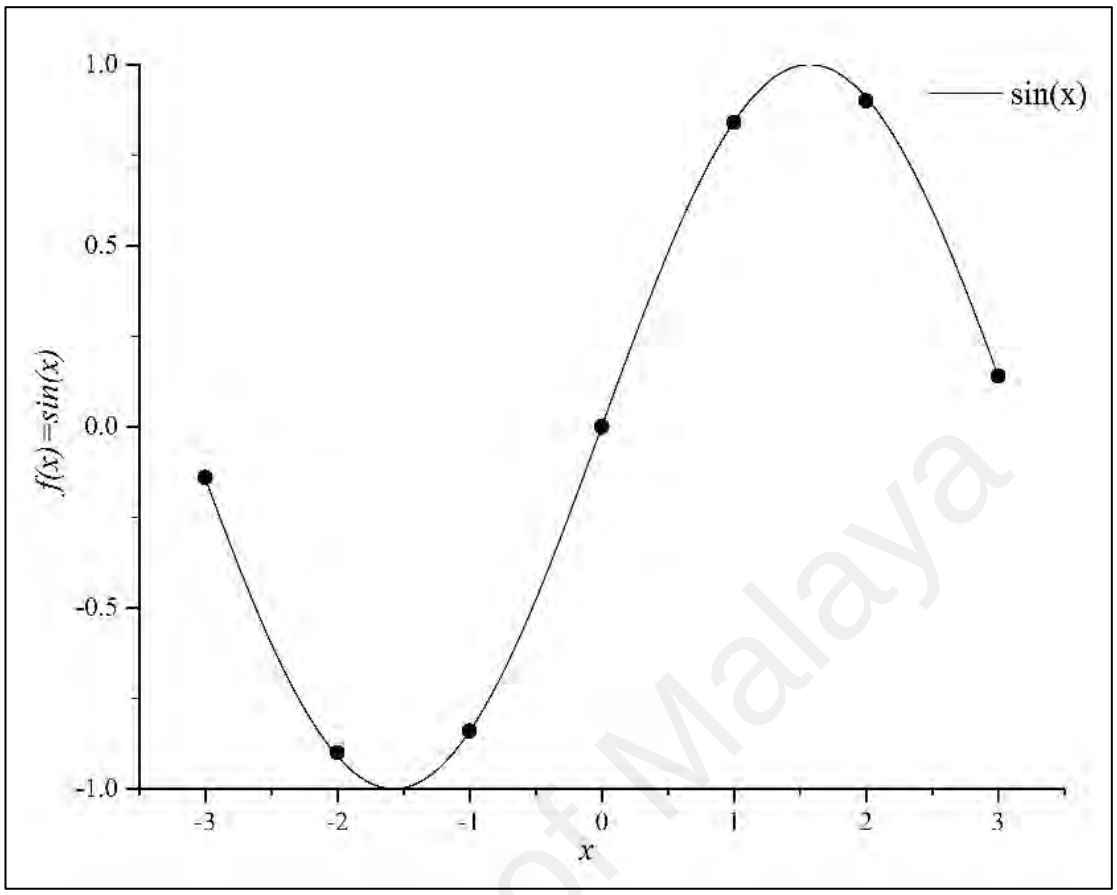

Figure 4.2: Sin(x) function.

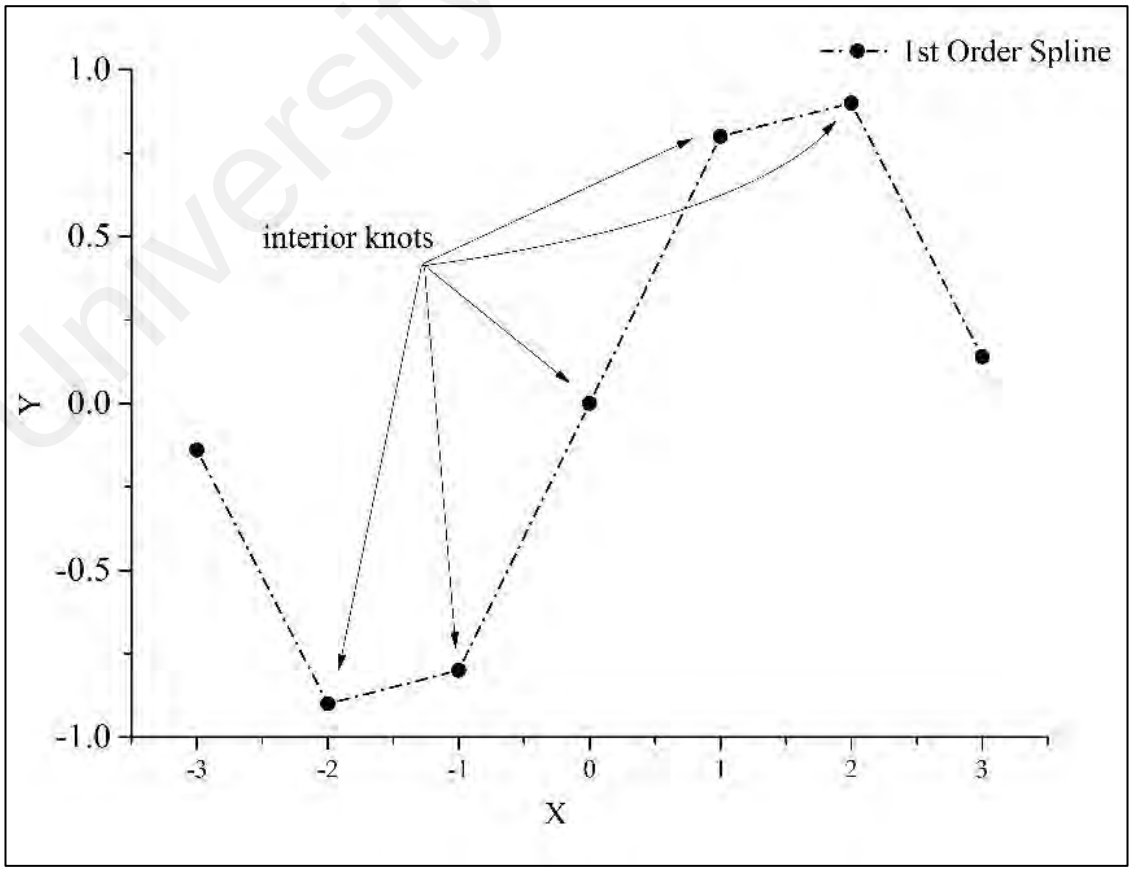

Figure 4.3: 1st order spline for selected points on the Sin(x) function.

4.3.2 2nd Order Spline

Due to its flexibility, 2nd Order Spline or Quadratic spline has more complicated form than linear spline form. In addition to the fact that connected spline functions are equal at interior knots, the first derivative of that functions are also equal at the interior knots in 2nd Order Spline. However, 2nd Order Spline takes the form shown in Equation 4.21

$$f(x) = \begin{cases} a_1x^2 + b_1x + c_1 & ;\ x_0 \le x \le x_1 \\ a_2x^2 + b_2x + c_2 & ;\ x_1 \le x \le x_2 \\ \vdots & \\ a_nx^2 + b_nx + c_n & ;\ x_{n-1} \le x \le n \end{cases} \tag{4.21}$$

Solving this type of equation requires certain conditions, these conditions are

1. Function values are equal at interior knots.
2. First and last functions pass through end points.
3. First derivatives are equal at interior knots.
4. Second derivative equal to zero at x_0 which sets $a_1 = 0$.

The polynomial for each interval can be represented generally as

$$f_i(x) = a_ix^2 + b_ix + c_i \tag{4.22}$$

For n + 1 data points (i= 0, 1, 2, . . . n), there are n intervals and, consequently, 3n unknown constants (the a's, b's, and c's) to evaluate. Therefore, 3n equations or conditions are required to evaluate the unknowns. These are:

1. The function values of adjacent polynomials must be equal at the interior knots. This condition can be represented as in Equations 4.23 and 4.24

$$f_i(x_{i-1}) = a_{i-1}x_{i-1}^2 + b_{i-1}x_{i-1} + c_{i-1} \tag{4.23}$$

$$f_i(x_{i-1}) = a_i x_{i-1}^2 + b_i x_{i-1} + c_i \quad (4.24)$$

for i = 2 to n. Because only interior knots are used, Equations 4.23 and 4.24 each provide

n-1 conditions for a total of 2n-2 conditions.

2. The first and last functions must pass through the end points. This adds two additional equations:

$$f_i(x_0) = a_1 x_0^2 + b_1 x_0 + c_1 \quad (4.25)$$

$$f_i(x_n) = a_n x_n^2 + b_n x_n + c_n \quad (4.26)$$

for a total of 2n-2+2=2n conditions.

3. The first derivatives at the interior knots must be equal. The first derivative of Equation 4.22 is

$$f'(x) = 2ax + b \quad (4.27)$$

Therefore, the condition can be represented generally as

$$2a_{i-1} x_{i-1} + b_{i-1} = 2a_i x_{i-1} + b_i \quad (4.28)$$

for i=2 to n. This provides another n-1 conditions for a total of 2n + n-1 = 3n-1. Because we have 3n unknowns, we are one condition short.

Unless we have some additional information regarding the functions or their derivatives, we must make an arbitrary choice to successfully compute the constants. Although there are a number of different choices that can be made, we select the following:

4. Assume that the second derivative is zero at the first point. Because the second derivative of Equation 4.25 is $2a_i$, this condition can be expressed mathematically as

$$a_1 = 0 \tag{4.29}$$

Continuing with previous example quadratic spline gives better fitted line for the data listed (Figure 4.4) (Chapra & Canale, 2015). After applying all conditions, the result is a set of equations with same number of un-knowns. These unknowns can be presented in matrix and easily numerically solved by the subroutine embedded in the code. This subroutine works on the principle of LDU decomposition or as it known LDL^T factorization described in (Chapra & Canale, 2015; Schnabel & Eskow, 1999).

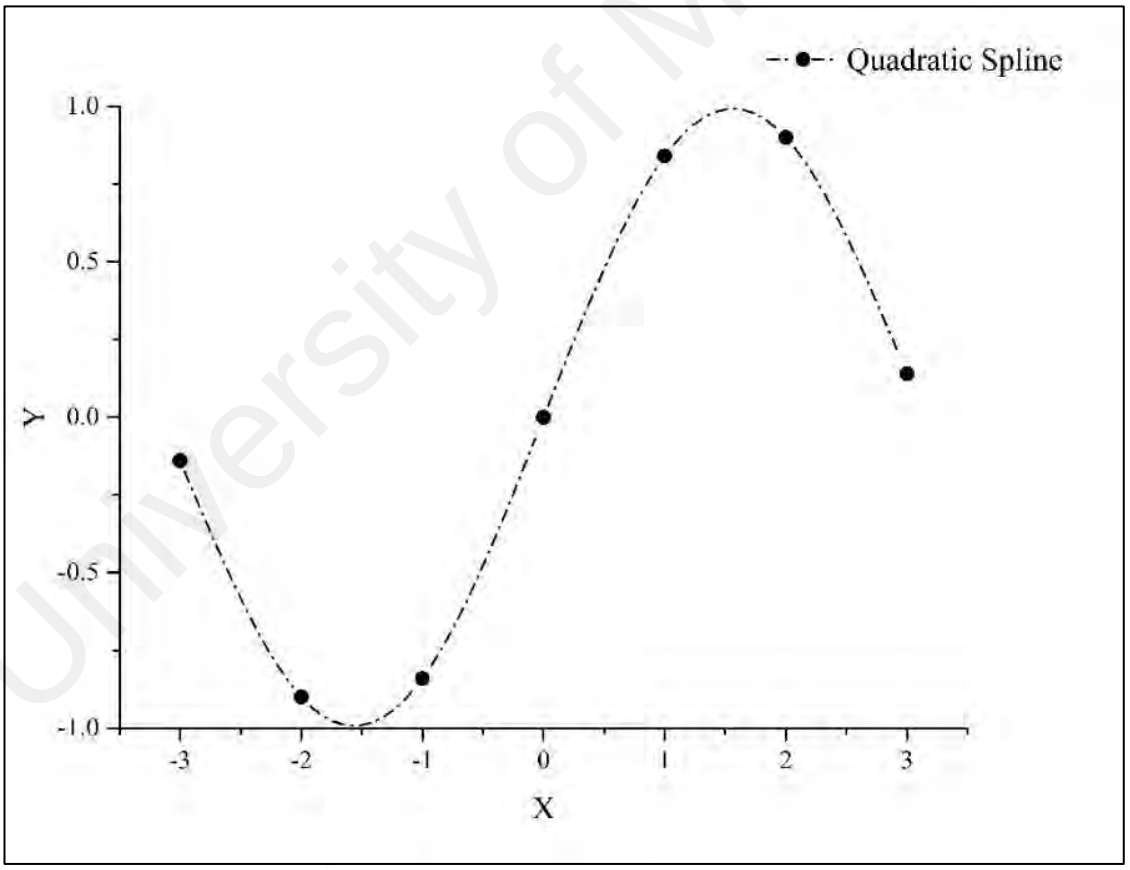

Figure 4.4: 2nd order spline for selected points on the Sin(x) function.

4.4 Variance and Covariance

The term 'Variance' is a measure of the variability or spread of data in one dataset. Mathematically, it is the average squared deviation from the mean value, and expressed by Equation 4.30

$$\text{Var. } (X) = \Sigma \, (X_i - X)^2 / N = \Sigma \, x_i^2 / N \tag{4.30}$$

Where, N is the number of data points in a dataset, X is the mean value of the N data point, Xi is the value of the i-th point data, xi is the deviation value of i-th point data from the mean value. On the other hand, 'Covariance' is a measure of the change of one particular element that is common to two sets of data, and can be computed by the Equation (4.31)

$$Cov. \, (X, \, Y) = \Sigma \, (X_i - X) \, (Y_j - Y) / N = \Sigma \, x_i y_j / N \tag{4.31}$$

Where, N is the number of data points in each set of data, X is the mean value of the first set of data, Xi is the value of the i-*th* point data in the first dataset, x_i is the deviation value of *i-th* point data from the mean value of the first dataset, Y is the mean value of the second set of data, Y_j is the value of the *j-th* point data in the second dataset, y_j is the deviation value of *j-th* point data from the mean value of the second dataset.

The obtained variance and covariance are often displayed together in a Covariance matrix. The variances appear along the diagonal and covariances appear in the off-diagonal elements, as shown in Equation 4.32:

$$\mathbf{V} = \begin{bmatrix} \Sigma \, x_1^2 / \mathrm{N} & \Sigma \, x_1 \, x_2 / \mathrm{N} & \ldots & \Sigma \, x_1 \, x_c / \mathrm{N} \\ \Sigma \, x_2 \, x_1 / \mathrm{N} & \Sigma \, x_2^2 / \mathrm{N} & \ldots & \Sigma \, x_2 \, x_c / \mathrm{N} \\ \ldots & \ldots & \ldots & \ldots \\ \Sigma \, x_c \, x_1 / \mathrm{N} & \Sigma \, x_c \, x_2 / \mathrm{N} & \ldots & \Sigma \, x_c^2 / \mathrm{N} \end{bmatrix} \tag{4.32}$$

Where, V is a $c \times c$ variance-covariance matrix, $\Sigma\, xi2 / N$ is the variance of elements from the *ith* data set, and $\Sigma\, xi\, xj / N$ is the covariance for elements from the *ith* and *jth* data sets. In order to understand the importance of covariance information in data evaluation procedure, we presented a simple example in Table 4.1 following the (Mannhart & Messreaktor, 1981) report.

Table 4.1: Uncertainty propagation via direct measurements and evaluation.

Gauge block length (mm)	**Variance for gauge length (mm^2)**	**Measured distance (mm)**	**Variance for measured distance (mm^2)**	**Final results (mm)**
$L_1 = 100 \pm 5$	5^2	$X_1 = L_1 - L_2 = 60$	5^2+2^2	$X_1 = 60 \pm 5.38$
$L_2 = 40 \pm 2$	2^2	$X_2 = L_1 + L_3 = 120$	5^2+1^2	$X_2 = 120 \pm 5.09$
$L_3 = 20 \pm 1$	1^2	$X_3 = L_2 + L_3 = 60$	2^2+1^2	$X_3 = 60 \pm 2.23$
		$X'_3 = X_2 - X_1 = 60$	$(5^2+1^2) + (5^2+2^2)$	$X'_3 = 60 \pm 7.40$
		Var. $(X'_3) = (5^2+2^2) + (5^2+1^2) - 2\times(5^2)$		$X'_3 = 60 \pm 2.23$

Table 4.1 shows a typical example of distance measurements by using three gauge block say L_1, L_2 and L_3. Here, the first three measurements (X_1, X_2 and X_3) are analogous to direct experimental results and the last process (X'_3) is analogous to the further data processing such as data evaluation. It can be observed that the gauge block L_1 made a common contribution in the final results of X_1 and X_2, while no contribution to X_3. On the other hand, one can reproduce the results of X_3 by using the final results of X_2 and X_1 via $X'_3=X_2-X_1$. It is interesting to mention that the standard deviation of X_3 and X'_3 is differing although the measured distance is same in both cases. This is because, the L_1 was a common parameter in calculations of X_1 and X_2, and the uncertainty of L_1 was propagated accordingly in X_1 and X_2. But when we calculate X_3, the common term L_1 was absent, thus the uncertainty (i.e., standard deviation) of X_3 is differing with X'_3. Such a difference could be resolved by introducing a term named 'covariance' (which is the common contributing term by the gauge L_1 in X_1 and X_2 measurements), and can be expressed as follows:

Var. (X'_3) = Var. (X_2) + Var. (X_1) - 2 Cov. (X_1, X_2)

Var. (X'_3) = (5^2+2^2) + (5^2+1^2) – 2×(5^2) = 2.23; which is same to the SD of (X_3)

i.e., SD (X'_3) = 2.23 = SD (X_3).

This example clearly shows that the information of covariance is important to ensure the accuracy of evaluated data.

To obtain the right uncertainty propagation in the final evaluated dataset, we have to avoid the common error from being taken into account more than one time. A practical example on how to construct correlation matrix is given in Table 4.2. Note that the data of (Wenrong et al., 1993) are used in constructing this correlation matrix presented herein. The reported cross-sections, corresponding systematic and statistical uncertainties are used to construct this matrix. The 'covariance' between any two energy points can be obtained by simply multiplying the systematic errors of the corresponding energy points. In practice, this 'covariance' goes to the off-diagonal position of the matrix after a further modification (i.e., by dividing with the total error of the representing energy points) which is then termed as 'correlation coefficient'. As for instance, correlation between the first two energy points (15.95, 16.23) in Table 4.2 can be calculated as follows: Correlation (15.95, 16.23) = Covariance (15.95, 16.23) / ((D-tot (15.95) × D-tot (16.23)) = 0.8951. Where, Covariance (15.95, 16.23) = D-sys (15.95) × D-sys (16.23) = 0.0569 × 0.1752 = 0.0099, and the Denominator D-tot (15.95) × D-tot (16.23) = 0.0602 × 0.1852 = 0.0111.

Table 4.2: A practical example on the construction of correlation matrix. The data of Wenrong et al. (1993) was used to construct this correlation matrix.

Energy / Energy	Sigma	Corrected Sigma	Syst. Err. (4.38%)	Stat. Err. (1.50%)	Total Err. (%)	15.95	16.23	16.78	17.31	17.83	18.36	18.86
MeV	mb	mb	mb	mb	mb							
15.95	1.3	1.299	0.056	0.019	0.060	1.000						
16.23	4	3.998	0.175	0.060	0.185	0.895	1.000					
16.78	13	12.995	0.569	0.194	0.601	0.895	0.895	1.000				
17.31	24	23.991	1.051	0.359	1.111	0.895	0.895	0.895	1.000			
17.83	24.4	24.391	1.068	0.365	1.129	0.895	0.895	0.895	0.895	1.000		
18.36	35.8	35.786	1.568	0.536	1.657	0.895	0.895	0.895	0.895	0.895	1.000	
18.86	39.2	39.185	1.717	0.587	1.814	0.895	0.895	0.895	0.895	0.895	0.895	1.000

However, it is possible to estimate covariance matrix of the evaluated data after solving the splines via the implementation of SOK code using the same equation for experimental data (Equation 4.32).

In fact, the diagonal elements represent the variance of cross-sections at the new proposed energy values x_i, and the off diagonal elements show the covariance between cross-sections at the new energy values x_i, x_j (Leo, 2012), which is the product of standard deviations of the evaluated cross-sections at the new energy values. Moreover, each element in the estimated covariance matrix implies how the two components in the data set (x_i, x_j) are related to each other. Covariance can take any value between -∞ to +∞. Similar to correlation, when the covariance sign is positive, it means that the elements are directly proportional to each other, while negative covariance value implies the elements are inversely related. However, if the covariance equals to zero, this means the two elements are independent.

4.5 EMPIRE and TALYS Nuclear Reaction Model Codes

EMPIRE is a modular system of nuclear reaction codes, comprising various nuclear models. In 1980, the first version of EMPIRE code was released, the Hauser-Feshbach theory and the classical HYBRID model were included in the code to account the pre-equilibrium effects, and the width fluctuation correction was implemented in terms of HRTW approach, henceforth, the code has been continuously developed.

The current version of EMPIRE-3.2.2 (Herman et al., 2007) was designed in two editions for Microsoft Windows operating system and Linux OS, furthermore, to simplify the dealing with both editions, EMPIRE can operated by Graphical User Interface shown in Figure 4.5. Such version makes use of several codes, written by different authors, which were converted into subroutines and adapted for the current version. However, the reaction cross-section calculation using EMPIRE code requires to prepare one input file

containing the primary reaction details such as projectile, ejectiles, target and the incident energy values. The code automatically construct the tables of involved nuclei and collect the required nuclear data for calculation from the included reference input parameters library.

The Reference Input Parameter Library (RIPL) covers nuclear masses and binding energies, optical model parameters, ground state deformations, shell corrections, discrete levels and decay schemes, level densities parameters, discrete and collective levels, fission barriers, and low energy observables (resonance spacing, γ-strength function).

Figure 4.7 shows the EMPIRE calculation steps flow chart. In the pre-equilibrium emission calculation step, usually not all of pre-equilibrium models available in EMPIRE are used. However, several calculations were done in pre-equilibrium step by different sub-codes

- Calculate double-differential cross-sections for inelastic scattering in terms of the MSD mechanism, populate residual nucleus continuum and discrete levels, store recoil spectra (first CN only).
- Calculate neutron, proton, γ, deuteron, triton, ^{3}H, and emission spectra in terms of the exciton model (code PCROSS), populate residual nuclei continuum and discrete levels (first CN only).
- Calculate neutron, proton, and emission spectra in terms of the HMS model (code DDHMS), populate residual nuclei continuum and discrete levels, store recoil spectra (first CN only).
- Calculate neutron, proton, and γ emission spectra in terms of the MSC mechanism, populate residual nuclei continuum and discrete levels (first CN only).

TALYS, is a software package for the simulation of nuclear reactions that developed at NRG Petten and CEA Bruyères-le-Châtel, and can easily be installed under Linux, UNIX, and Windows. TALYS can treats n, γ, p, d, t, h, and α as projectiles and ejectiles in the 1keV – 200 MeV incident energy range. TALYS incorporates modern nuclear models for the optical model, level densities, direct reactions, compound reactions, pre-equilibrium reactions, fission reactions, and a large nuclear structure database. It can calculates total and partial cross-sections, energy spectrum angular distributions, double-differential spectra, residual production cross-sections and recoils. Figure 4.7 shows the TALYS calculation steps together with a flow chart taken from "TALYS-1.8 user manual by Arjan Koning, Stephane Hilaire and Stephane Goriely p.42" Evaluation of nuclear data for the same selected reactions were also performed via widely used nuclear model code system TALYS (Koning & Rochman, 2012) and EMPIRE (Herman et al., 2007). These model code systems are designed for theoretical investigations of nuclear reactions as well as for nuclear data evaluation work. They can be used to simulate different nuclear reactions over a broad range of energies. Many state-of-the-art nuclear models are included in these code systems. As an example EMPIRE code accounts for the major nuclear reaction models such as optical model, coupled channel and DWBA, multi-step direct reaction (MSD), multi-step compound processes (MSC), exciton model, hybrid Monte Carlo simulation, and the full featured Hauser-Feshbach model including width fluctuations correction and many other models.

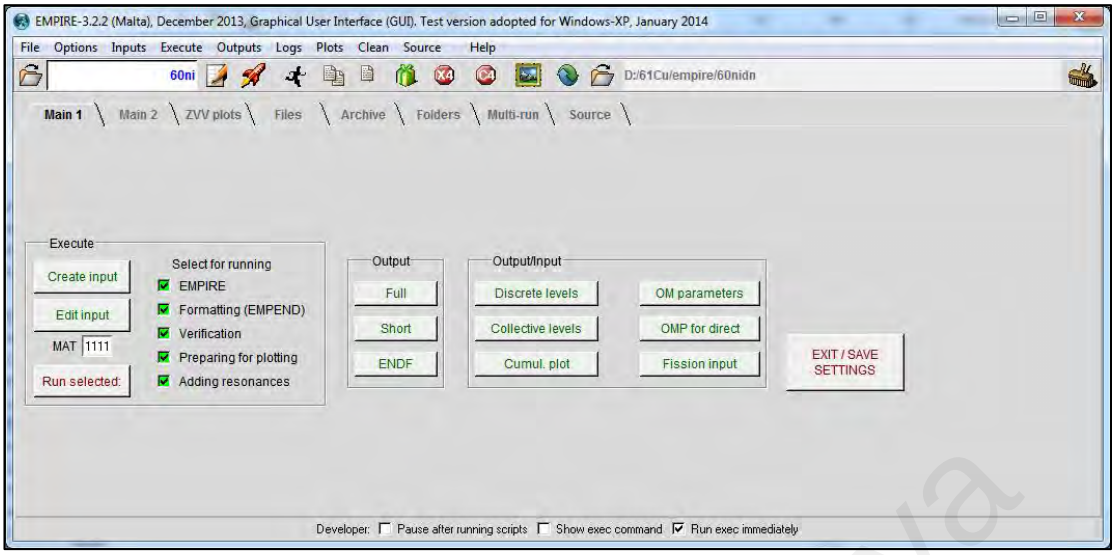

Figure 4.5: EMPIRE graphical user interface.

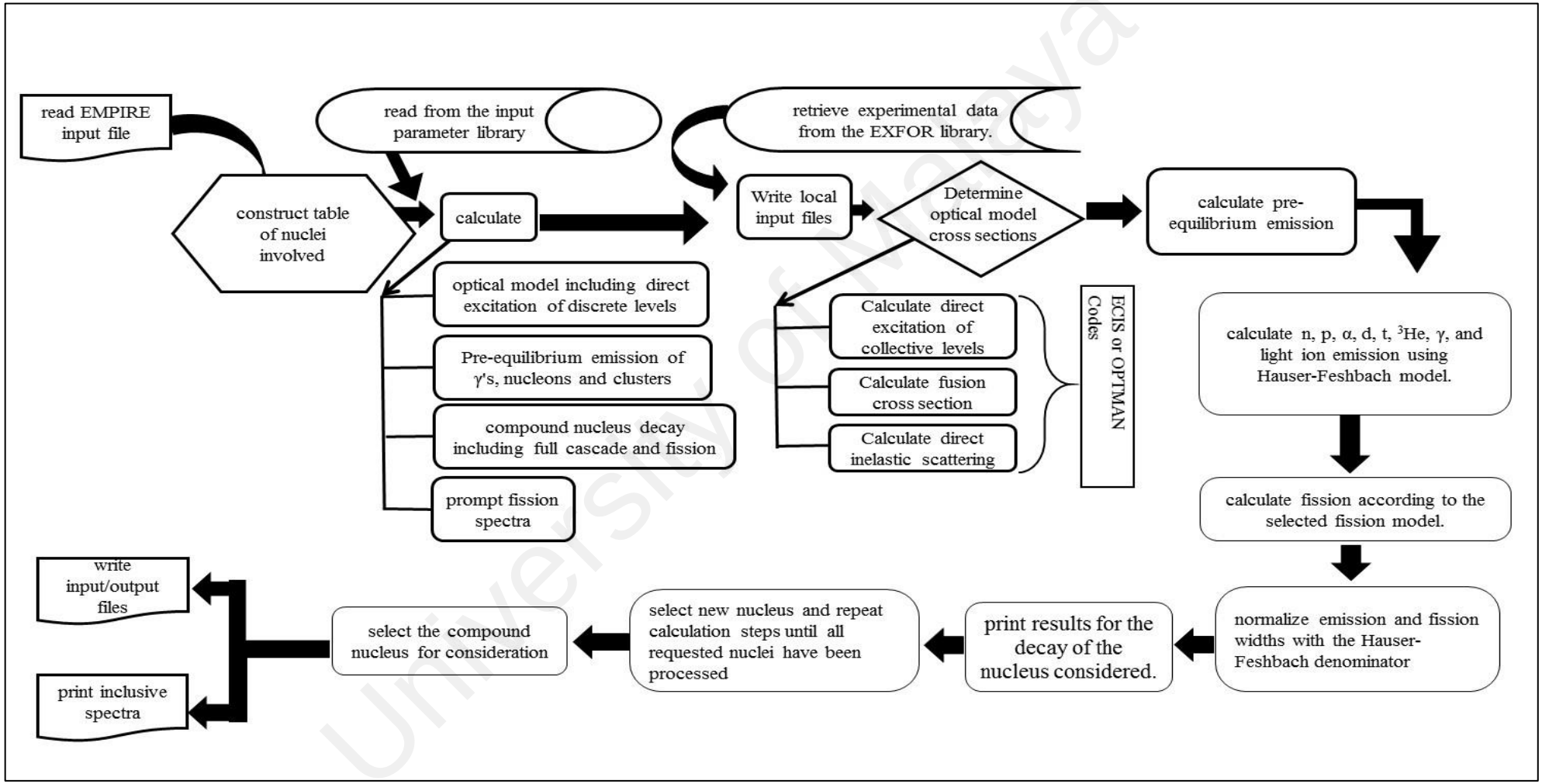

Figure 4.6: EMPIRE calculation steps flow chart.

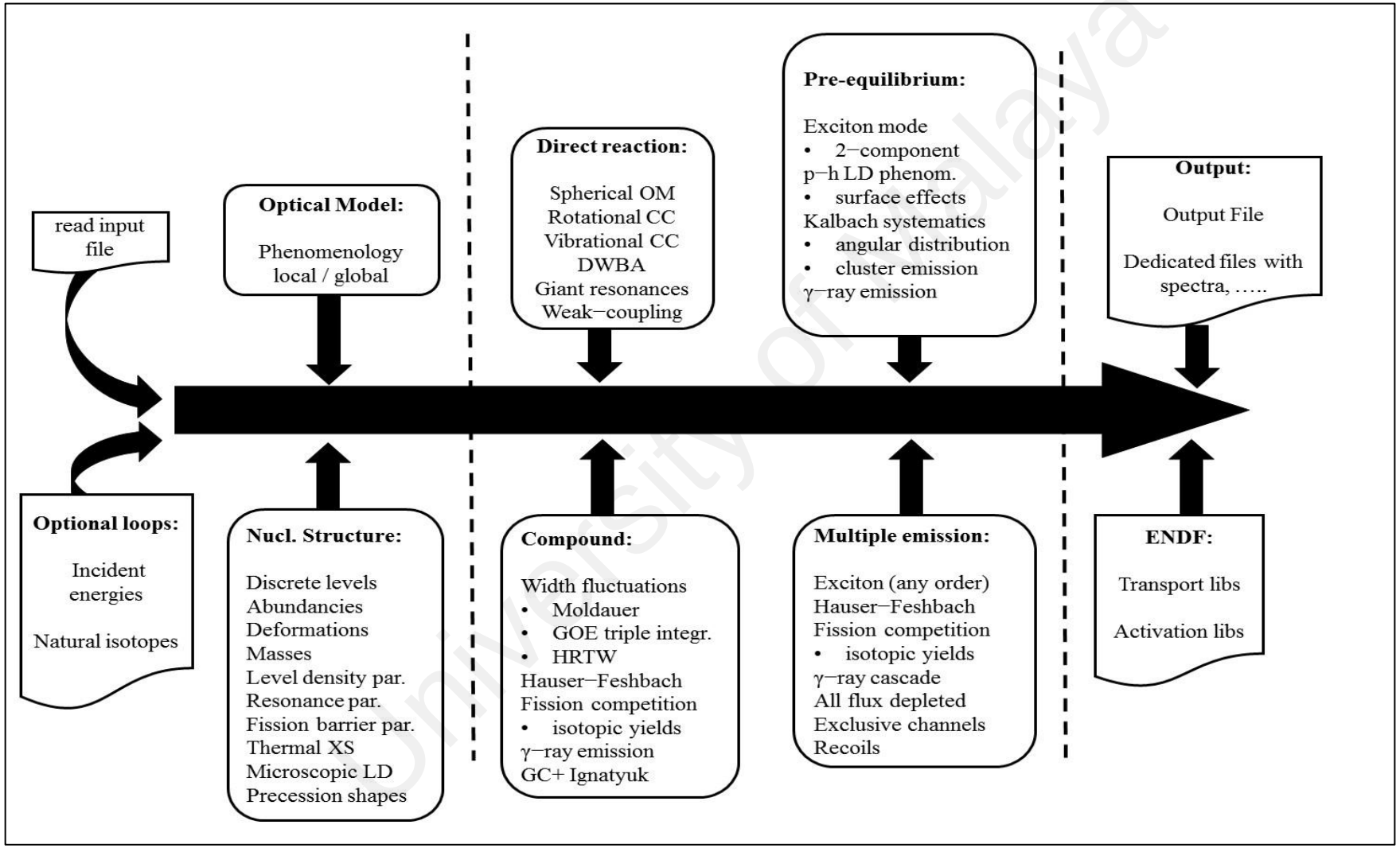

Figure 4.7: TALYS calculation steps flow chart.

For comparison purposes of the SOK code evaluated data, calculations of cross-sections for the reactions of interest were performed using the newest version of the EMPIRE code, which incorporates the newest reference input parameters library RIPL-3 (Capote et al., 2009). These calculations were made by using the default input parameters and taking into account all possible reactions, including emission of complex particles at the given bombarding energies.

For TALYS calculation, we used an online database called the TENDL library which provides the output of the TALYS nuclear model code system for direct use in both basic physics and applications. In the present case, the calculated data were extracted from the 9th version of the library TENDL-2017 (Koning et al., 2017), which is based on both default and adjusted TALYS calculations. In practice, these comparisons may help the developers of the above codes to further improve the theory behind these calculations.

CHAPTER 5: RESULTS AND DISCUSSION

Evaluation of nuclear data is largely practiced, especially in the evaluation of neutron induced reaction cross-sections due to its significance in safe operation of nuclear power plants or reactor dynamics applications. A number of nuclear reaction model codes and well established data evaluators are engaged to perform such evaluation.

However, during the last few decades numerous efforts have been devoted to study the nuclear reaction cross-sections for various purposes by using the available accelerator and reactor facilities worldwide. Among the different studies, neutron activation and charged-particles-induced reactions for production of medically and technologically important radionuclides received more attention to the scientific community. For the convenience of end user, the International Atomic Energy Agency (IAEA) developed an online database entitled EXFOR, where most of the published nuclear reactions data including reference materials, charts, tables etc. are updated and maintained in a timely manner. In brief, EXFOR is the EXchange FORmat for the transmission of experimental nuclear reaction data between national and international nuclear data centres for the benefit of nuclear data users in all countries (EXFOR, 2018). However, a careful observation on the archived cross-sections for a particular reaction in the EXFOR database often show a significant discrepancy among the different measurements even at the same energy region. Although it is very difficult to identify the real reason of discrepancy, but it is generally assumed that such discrepancy is attributed to many known/unknown sources of uncertainties such as monitor cross-sections, calibration sources, detector efficiency etc. However, a reliable and/or agreed set of data for a particular reaction can be obtained via a rigorous process called data evaluation. Thus, it is not feasible to use the raw data available in the EXFOR in practical applications (such as medical and industrial) without any pre-treatment or further processing. Beside this, an accurate form of nuclear reaction

cross-sections is important not only for optimization of production route of a particular radionuclide but also for a better understanding of nuclear reaction mechanisms and validation of different nuclear models.

This chapter talks about the evaluated cross-sections for each nuclear reaction previously selected in Chapter 3. However, plots for the reactions cross-sections including the present results are illustrated in this chapter, curves of cross-sections calculated by EMPIRE-3.2.2 and TALYS-1.8 nuclear reaction modelling code and plots for covariances were also included.

5.1 Evaluated Cross-Sections for $^{56}Fe(p,2n)^{55}Co$

The emission of high energy positrons and cascade γ-rays makes this radionuclide suitable for using in specific applications such as PET or SPECT. Due to its potential medical applications, production of ^{55}Co was studied by numerous authors (as mentioned in the Chapter 3) via charged-particle irradiations on metallic targets such as iron, nickel etc. Among the studied reactions in the literature, the $^{56}Fe(p,2n)^{55}Co$ reaction showed the most promising towards the no carrier added (NCA) production of ^{55}Co by cyclotron.

Although, a number of experimental investigations is available in the literature, a non-negligible discrepancy can be seen among the reported data (See in Figure 3.2). It is therefore important to understand the reason of discrepancies following the experimental parameters, decay data, monitor reactions etc, and produce an agreed set of evaluated data for this $^{56}Fe(p,2n)^{55}Co$ reaction.

A total of thirteen measurements on $^{56}Fe(p,2n)^{55}Co$ reaction cross-sections are available in the literature, and six measurements having obvious reasons were selected to perform the present evaluation. In addition, two experiments performed by Read (1968) and Remsberg & Miller (1963) were in the high energy region. So those experiments were

not considered in this evaluation. Figure 3.2 represents all reported measurements before renormalization within the energy range of 0–50 MeV. Note that, this energy range is important for NCA production ^{55}Co radionuclide. However, data reported by Zhuravlev et al. (1984) and Cohen & Newman (1955) was found to be very discrepant as compared to other experimental data, and hence discarded from this evaluation. Furthermore, experiments done by Michel et al. (1979) and Williams & Fulmer (1967) were excluded from this evaluation due to the unavailability of the sources of uncertainties in their article which restricts the construction of SOK code input file such as the correlation matrix. Reported data of other measurements were renormalized based on the latest agreed values of various parameters, and presented in Figure 3.3.

Although, the reported data by Kim et al. (2014) show clear discrepancy compared to the other selected and renormalized data, but no probable reason is mentioned in their original publication about this discrepancy. In principle, many known and unknown reasons are responsible for a discrepant result. As for instance, the ^{55}Co could be identified by using its intense 931.1 keV γ-line ($I\gamma$ = 75%) or relatively less intense 477.2 keV ($I\gamma$ = 20.2%) and 1408.5 keV ($I\gamma$ = 16.9%) γ-lines. The 931.1 keV γ-line has a high possibility to be interfered by the simultaneously produced ^{52}Mn radionuclide via the 935.5 keV γ-line. Contamination by ^{52}Fe via the 929.5 keV γ-line cannot also be neglected. The use of less intense 477.2 keV γ-line may overcome this contamination problem. However, use of the 477.2 keV γ-line may not provide enough good counting statistics if the relevant gamma-ray spectrum is acquired after a decay time of 35 hrs or longer. In such a situation, the deduced cross-sections show discrepant results. Since, it is not explicitly mentioned about which gamma-line was used in their measurement, therefore no particular correction was taken for this data set.

SOK code (Kawano et al., 2000) was then applied to the normalized datasets and their corresponding correlation matrices to obtain evaluated cross-sections of ^{55}Co radionuclide together with the covariance information. The evaluated cross-sections together with uncertainties are presented numerically in Table 5.1. Figure 5.1 presents the SOK evaluated curve for the ^{56}Fe(p,2n)^{55}Co reaction which shows agreement with the trend of the experimental cross-sections. EMPIRE model calculation for the ^{56}Fe(p,2n)^{55}Co reaction shows agreement with the evaluated cross-sections up to the energy of 30.0 MeV, in the energy range 30.0 to 40.0 MeV EMPIRE calculation clearly deviates toward zero. In TALYS model calculation, the calculated cross-sections shows higher values from 17.0 to 27.0 MeV while in the range 27.0 to 35.0 MeV shows lower values of cross-sections for the ^{56}Fe(p,2n)^{55}Co reaction. The generated covariance matrix is shown in Figure 5.2 . Covariance matrix was plotted using ZV-View tool developed by IAEA - NDS division (Zerkin, 2009)

Table 5.1: Evaluated cross-sections with uncertainties in the energy region of interest for the production ^{55}Co towards medical application.

Energy (MeV)	Cross-sections (mb)	Energy (MeV)	Cross-sections (mb)	Energy (MeV)	Cross-sections (mb)	Energy (MeV)	Cross-sections (mb)
15.00	00.10±0.05	21.50	54.62±7.31	28.00	52.32±0.94	34.50	26.15±6.89
15.50	03.15±0.12	22.00	56.26±0.37	28.50	50.61±3.58	35.00	24.37±0.72
16.00	06.29±0.03	22.50	57.53±1.19	29.00	48.78±23.1	35.50	22.72±7.22
16.50	13.33±0.35	23.00	58.44±3.77	29.50	46.85±0.29	36.00	21.22±7.66
17.00	19.78±0.32	23.50	59.02±0.75	30.00	44.83±0.36	36.50	19.89±7.58
17.50	25.67±0.77	24.00	59.28±0.22	30.50	42.75±0.43	37.00	18.75±7.29
18.00	31.01±0.21	24.50	59.25±3.17	31.00	40.62±0.87	37.50	17.82±6.47
18.50	35.81±0.97	25.00	58.93±4.23	31.50	38.48±0.71	38.00	17.12±0.86
19.00	40.11±0.22	25.50	58.36±0.21	32.00	36.32±0.53	38.50	16.66±1.89
19.50	43.92±2.74	26.00	57.55±0.21	32.50	34.18±3.62	39.00	16.47±0.47
20.00	47.25±1.88	26.50	56.53±2.21	33.00	32.07±2.16	39.50	16.47±7.01
20.50	50.13±0.63	27.00	55.30±2.77	33.50	30.02±3.49	40.00	16.47±7.28
21.00	52.58±5.72	27.50	53.89±3.02	34.00	28.04±3.71		

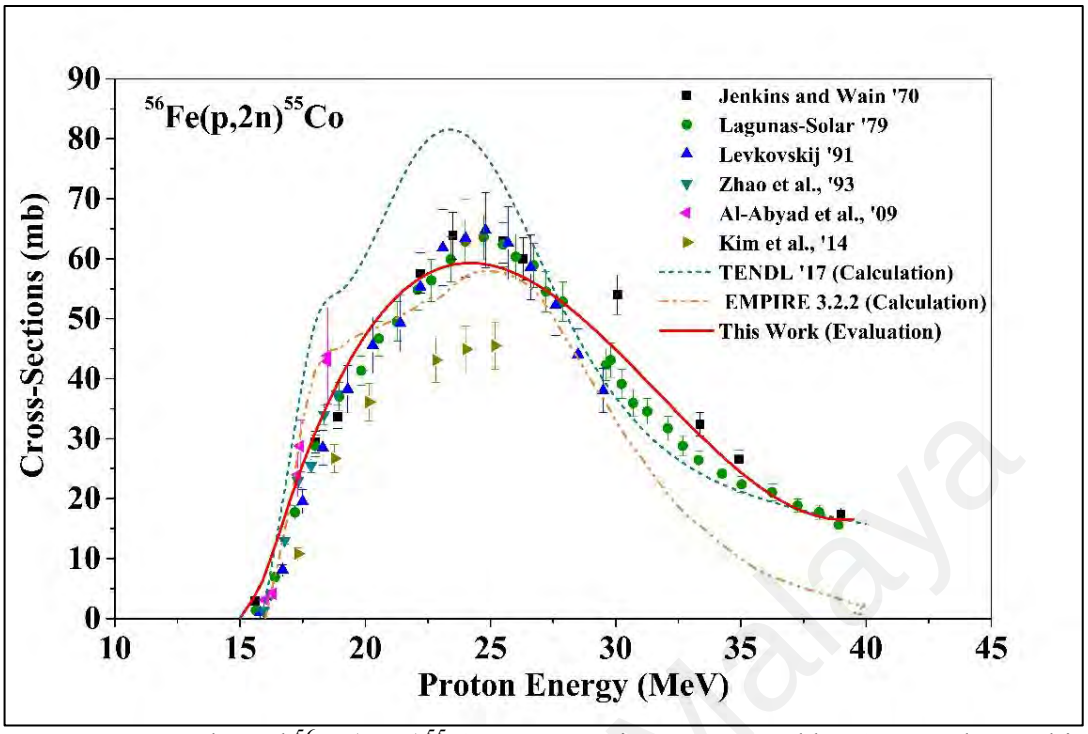

Figure 5.1: Evaluated ^{56}Fe(p,2n)^{55}Co cross-sections generated by SOK code combined with the least squares method.

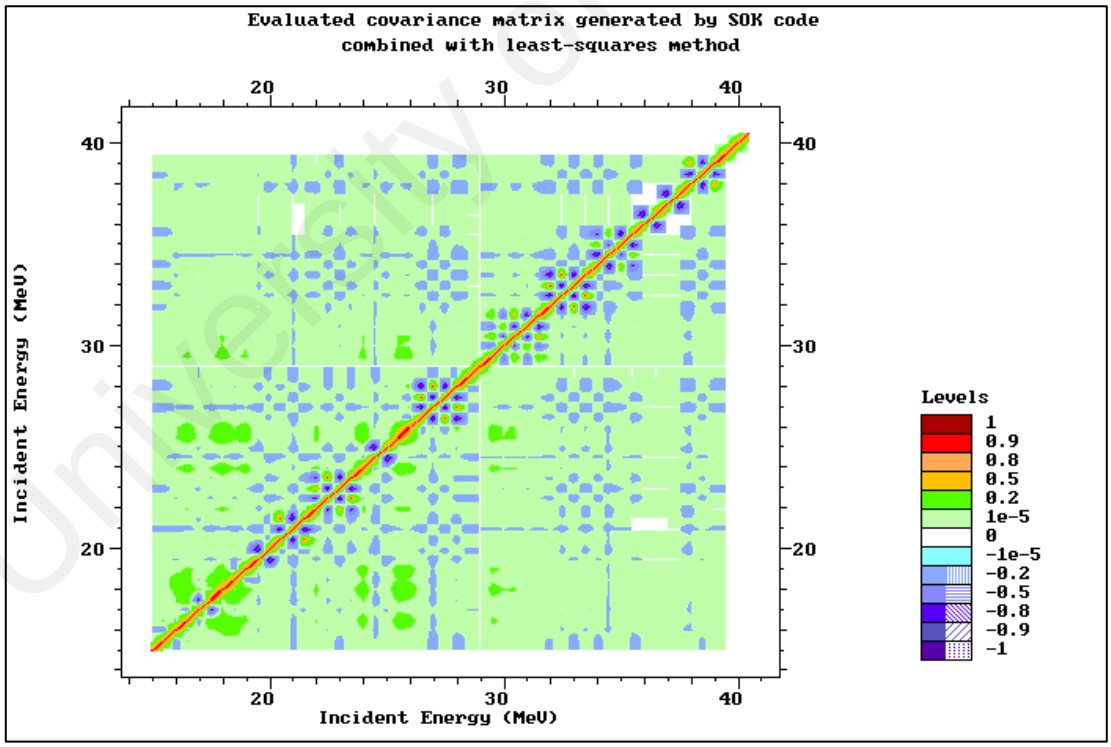

Figure 5.2: Evaluated covariance matrix generated by SOK code combined with least-squares method for ^{56}Fe(p,2n)^{55}Co reaction.

5.2 Evaluated Cross-Sections for ^{61}Cu Produced via Selected Routes

In Chapter 3 we have shown that several charged-particle-induced nuclear reactions on different targets lead to the production of ^{61}Cu in no carrier added form. Based on the detailed discussion in Chapter 3, the ^{58}Ni(α,p)^{61}Cu, ^{59}Co(α,2n)^{61}Cu, ^{60}Ni(d,n)^{61}Cu and ^{64}Zn(p,α)^{61}Cu reactions show promising for NCA production of ^{61}Cu, but the reported experimental cross-sections of these reactions by different authors contains higher order of discrepancy. It is thus important to evaluate those cross-sections and obtain an agreed set of data for each reaction. To reduce these discrepancies in the literature data, the KALMAN principle combined with least-squared method was applied. Evaluation procedure using KALMAN principle implemented in SOK code were described in details in Chapter 4. However, some salient features relevant to the present work is given as follows:

All experimental cross-sections for the selected ^{58}Ni(α,p)^{61}Cu, ^{59}Co(α,2n)^{61}Cu, ^{60}Ni(d,n)^{61}Cu and ^{64}Zn(p,α)^{61}Cu reactions were renormalized following the standard procedure (as mentioned in Chapter 3), and several input files such as experimental cross-sections, relevant uncertainties and correlation matrices were prepared for each experiment. Two more files were also prepared to be used as the input file in the SOK code: one is a proposed set of cross-sections and the other is the proposed uncertainty which normally contains a larger uncertainty corresponding to the proposed cross-sections. All of the prepared items are organized as input files in the working directory of SOK code, and then run the code using Linux platform. Since the systematic errors sources were differ from one experimental setup to another, discrepancies in results from different experimental setups that measure the same physical quantity provide a clue on ways to go beyond the lower limits imposed by each individual experiment, where the systematic uncertainties mark out the lower accuracy limit for particular experiment setup (Chadwick et al., 2005). The key role of SOK code is to find an estimated value with

uncertainty lower than the uncertainty of the original experimental value through principle of KALMAN filter. To find the best fitted line, SOK code applied the least squares method together with spline function on the evaluated data.

Tables 5.2, 5.3, 5.4, 5.5 show the numerical values of the evaluated cross-sections by SOK code for the reactions $^{59}Co(\alpha,2n)^{61}Cu$, $^{58}Ni(\alpha,p)^{61}Cu$, $^{60}Ni(d,n)^{61}Cu$ and $^{64}Zn(p,\alpha)^{61}Cu$, respectively. Figure 5.3, 5.5, 5.7 and 5.9 compare the evaluated cross-sections with the results of theoretical calculations by TALYS-1.8 and EMPIRE-3.2.2 nuclear model codes, while Figures 5.4, 5.6, 5.8 and 5.10 show the corresponding covariance matrices for the studied reactions for the reactions $^{59}Co(\alpha,2n)^{61}Cu$, $^{58}Ni(\alpha,p)^{61}Cu$, $^{60}Ni(d,n)^{61}Cu$ and $^{64}Zn(p,\alpha)^{61}Cu$, respectively.

Table 5.2: Evaluated $^{59}Co(\alpha,2n)^{61}Cu$ cross-sections generated by SOK code combined with the least squares method.

Energy (MeV)	Cross-Section (mb)	Energy (MeV)	Cross-Section (mb)	Energy (MeV)	Cross-Section (mb)	Energy (MeV)	Cross-Section (mb)
12.0	0.6 ± 0.1	23.0	335.6 ± 60.9	34.0	272.3 ± 14.6	45.0	61.8 ± 6.8
12.5	0.8 ± 0.1	23.5	357.6 ± 16.3	34.5	257.7 ± 9.7	45.5	57.3 ± 9.9
13.0	1.4 ± 0.1	24.0	376.8 ± 34.4	35.0	243.5 ± 29.4	46.0	53.1 ± 6.1
13.5	2.3 ± 0.3	24.5	393.1 ± 42.5	35.5	229.6 ± 24.3	46.5	49.3 ± 5.7
14.0	3.9 ± 0.7	25.0	406.3 ± 49.3	36.0	216.2 ± 20.2	47.0	45.7 ± 2.8
14.5	6.3 ± 1.2	25.5	416.3 ± 79.9	36.5	203.3 ± 17.5	47.5	42.3 ± 6.1
15.0	9.9 ± 1.9	26.0	423.2 ± 41.4	37.0	190.9 ± 14.8	48.0	39.2 ± 7.5
15.5	15.2 ± 3.0	26.5	427.0 ± 53.2	37.5	179.0 ± 15.3	48.5	36.3 ± 7.7
16.0	22.4 ± 4.2	27.0	427.9 ± 41.4	38.0	167.7 ± 33.1	49.0	33.6 ± 2.4
16.5	31.8 ± 2.7	27.5	426.2 ± 17.3	38.5	156.9 ± 15.2	49.5	31.2 ± 2.9
17.0	43.9 ± 10.4	28.0	422.0 ± 32.1	39.0	146.6 ± 18.3	50.0	28.9 ± 5.5
17.5	58.8 ± 3.8	28.5	415.6 ± 53.6	39.5	136.9 ± 5.1	50.5	26.7 ± 5.1
18.0	76.5 ± 10.8	29.0	407.3 ± 30.3	40.0	127.8 ± 8.3	51.0	24.7 ± 4.7
18.5	97.0 ± 14.1	29.5	397.4 ± 30.4	40.5	119.1 ± 13.3	52.0	21.2 ± 2.5
19.0	120.0 ± 4.4	30.0	386.0 ± 24.0	41.0	111.0 ± 20.8	53.0	18.2 ± 3.4
19.5	145.3 ± 20.2	30.5	373.6 ± 41.1	41.5	103.3 ± 10.3	54.0	15.6 ± 2.2
20.0	172.2 ± 16.6	31.0	360.2 ± 27.7	42.0	96.1 ± 11.2	55.0	13.3 ± 2.5
20.5	200.3 ± 22.8	31.5	346.2 ± 15.8	42.5	89.4 ± 7.1	56.0	11.4 ± 2.1
21.0	228.9 ± 25.8	32.0	331.7 ± 28.3	43.0	83.1 ± 11.8	57.0	9.8 ± 2.7
21.5	257.4 ± 34.9	32.5	316.9 ± 27.5	43.5	77.2 ± 7.9	58.0	8.4 ± 2.8
22.0	285.0 ± 51.9	33.0	302.0 ± 24.5	44.0	71.7 ± 10.1	59.0	7.2 ± 1.5
22.5	311.3 ± 36.8	33.5	287.0 ± 24.9	44.5	66.6 ± 4.7	60.0	6.2 ± 0.9

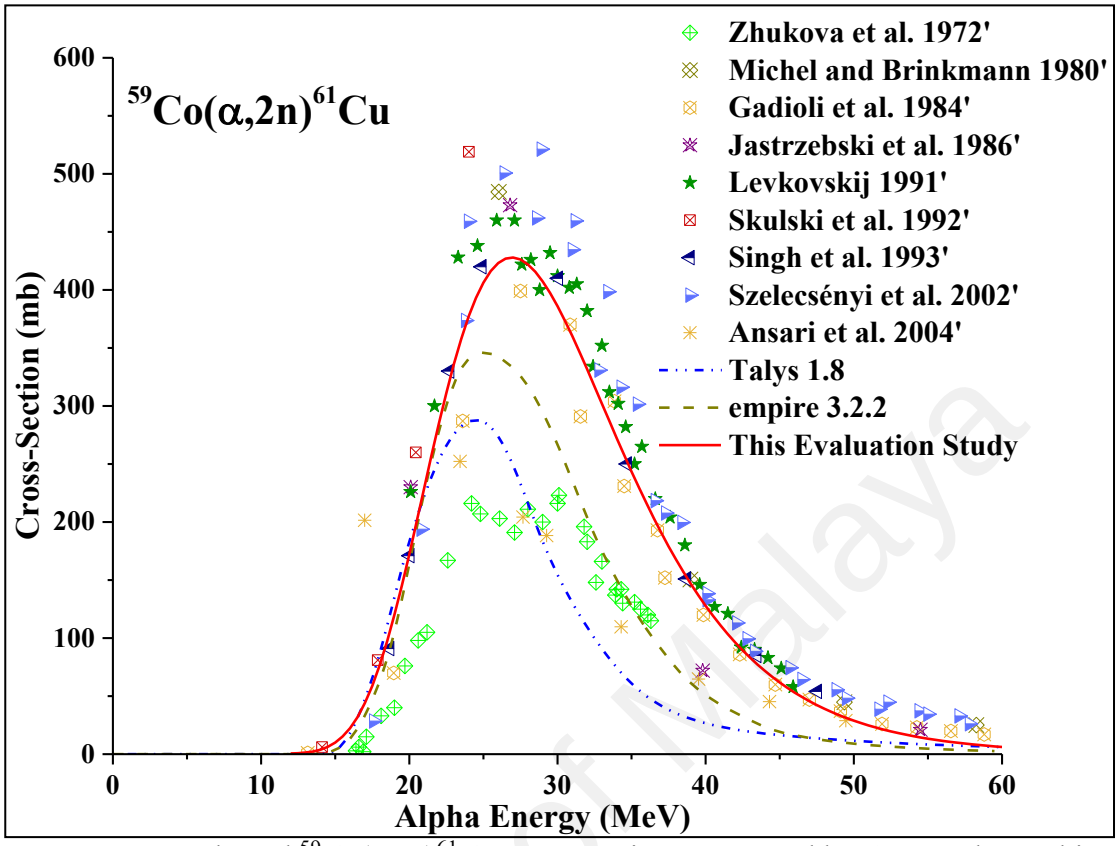

Figure 5.3: Evaluated ^{59}Co(α,2n)^{61}Cu cross-sections generated by SOK code combined with the least squares method.

Figure 5.3 shows that the SOK code evaluated data for the ^{59}Co(α,2n)^{61}Cu reaction is in agreement with the theoretical prediction by TALYS-1.8 and EMPIRE-3.2.2 codes for up to 22 MeV energy. At higher energy region (>22 MeV), both the model codes reproduced only the shape of the excitation function generated by the SOK code but with a slight energy shifting in the downward scale, and predicts a maximum value of about 40% and 20% lower, respectively, than the SOK code evaluated one. Moreover, the model codes prediction are also showing considerable discrepancies with most of the experimental data. The evaluated excitation function reveals that an energy window of 36→18 MeV is suitable to produce a considerable amount of ^{61}Cu via alpha-particle irradiation on monoisotopic ^{59}Co target material.

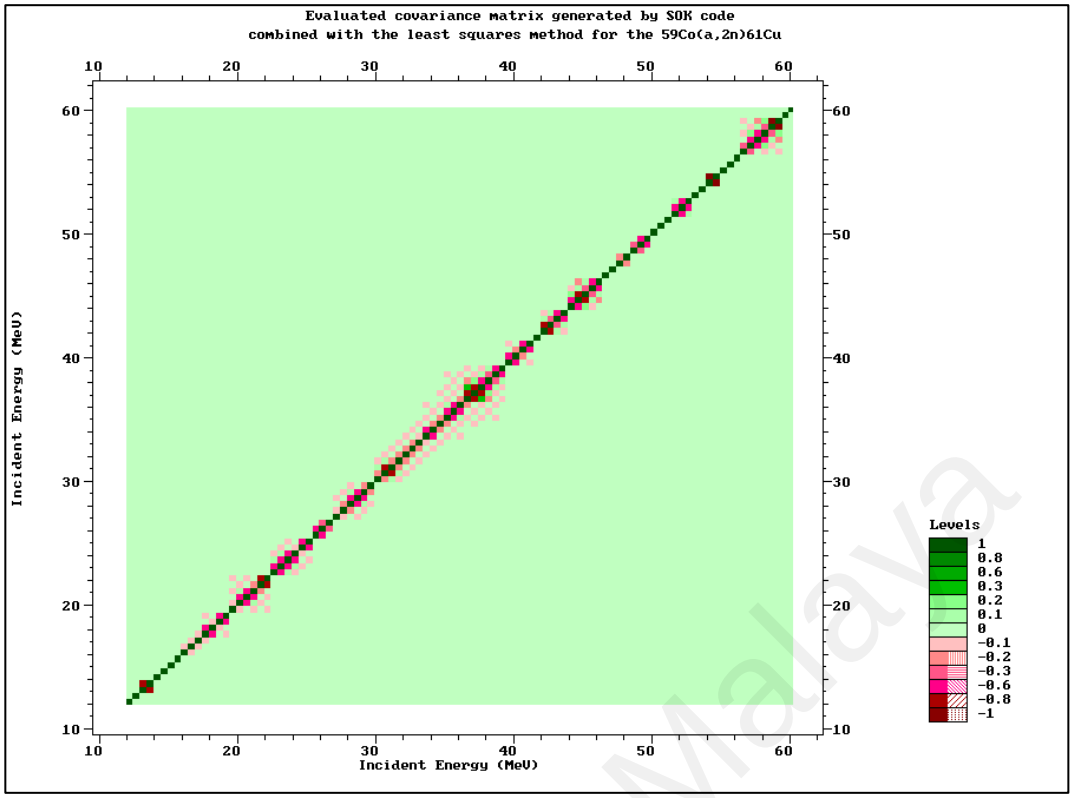

Figure 5.4: Evaluated covariance matrix generated by SOK code combined with the least squares method for the $^{59}Co(\alpha,2n)^{61}Cu$ reaction.

Table 5.3: Evaluated $^{58}Ni(\alpha,p)^{61}Cu$ cross-sections generated by SOK code combined with the least squares method.

Energy (MeV)	Cross-Section (mb)	Energy (MeV)	Cross-Section (mb)	Energy (MeV)	Cross-Section (mb)	Energy (MeV)	Cross-Section (mb)
2.0	0.2 ± 0.2	8.0	36.3 ± 12.2	14.0	525.6 ± 35.7	20.0	546.8 ± 63.3
2.5	0.2 ± 0.3	8.5	60.4 ± 15.6	14.5	563.2 ± 98.1	20.5	504.1 ± 74.3
3.0	1.4 ± 0.5	9.0	90.4 ± 19.5	15.0	596.3 ± 43.0	21.0	457.7 ± 30.4
3.5	2.6 ± 0.8	9.5	125.9 ± 24.2	15.5	623.9 ± 132.8	21.5	409.1 ± 15.2
4.0	3.9 ± 1.1	10.0	166.5 ± 22.2	16.0	645.3 ± 114.6	22.0	359.7 ± 19.3
4.5	5.1 ± 1.5	10.5	210.2 ± 12.1	16.5	659.8 ± 45.1	22.5	311.1 ± 34.7
5.0	6.3 ± 2.2	11.0	260.0 ± 7.7	17.0	666.8 ± 43.2	23.0	264.4 ± 28.7
5.5	7.5 ± 3.0	11.5	303.9 ± 22.1	17.5	666.0 ± 118.5	23.5	220.9 ± 44.3
6.0	8.7 ± 4.1	12.0	349.2 ± 57.8	18.0	657.2 ± 116.6	24.0	181.3 ± 38.4
6.5	9.9 ± 5.5	12.5	395.1 ± 66.0	18.5	640.4 ± 113.2	24.5	146.2 ± 8.4
7.0	11.1 ± 7.2	13.0	440.5 ± 83.4	19.0	615.9 ± 22.9	25.0	115.9 ± 7.8
7.5	17.9 ± 9.5	13.5	484.4 ± 38.2	19.5	584.4 ± 73.1		

Figure 5.5 exhibits a comparative scenario of the SOK code evaluated data for the $^{58}Ni(\alpha,p)^{61}Cu$ reaction together with the theoretical prediction by TALYS-1.8 and EMPIRE-3.2.2 codes in the energy region of 8-26 MeV. Although the status of $^{58}Ni(\alpha,p)^{61}Cu$ reaction cross-sections is rather poor but the evaluated excitation function by SOK code shows the representation of maximum number of experimental data points compared to the predicted excitation functions by TALYS-1.8 and EMPIRE-3.2.2 nuclear model codes. Both the model codes TALYS-1.8 and EMPIRE-3.2.2 respectively underestimate and overestimate the peak energy region of the SOK code evaluated excitation function. The evaluated excitation function indicates that a relatively good amount of ^{61}Cu can be produced using an energy window of 24→10 MeV via an alpha-particle irradiation on enriched ^{58}Ni target material.

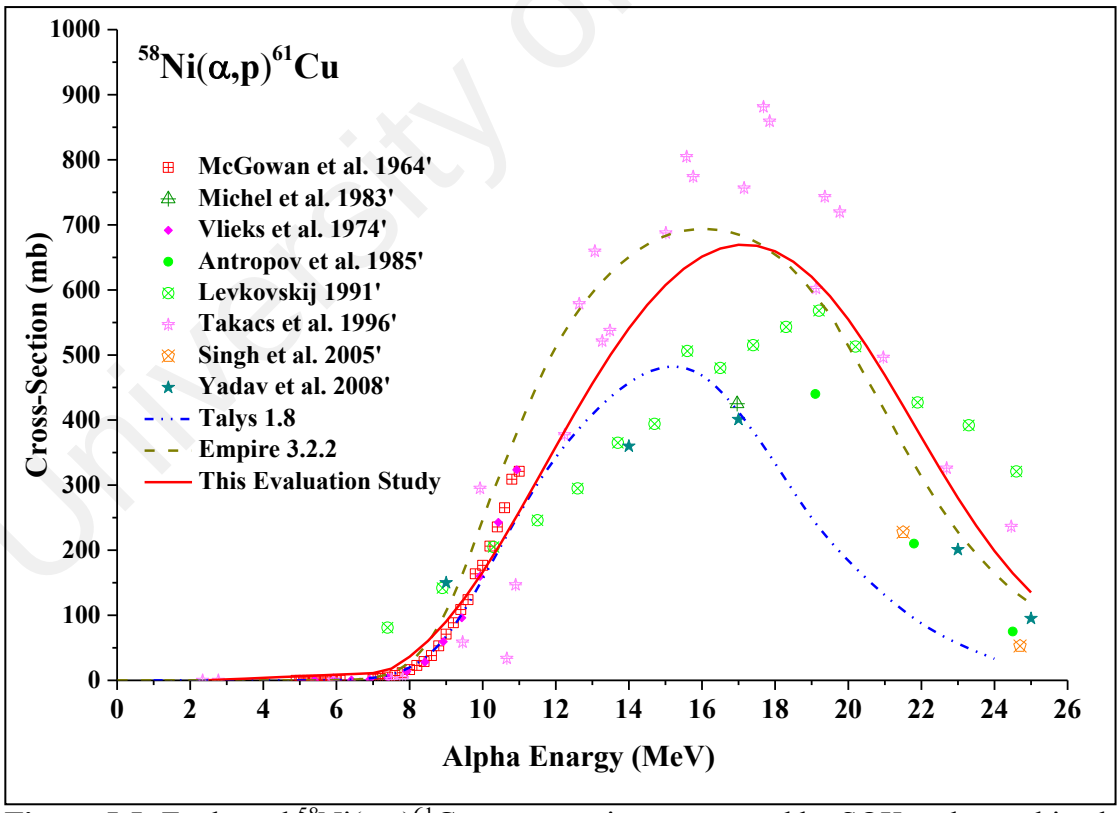

Figure 5.5: Evaluated $^{58}Ni(\alpha,p)^{61}Cu$ cross-sections generated by SOK code combined with the least squares method.

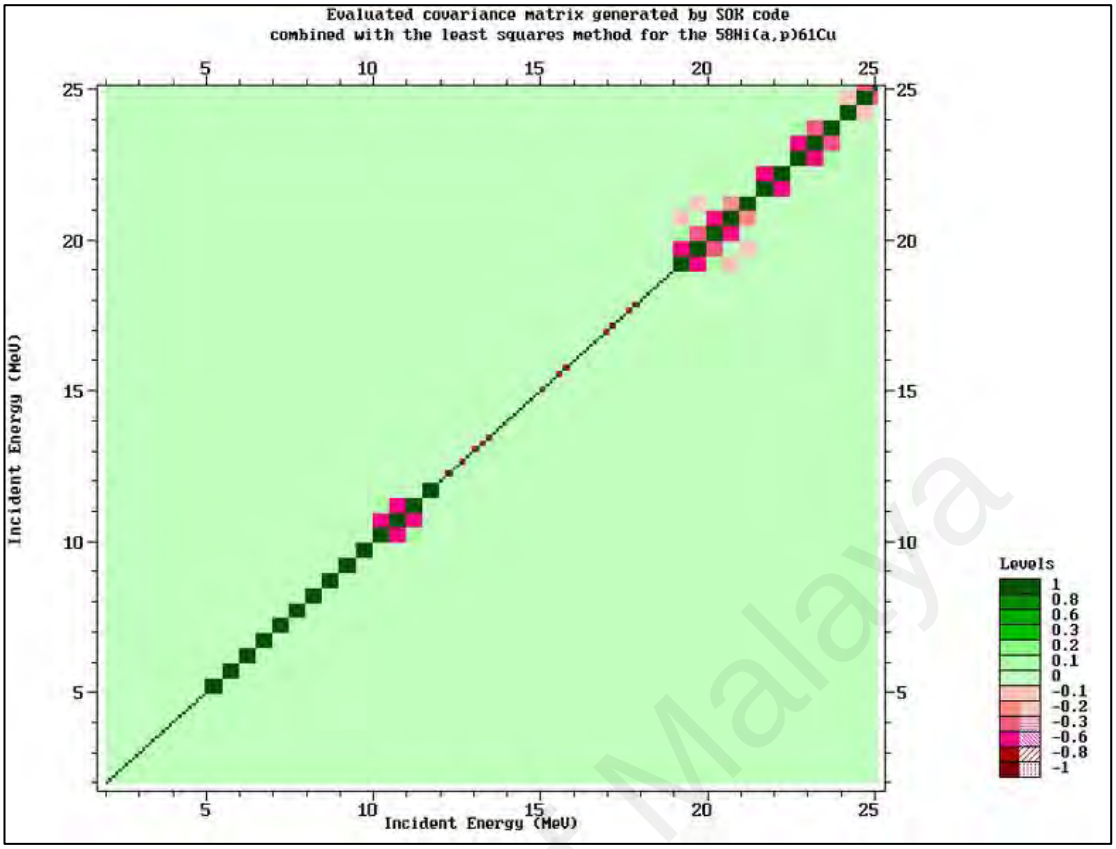

Figure 5.6: Evaluated covariance matrix generated by SOK code combined with the least squares method for the $^{58}Ni(\alpha,p)^{61}Cu$ reaction.

Table 5.4: Evaluated $^{60}Ni(d,n)^{61}Cu$ cross-sections generated by SOK code combined with the least squares method.

Energy (MeV)	Cross-Section (mb)	Energy (MeV)	Cross-Section (mb)	Energy (MeV)	Cross-Section (mb)	Energy (MeV)	Cross-Section (mb)
2.0	2.5 ± 0.4	14.5	99.1 ± 4.8	26.5	52.1 ± 4.1	38.5	44.6 ± 3.8
2.5	8.3 ± 1.2	15.0	94.1 ± 13.4	27.0	51.6 ± 8.2	39.0	44.4 ± 6.4
3.0	29.0 ± 3.8	15.5	89.7 ± 8.7	27.5	51.0 ± 8.1	39.5	44.3 ± 6.3
3.5	54.0 ± 11.1	16.0	85.8 ± 5.7	28.0	50.5 ± 8.0	40.0	44.1 ± 5.8
4.0	94.6 ± 3.1	16.5	82.3 ± 4.2	28.5	50.0 ± 7.9	40.5	44.0 ± 6.2
4.5	137.1 ± 11.0	17.0	79.1 ± 11.6	29.0	49.6 ± 7.8	41.0	43.9 ± 6.1
5.0	190.3 ± 18.5	17.5	76.2 ± 5.4	29.5	49.2 ± 3.4	41.5	43.7 ± 6.0
5.5	239.9 ± 22.5	18.0	73.6 ± 5.4	30.0	48.8 ± 7.7	42.0	43.6 ± 5.9
6.0	273.6 ± 36.1	18.5	71.3 ± 10.8	30.5	48.4 ± 7.6	42.5	43.5 ± 1.9
6.5	287.9 ± 39.0	19.0	69.2 ± 5.3	31.0	48.0 ± 7.5	43.0	43.4 ± 5.8
7.0	286.4 ± 37.0	19.5	67.2 ± 10.0	31.5	47.7 ± 4.6	43.5	43.3 ± 5.7
7.5	274.7 ± 21.1	20.0	65.5 ± 10.0	32.0	47.4 ± 7.4	44.0	43.2 ± 5.7
8.0	257.7 ± 33.5	20.5	63.9 ± 2.6	32.5	47.1 ± 7.3	44.5	43.1 ± 1.7
8.5	238.7 ± 12.5	21.0	62.4 ± 9.7	33.0	46.8 ± 7.2	45.0	43.0 ± 5.5
9.0	219.6 ± 26.3	21.5	61.1 ± 9.5	33.5	46.6 ± 2.5	45.5	42.9 ± 5.4
9.5	201.6 ± 24.5	22.0	59.8 ± 9.4	34.0	46.3 ± 3.4	46.0	42.9 ± 5.4
10.0	185.1 ± 12.5	22.5	58.7 ± 9.2	34.5	46.1 ± 7.0	46.5	42.8 ± 2.4
10.5	170.3 ± 23.8	23.0	57.6 ± 2.6	35.0	45.8 ± 6.9	47.0	42.7 ± 2.2
11.0	157.1 ± 12.0	23.5	56.7 ± 4.1	35.5	45.6 ± 6.2	47.5	42.6 ± 2.5
11.5	145.4 ± 8.5	24.0	55.8 ± 8.5	36.0	45.4 ± 6.8	48.0	42.6 ± 5.1
12.0	135.1 ± 7.4	24.5	54.9 ± 8.7	36.5	45.2 ± 6.7	48.5	42.5 ± 2.2
12.5	126.0 ± 17.8	25.0	54.2 ± 8.6	37.0	45.1 ± 6.6	49.0	42.4 ± 4.9
13.0	118.0 ± 5.0	25.5	53.4 ± 8.5	37.5	44.9 ± 6.6	49.5	42.4 ± 4.8
13.5	110.9 ± 15.1	26.0	52.8 ± 8.4	38.0	44.7 ± 6.5	50.0	42.3 ± 4.7
14.0	104.6 ± 14.7						

The evaluated excitation function for $^{60}Ni(d,n)^{61}Cu$ reaction by SOK code together with the available literature data, theoretical predictions by TALYS-1.8 model code and IAEA recommended data is presented in Figure 5.7. Evaluated data by SOK code show an excellent agreement with the IAEA fitted data while the model code TALYS-1.8 underestimates the magnitudes (~ 20%) of the excitation function in the energy region at >7 MeV. The excitation function predicted by the EMPIRE-3.2.2 code show a large discrepancy (in both shape and magnitude) compared to the all other data for the $^{60}Ni(d,n)^{61}Cu$ reaction. The evaluated excitation function indicates that a low energy cyclotron with an energy window of 15→2 MeV is suitable to produce ^{61}Cu in NCA form via deuteron irradiation on enriched ^{60}Ni target material.

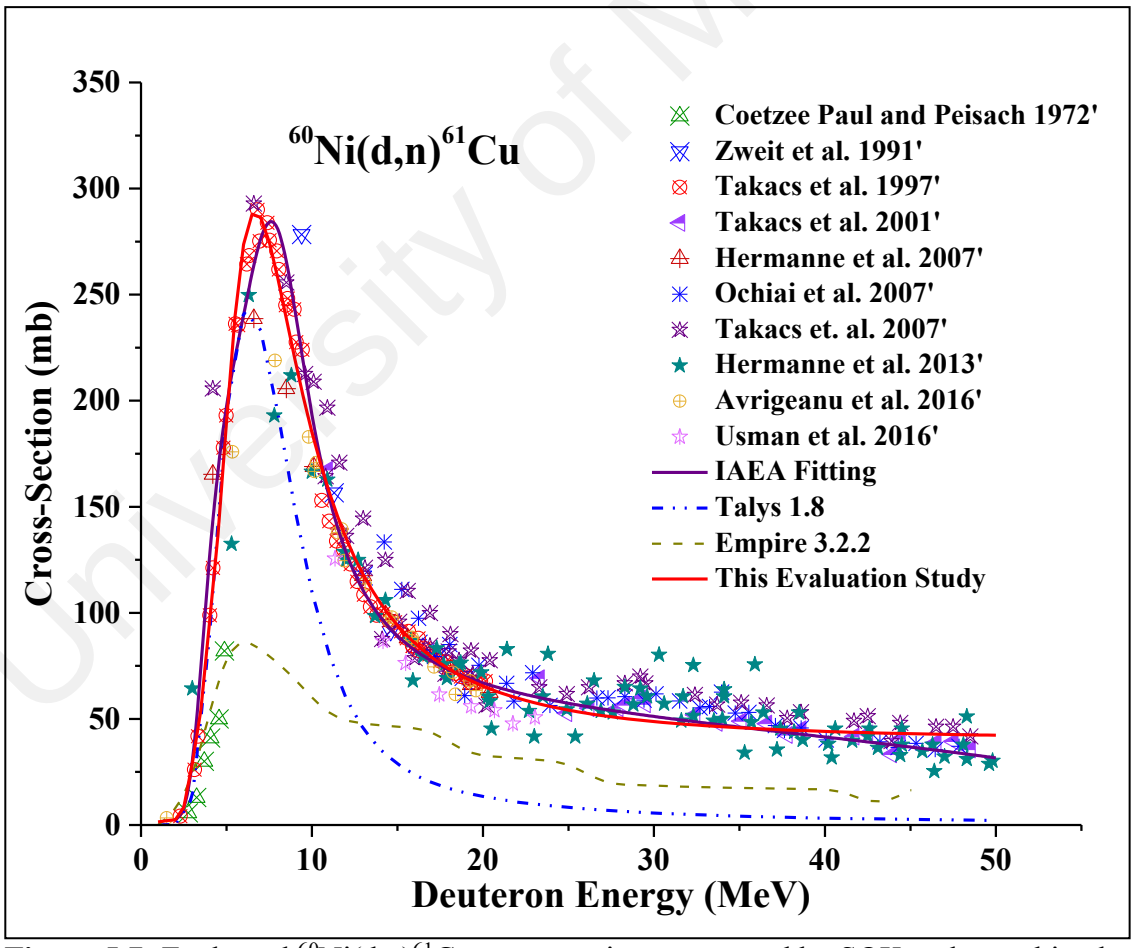

Figure 5.7: Evaluated $^{60}Ni(d,n)^{61}Cu$ cross-sections generated by SOK code combined with the least squares method.

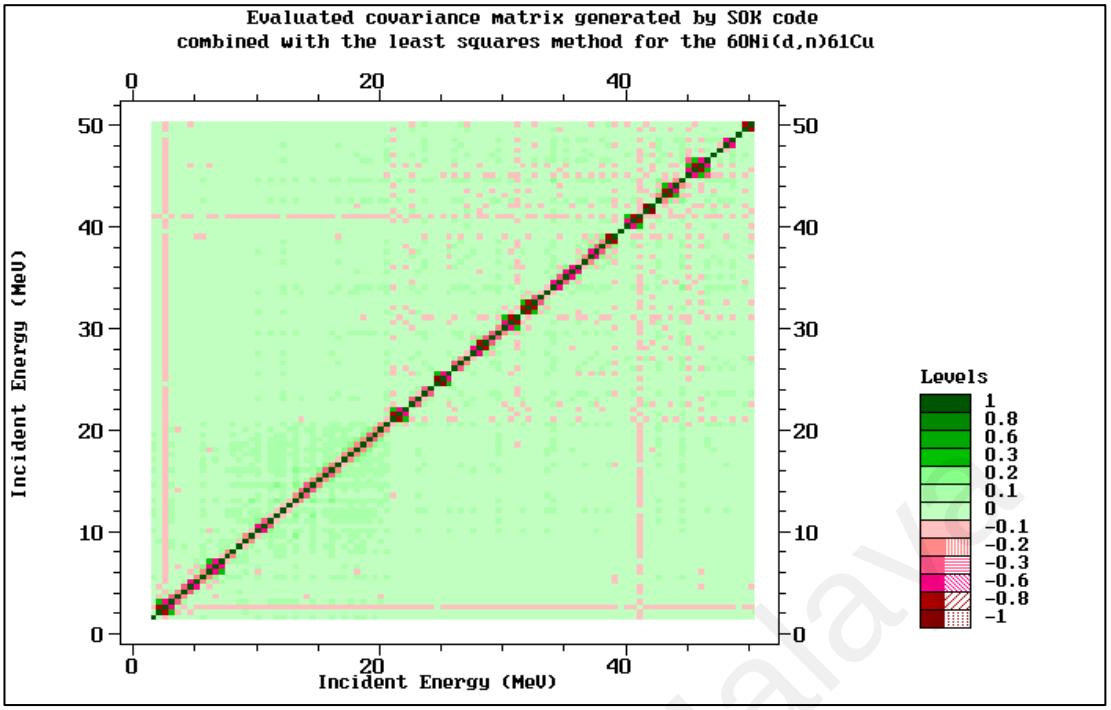

Figure 5.8: Evaluated covariance matrix generated by SOK code combined with the least squares method for the ^{60}Ni(d,n)^{61}Cu reaction.

Table 5.5: Evaluated ^{64}Zn(p,α)^{61}Cu cross-sections generated by SOK code combined with the least squares method.

Energy (MeV)	Cross-Section (mb)	Energy (MeV)	Cross-Section (mb)	Energy (MeV)	Cross-Section (mb)
3.0	1.5 ± 0.2	10.5	76.9 ± 0.4	18.0	53.0 ± 15.1
3.5	1.6 ± 0.1	11.0	85.8 ± 0.3	18.5	47.8 ± 8.6
4.0	1.6 ± 0.1	11.5	92.7 ± 0.3	19.0	43.0 ± 11.1
4.5	1.7 ± 0.1	12.0	97.5 ± 0.3	19.5	38.5 ± 7.3
5.0	1.9 ± 0.1	12.5	100.1 ± 0.8	20.0	34.4 ± 8.3
5.5	2.5 ± 0.6	13.0	100.7 ± 1.5	20.5	30.7 ± 5.3
6.0	3.7 ± 0.8	13.5	99.4 ± 5.3	21.0	27.3 ± 6.7
6.5	6.1 ± 1.0	14.0	96.6 ± 8.0	21.5	24.3 ± 1.9
7.0	10.0 ± 2.1	14.5	92.6 ± 4.9	22.0	21.6 ± 4.0
7.5	15.8 ± 2.1	15.0	87.7 ± 5.1	22.5	19.2 ± 2.8
8.0	23.5 ± 1.1	15.5	82.1 ± 5.8	23.0	17.1 ± 1.5
8.5	33.0 ± 0.5	16.0	76.3 ± 9.6	23.5	15.2 ± 3.5
9.0	43.8 ± 0.4	16.5	70.3 ± 4.3	24.0	13.5 ± 0.7
9.5	55.3 ± 0.3	17.0	64.4 ± 4.0	24.5	12.0 ± 2.8
10.0	66.5 ± 0.5	17.5	58.6 ± 2.8	25.0	10.7 ± 2.0

Figure 5.9 shows the results of SOK code generated cross-sections for the ^{64}Zn(p,α)^{61}Cu reaction together with the selected literature data and the predicted data by the theoretical codes TALYS-1.8 and EMPIRE-3.2.2. The SOK code generated data show a better representation of the literature data, while the theoretical model calculations fail

to predict the correct behaviour of the experimental excitation function. Above 8 MeV TALYS-1.8 underestimates the magnitude of the excitation function, whereas EMPIRE-3.2.2 predicts a mix behaviour (i.e., underestimates the peak energy region and slightly overestimate the tail part after 16 MeV). An energy window of 20→7 MeV is suitable for the production of ^{61}Cu via proton irradiation on ^{64}Zn target but this route yield ^{61}Cu in relatively lower amount compared to the previously discussed routes. Moreover, both model codes (EMPRE and TALYS) predicted data show clear deviation than the experimental cross-sections and also the SOK evaluated cross-sections. But the EMPIRE code calculated data show a considerable energy shifting for ^{64}Zn(p,α)^{61}Cu reaction compared to the available experimental and other evaluated data.

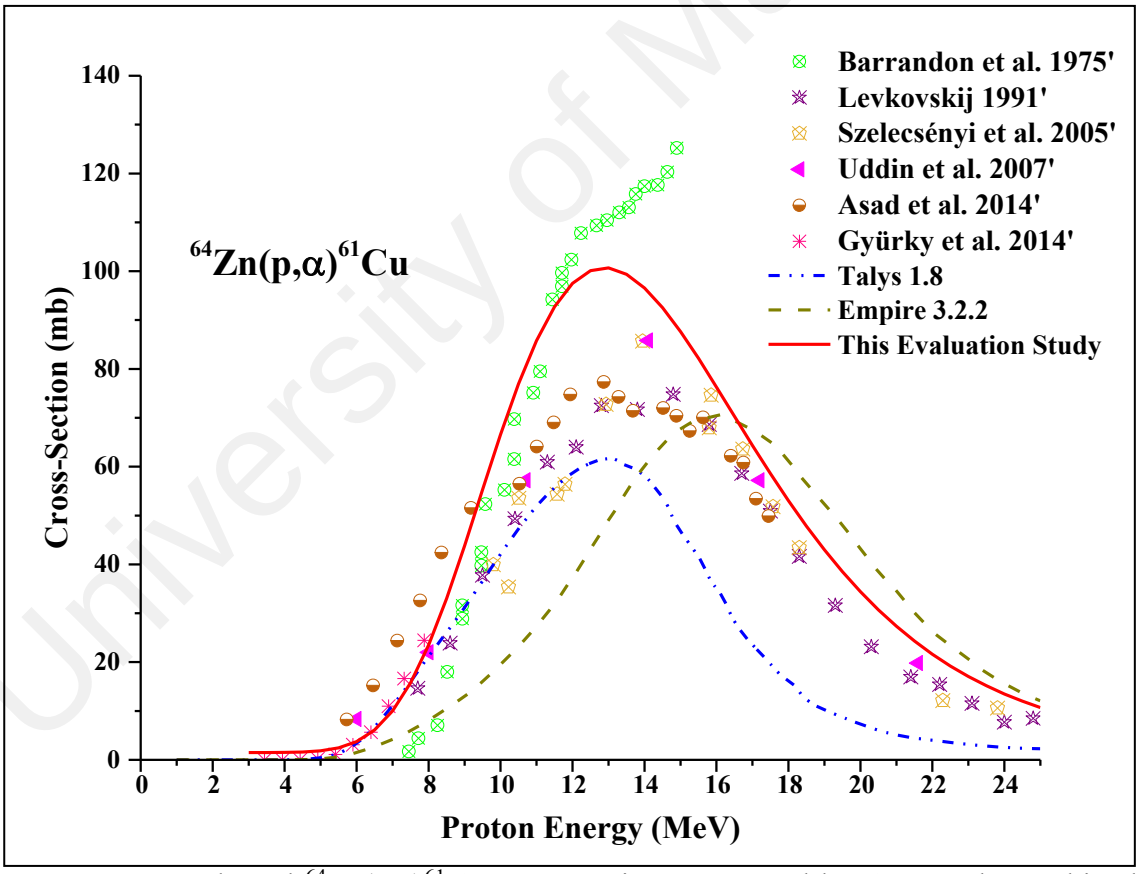

Figure 5.9: Evaluated ^{64}Zn(p,α)^{61}Cu cross-sections generated by SOK code combined with the least squares method.

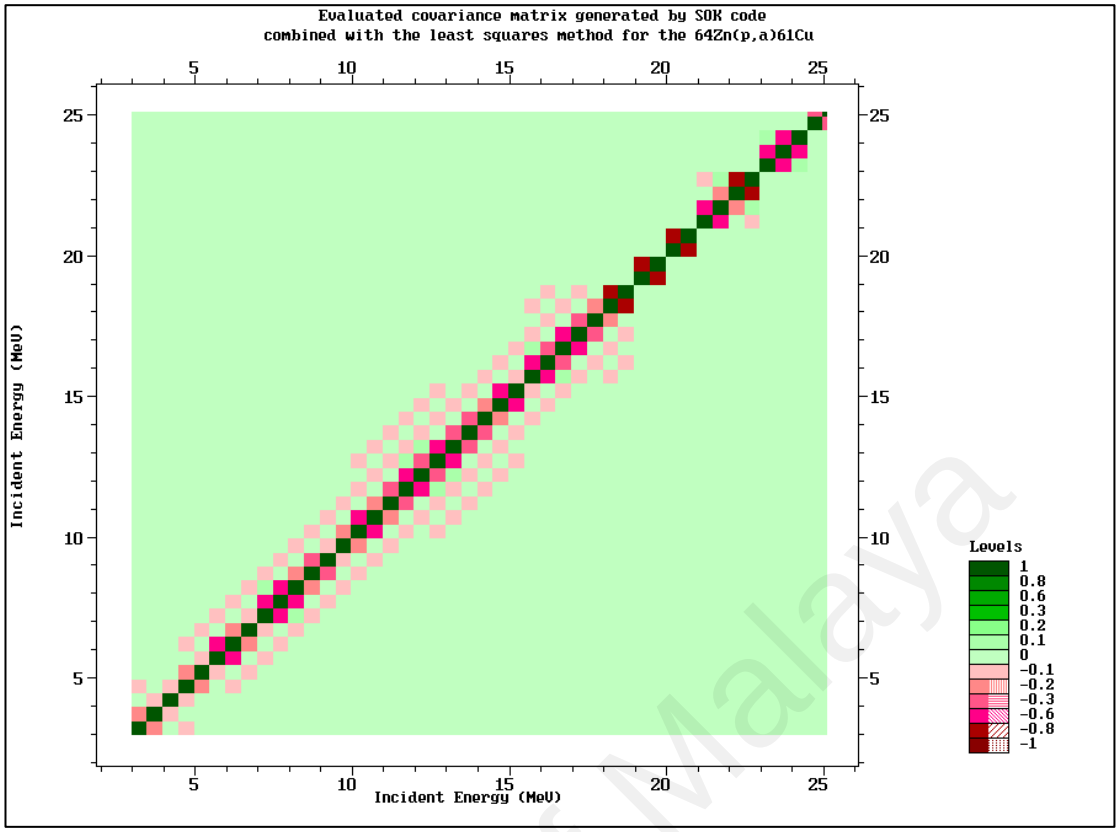

Figure 5.10: Evaluated covariance matrix generated by SOK code combined with the least squares method for the $^{64}Zn(p,\alpha)^{61}Cu$ reaction.

5.3 Evaluated Cross-Section for the $^{186}W(p,n)^{186}Re$ and $^{186}W(d,2n)^{186}Re$ Reactions

Applications of charged-particle induced reaction cross-sections currently show greater importance in various fields including isotope production for medical and industrial applications. Thus, the evaluation of such data is currently practiced by some authors via the use of pure experimental data while others are using the model codes. Here, we applied a least-squares fitting technique to evaluate the experimental cross-sections for the $^{186}W(p,n)^{186}Re$ and $^{186}W(d,2n)^{186}Re$ reactions.

The original experimental cross-sections and their corresponding uncertainties were retrieved from the EXFOR database (EXFOR, 2017) and also from the original publications. The experimental data were then corrected mainly based on the latest agreed set of decay data and monitor reaction cross-sections etc. On the other hand, no correction has been done for the nuclide half-life due to the lack of detailed information on

experimental conditions such as irradiation time, cooling and measurement time. To obtain the best fitted curve that virtually represents all of the experimental data points, a simultaneous evaluation method was applied on the normalized data points and corresponding experimental correlation matrices. This procedure can estimate the covariance matrices as well as the evaluated cross-sections together with their uncertainties. In general, the evaluated cross-sections provide a fair description of the observables, and the obtained values are listed in the Tables 5.6 and 5.7 for the ^{186}W(p,n)^{186}Re, ^{186}W(d,2n)^{186}Re reactions, respectively.

Furthermore, the obtained evaluated cross-sections are compared in the Figures 5.13 and 5.15 with the similar evaluation work available in the literature (Hussain et al., 2010), and also with evaluated data extracted from the TENDL library. Note that TENDL library (Koning et al., 2017) contains the evaluated data for a range of nuclides via the use of TALYS nuclear model code (Koning & Rochman, 2012).

Overall, it can be seen that the three theoretical works have the same trend for both reactions ^{186}W(p,n)^{186}Re and ^{186}W(d,2n)^{186}Re, which is similar to the shape/behavior of the experimental cross-sections in our region of interest. On the other hand, it is clearly observed that TALYS-1.8 code provides an underestimated magnitude for both the reactions compared to the present evaluations and most of the experimental measurements as well. Furthermore, the evaluated cross-sections by Hussain et al. (2010) for the ^{186}W(p,n)^{186}Re reaction show some clear discrepancy at the peak energy region while a little energy shift for the ^{186}W(d,2n)^{186}Re reaction at the peak region too. One of the probable reason is that Hussain et al. performed the evaluation by the use of parameter adjustment of nuclear reaction model codes while our evaluation is fully based on the update of experimental data and their documented uncertainties using the latest set of agreed parameters. On the other hand, the estimated covariance matrices by the SOK code

for the $^{186}W(p,n)^{186}Re$ and $^{186}W(d,2n)^{186}Re$ reactions are presented in Figure 5.12 and Figure 5.14, respectively.

Table 5.6: Evaluated cross-sections for the $^{186}W(p,n)^{186}Re$ reaction generated by the SOK code combined with least squares method.

Proton Energy (MeV)	Cross-Sections (mb)	Proton Energy (MeV)	Cross-Sections (mb)	Proton Energy (MeV)	Cross-Sections (mb)	Proton Energy (MeV)	Cross-Sections (mb)
5.0	0.2 ± 0.2	14.5	32.5 ± 1.6	24.0	25.0 ± 1.9	40.0	16.6 ± 1.8
5.5	0.4 ± 0.1	15.0	31.7 ± 0.8	24.5	24.7 ± 3.1	41.0	16.2 ± 4.9
6.0	2.2 ± 0.6	15.5	31.1 ± 0.7	25.0	24.4 ± 5.7	42.0	15.8 ± 4.8
6.5	5.7 ± 0.7	16.0	30.6 ± 0.8	25.5	24.1 ± 1.7	43.0	15.4 ± 4.7
7.0	11.8 ± 0.9	16.5	30.2 ± 0.6	26.0	23.8 ± 3.6	44.0	15.0 ± 4.6
7.5	21.3 ± 0.3	17.0	29.9 ± 0.8	26.5	23.5 ± 4.9	45.0	14.6 ± 4.5
8.0	34.1 ± 2.7	17.5	29.5 ± 1.2	27.0	23.2 ± 1.6	46.0	14.2 ± 1.2
8.5	48.7 ± 4.1	18.0	29.1 ± 3.3	28.0	22.6 ± 1.6	47.0	13.8 ± 4.3
9.0	62.4 ± 3.3	18.5	28.7 ± 1.6	29.0	22.0 ± 1.8	48.0	13.5 ± 4.2
9.5	72.0 ± 1.6	19.0	28.4 ± 0.7	30.0	21.5 ± 1.5	49.0	13.1 ± 4.1
10.0	74.9 ± 3.0	19.5	28.0 ± 7.9	31.0	20.9 ± 1.2	50.0	12.8 ± 4.1
10.5	71.0 ± 1.6	20.0	27.7 ± 3.0	32.0	20.4 ± 3.4	51.0	12.5 ± 4.0
11.0	62.8 ± 3.9	20.5	27.3 ± 1.5	33.0	19.9 ± 3.6	52.0	12.1 ± 2.4
11.5	54.6 ± 1.6	21.0	27.0 ± 3.9	34.0	19.4 ± 5.3	53.0	11.8 ± 3.8
12.0	48.7 ± 5.2	21.5	26.6 ± 1.1	35.0	18.9 ± 2.5	54.0	11.5 ± 3.8
12.5	44.2 ± 0.9	22.0	26.3 ± 3.2	36.0	18.4 ± 6.2	55.0	11.2 ± 3.7
13.0	39.8 ± 2.5	22.5	26.0 ± 5.6	37.0	17.9 ± 2.2		
13.5	36.3 ± 1.5	23.0	25.6 ± 7.2	38.0	17.5 ± 3.3		
14.0	33.9 ± 0.7	23.5	25.3 ± 2.7	39.0	17.0 ± 5.0		

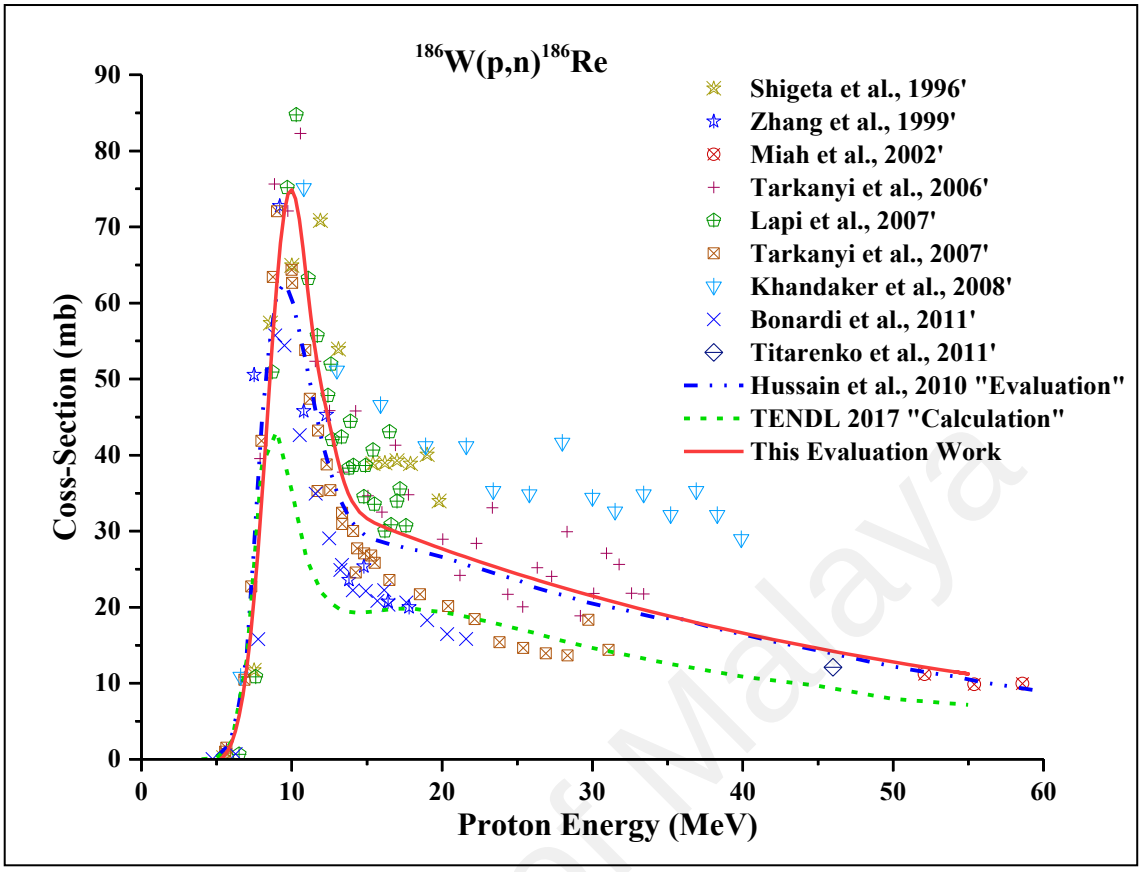

Figure 5.11: Evaluated cross-sections generated by SOK code combined with least squares method for the $^{186}W(p,n)^{186}Re$ reaction.

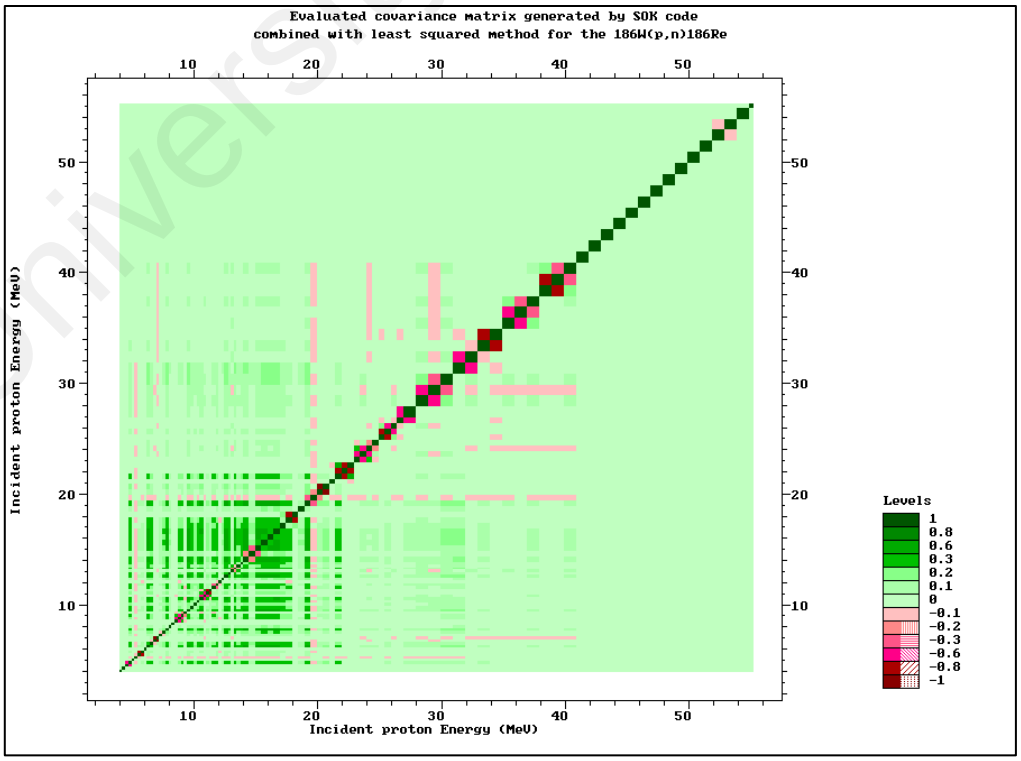

Figure 5.12: Evaluated covariance matrix generated by SOK code combined with least squares method for the $^{186}W(p,n)^{186}Re$ experiment.

Table 5.7: Evaluated cross-sections for the $^{186}W(d,2n)^{186}Re$ reaction generated by SOK code combined with the least squares method.

Deuteron Energy (MeV)	Cross-Sections (mb)	Deuteron Energy (MeV)	Cross-Sections (mb)	Deuteron Energy (MeV)	Cross-Sections (mb)	Deuteron Energy (MeV)	Cross-Sections (mb)
6.0	4.3 ± 0.2	14.0	372.6 ± 13.8	24.0	87.9 ± 5.4	40.0	30.8 ± 8.7
6.5	8.2 ± 0.0	14.5	327.7 ± 14.5	25.0	82.3 ± 4.4	41.0	28.8 ± 10.1
7.0	15.2 ± 0.2	15.0	283.0 ± 32.1	26.0	77.1 ± 4.5	42.0	27.0 ± 9.6
7.5	26.9 ± 2.0	15.5	242.6 ± 13.8	27.0	72.2 ± 4.7	43.0	25.3 ± 6.2
8.0	45.4 ± 2.4	16.0	208.8 ± 20.7	28.0	67.6 ± 3.7	44.0	23.7 ± 8.9
8.5	73.2 ± 3.1	16.5	182.2 ± 8.7	29.0	63.3 ± 4.0	45.0	22.2 ± 8.4
9.0	112.5 ± 3.9	17.0	162.3 ± 15.8	30.0	59.3 ± 3.1	46.0	20.8 ± 8.6
9.5	164.5 ± 7.2	17.5	147.8 ± 7.0	31.0	55.5 ± 3.1	47.0	19.4 ± 5.9
10.0	226.2 ± 8.7	18.0	137.4 ± 14.7	32.0	52.0 ± 2.7	48.0	18.2 ± 7.9
10.5	293.3 ± 9.5	18.5	129.7 ± 15.6	33.0	48.7 ± 2.9	49.0	17.1 ± 7.1
11.0	357.5 ± 15.8	19.0	123.8 ± 14.2	34.0	45.6 ± 3.1	50.0	16.0 ± 7.6
11.5	409.2 ± 11.7	19.5	118.9 ± 12.5	35.0	42.7 ± 3.5	51.0	15.0 ± 7.0
12.0	441.6 ± 17.5	20.0	114.6 ± 10.4	36.0	40.0 ± 3.3	52.0	14.0 ± 6.8
12.5	451.6 ± 15.4	21.0	107.1 ± 6.9	37.0	37.5 ± 2.7	53.0	13.1 ± 6.6
13.0	440.5 ± 25.0	22.0	100.2 ± 6.3	38.0	35.1 ± 3.5	54.0	12.3 ± 0.9
13.5	412.3 ± 45.4	23.0	93.9 ± 4.2	39.0	32.9 ± 10.7		

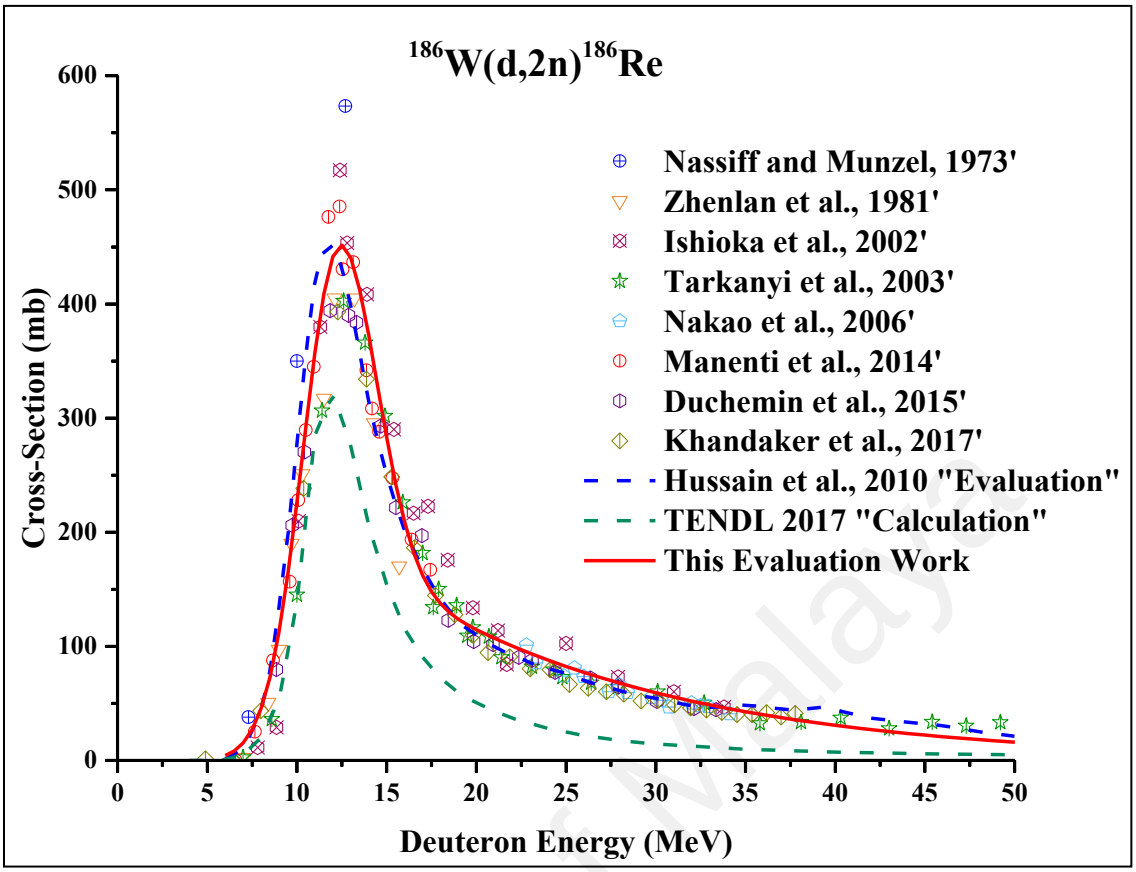

Figure 5.13: Evaluated cross-sections generated by SOK code combined with the least squares method for the ^{186}W(d,2n)^{186}Re reaction.

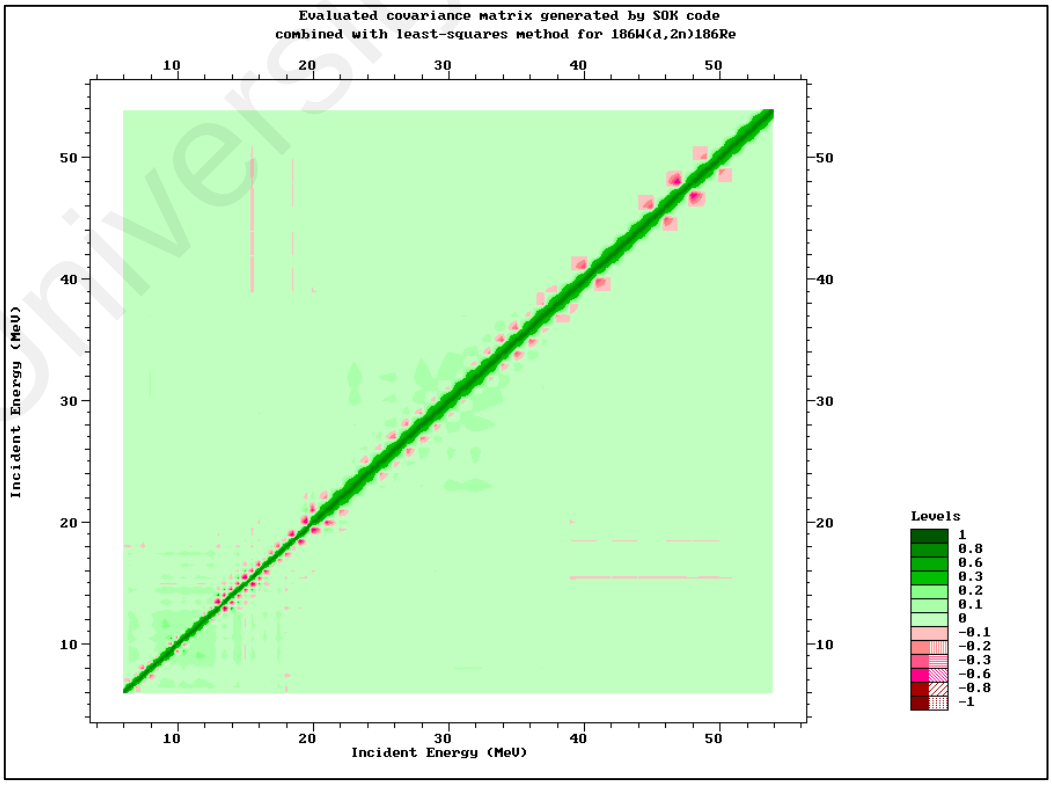

Figure 5.14: Evaluated covariance matrix generated by SOK code combined with the least squares method for the ^{186}W(d,2n)^{186}Re reaction.

5.4 Covariance Matrices Discussion

According to probability theory and statistics, the covariance between any two variables x and y is a representation on how the two variables move together. In other words, it figure out the extent to the fact that when variable (x) lies above its mean value the other variable (y) has also the same behaviour or not. Covariance may have negative or positive sign: positive sign implies that the two variables tend to move together and the negative sign implies that one of the two variables is above its mean and the other is below its mean value.

The covariance matrices showed in Figures 5.2, 5.4, 5.6, 5.8, 5.10, 5.12 and 5.14 were plotted by using "ZV View tool" developed by the IAEA-NDS division (Zerkin, 2009). In such matrices, the elements that have zero value in the off diagonal regions indicate that estimated error for the first parameter is completely independent on the other parameters. In other words no adjustments are made to the estimates of one variable due to the processing errors of other variables.

The degree of association and linear relationship that may exist among the various experimental parameters for a particular reaction cross-sections is revealed by a value of in between ±1. On the other hand, the cross-section error of the first energy point strongly affects the estimated cross-section of the second energy point (see Equations 4.1, 4.2 and 4.3) as the covariance value between two energy points becomes closer to ±1, where a positive covariance value reflects a directly proportional trend and the negative one reflects the inversely proportional trend.

However, relatively higher values of covariance data are generated in the energy region where the maximum number of experimental data points are available and showed lower values of covariance data in the energy region following the existence of less

experimental data points. A detailed information about the significance of covariance and correlation matrices in data evaluation is available in elsewhere (Badwar et al., 2018; Otuka et al., 2017).

For example, Table 5.8 shows part of SOK code generated covariance matrix for the $^{56}Fe(p,2n)^{55}Co$ reaction presented in Figure 5.2. Note that the covariance data for only first 10 energy points are presented in this table. This is because, the size of the combined covariance matrix is very large, and it is not rational to present all the data points of the matrix, rather more practical to show them in graphical form.

In the generated covariance matrix presented in Table 5.8 (partial) and in Figure 5.2, some energy points shows positive correlation between them but none of these correlations were observed to be particularly strong. Whereas, a very weak negative correlation (Table 5.8) also obtained among some of the energy points. Such negative values in the off-diagonal position indicates that the correlation between the corresponding energy points is insignificant. While the positive value of 0.016 represents that there is weak correlation exist between the 15.5 MeV and 17.0 MeV energy points. The bold marked off-diagonal values in Table 5.8 represents relatively strong correlation among the energy points. Generally, if the off-diagonal term shows a positive value of $\geq$ 0.5, it means a strong correlation while the value of $\leq$ 0.5 represents a weak correlation.

Table 5.8: Part of SOK code generated covariance matrix for the $^{56}Fe(p,2n)^{55}Co$ reaction.

Proton Energy (MeV)	15.0	15.5	16.0	16.5	17.0	17.5	18.0	18.5	19.0	19.5	20.0
15.0	1.000										
15.5	0	1.000									
16.0	0	-0.222	1.000								
16.5	0	0.230	-0.033	1.000							
17.0	0	0.016	0.121	-0.191	1.000						
17.5	0	0.087	0.191	**0.475**	-0.646	1.000					
18.0	0	0.172	0.216	**0.348**	0.211	0.161	1.000				
18.5	0	0.050	**0.358**	**0.329**	-0.022	**0.348**	0.196	1.000			
19.0	0	0.152	0.069	0.244	0.154	0.105	**0.377**	-0.184	1.000		
19.5	0	0.023	-0.004	0.009	0.021	-0.023	0.023	-0.019	0.008	1.000	
20.0	0	0.006	0.038	0.056	0.006	0.064	0.057	0.060	0.057	-0.982	1.000

CHAPTER 6: CONCLUSION

^{55}Co, ^{61}Cu and ^{186}Re radionuclides show increasing significance in imaging and radiotherapy. In general, positron emitters play a vital role in Positron Emission Tomography (PET scans) for organs imaging. However, these non-standards positron emitters have a relatively long half-life and can be produced from cheap raw materials that have good abundance. Different nuclear reactions lead to the formation of these radionuclides using nuclear reactors and accelerators.

Nowadays, a large number of cyclotrons throughout the world are involved in some aspects of radionuclide production. Investigation was done on experiments performed by accelerators to evaluate the production of ^{55}Co, ^{61}Cu and ^{186}Re radionuclides. Since production cross-section of these promising positron emitters have been listed with high order of discrepancy in EXFOR library, thus an accurate and clear nuclear data is essential for various fields especially in nuclear medicine.

Production cross-sections of promising non-standard radionuclide ^{55}Co, ^{61}Cu and ^{186}Re were evaluated via the ^{56}Fe(p,2n)^{55}Co; ^{59}Co(α,2n)^{61}Cu, ^{58}Ni(α,p)^{61}Cu, ^{60}Ni(d,n)^{61}Cu ^{64}Zn(p,α)^{61}Cu; and ^{186}W(p,n)^{186}Re, ^{186}W(d,2n)^{186}Re, respectively, nuclear processes due to its importance in medical applications. In this work, the most efficient production routes were evaluated, and thus this evaluation found great importance to obtain accurate values of production cross-sections toward the NCA production of ^{55}Co, ^{61}Cu and ^{186}Re radionuclides. In order to reduce the discrepancy exists between experimental datasets, KALMAN filter combined with least squares method together with spline function were employed to carry out this study.

This work presents a very practical approach of evaluation of nuclear data since only the experimental parameters, nuclide decay data etc. but not any other external parameters

or hypothesis are considered herein. The use of SOK code which works based on the least squares technique was found very effective to remove the existing discrepancies among the experiments and finally produce recommended cross-sections together with the covariance matrix. The produced dataset was very significant for the end users, since the results obtained by the applied mathematical approaches were consistent with experimental data and the real values as well.

Since the TENDL and EMPIRE-3.2.2 data show a clear discrepancy with the present work and also the available literature, the obtained data might be helpful to improve the predicting capability of the widely used model codes TALYS and EMPIRE.

REFERENCES

Adrian, L., & Marco-Urrea, E. (2016). Isotopes in geobiochemistry: tracing metabolic pathways in microorganisms of environmental relevance with stable isotopes. *Current Opinion in Biotechnology, 41*, 19-25.

Ajzenberg-Selove, F. (1991). Energy Levels of Light Nuclei A= 14. *Nuclear Physics, 523*, 1.

Al-Abyad, M., Comsan, M., & Qaim, S. (2009). Excitation functions of proton-induced reactions on ^{nat}Fe and enriched ^{57}Fe with particular reference to the production of ^{57}Co. *Applied Radiation and Isotopes, 67*(1), 122-128.

Al Saleh, F. S., Al Mugren, K. S., & Azzam, A. (2007). Excitation functions of (p,x) reactions on natural nickel between proton energies of 2.7 and 27.5 MeV. *Applied Radiation and Isotopes, 65*(1), 104-113.

Aleksandrov, Yu. V., Vasilev, S.K., Zelinski, A., Ivanov, R.B., Kolachkovski, A., Misiak, R., … Prikhodtseva, V.P. (1990). *Production cross-sections of spallation radioactive nuclides in thin targets of Co, Ni, Cu and Zn irradiated by 660 MeV protons.* nuclear spectroscopy and nuclear strucrutre, Joint Institution for Nuclear Research, (pp. 498). Leningrad, USSR.

Alekseev, I., & Lazarev, V. (2006). Cyclotron production and radiochemical isolation of the therapeutical radionuclide ^{186}Re. *Radiochemistry, 48*(5), 497-500.

Ansari, M. A., Abd. Al Slam, M. A., Sathik, N. P. M., Ismail, M., & Rashid, M. H. (2004). Excitation functions of α-induced reactions in Cobalt and pre-equilibrium effects. *International Journal of Modern Physics E, 13*(03), 585-595.

Antropov, A., Zarubin, P., Aleksandrov, Y. A., & Gorshkov, I. Y. (1985). *Measurement of cross-sections of the (p, n),(α, pn),(α, xn) reactions on intermediate mass nuclei*. Paper presented at the Conference on nuclear spectroscopy and nuclear structure, (pp. 369). Leningrad, USSR.

Asad, A. H., Chan, S., Morandeau, L., Cryer, D., Smith, S. V., & Price, R. I. (2014). Excitation functions of ^{nat}Zn(p,x) nuclear reactions with proton beam energy below 18 MeV. *Applied Radiation and Isotopes, 94*, 67-71.

Asscher, Y., Weiner, S., & Boaretto, E. (2017). A new method for extracting the insoluble occluded carbon in archaeological and modern phytoliths: Detection of ^{14}C depleted carbon fraction and implications for radiocarbon dating. *Journal of Archaeological Science, 78*, 57-65.

Aubrecht, G. (2003). A teachers guide to the nuclear science wall chart *Contemporary Physics Education Project* (pp. 1-4).

Avrigeanu, M., Šimečková, E., Fischer, U., Mrázek, J., Novak, J., Štefánik, M., . . . Avrigeanu, V. (2016). Deuteron-induced reactions on Ni isotopes up to 60 MeV. *Physical Review C, 94*(1), 014606.

Badwar, S., Ghosh, R., Yerraguntla, S. S., Jyrwa, B. M., Lawriniang, B. M., Naik, H., . . . Ganesan, S. (2018). Measurements and uncertainty propagation for the $^{nat}Ni(p,x)^{61}Cu$ reaction cross-section up to the proton energies of 20 MeV. *Nuclear Physics A, 977*, 112-128.

Baglin, C. M. (2003a). Nuclear Data Sheets 99, 1. Retrieved on 12 April 2017, from http://www.nndc.bnl.gov/nudat2.

Baglin, C. M. (2003b). Nuclear Data Sheets for A = 186. *Nuclear Data Sheets, 99*(1), 1-196.

Barrandon, J., Debrun, J., Kohn, A., & Spear, R. (1975). A study of the main radioisotopes obtained by irradiation of Ti, V, Cr, Fe, Ni, Cu and Zn with protons from 0 to 20 MeV. *Nuclear Instruments and Methods, 127*(2), 269-278

Barrandon, J. N., Debrun, J. L., Kohn, A., & Spear, R. H. (1975). Étude du dosage de Ti, V, Cr, Fe, Ni, Cu et Zn par activation avec des protons d'énergie limitée a 20 MeV. *Nuclear Instruments and Methods, 127*(2), 269-278.

Bertulani, C. A. (2007). *Nuclear physics in a nutshell*: Princeton University Press.

Bianchi, G., & Tinnirello, I. (2003, March). *Kalman filter estimation of the number of competing terminals in an IEEE 802.11 network.* Paper presented at the INFOCOM 2003. Twenty-Second Annual Joint Conference of the IEEE Computer and Communications. IEEE Societies (pp.844-852). San Francisco, USA.

Bissem, H. H., Georgi, R., Scobel, W., Ernst, J., Kaba, M., Rao, J. R., & Strohe, H. (1980). Entrance and exit channel phenomena in d- and ^{3}He- induced preequilibrium decay. *Physical Review C, 22*(4), 1468-1484.

Bonardi, M., Groppi, F., Persico, E., Manenti, S., Abbas, K., Holzwarth, U., . . . Alfassi, Z. (2011). Excitation functions and yields for cyclotron production of radiorhenium via ^{nat}W (p, ŧxn) $^{181-186g}Re$ nuclear reactions and tests on the production of ^{186g}Re using enriched ^{186}W. *Radiochimica Acta International Journal for Jhemical Aspects of Nuclear Science and Technology, 99*(1), 1-11.

Bonardi, M. L., Groppi, F., Manenti, S., Persico, E., & Gini, L. (2010). Production study of high specific activity NCA Re-186g by proton and deuteron cyclotron irradiation. *Applied Radiation and Isotopes, 68*(9), 1595-1601.

Browne, E., Firestone, R. B., & Shirley, V. S. (1986). *Table of radioactive isotopes*. Lawrence Berkeley Laboratory, University of California, Clifornia, USA: Wiley-interscience Publication.

Budzanowski, A., Freindl, L., Grotowski, K., Rzeszutko, M. M., Słapa, M., Szmider, J., & Hodgson, P. E. (1963). Elastic scattering and total reaction cross-sections for the interaction of 12.8 MeV deuterons with ^{12}C, ^{58}Ni, ^{60}Ni and ^{209}Bi nuclei. *Nuclear Physics, 49*, 144-160.

Budzanowski, A., Grotowski, K., Kuźmiński, J., Niewodniczański, H., Strzałkowski, A., Sykutowski, S., . . . Wolski, R. (1967). Total reaction cross-section and elastic

scattering of 24.7 MeV alpha particles in the region of A = 60 nuclei. *Nuclear Physics A, 106*(1), 21-34.

Burrows, H. B., Gibson, W. M., & Rotblat, J. (1950). Angular Distributions of Protons from the Reaction $^{16}O(d,p)^{17}O$. *Physical Review, 80*(6), 1095.

Capote, R., Herman, M., Obložinský, P., Young, P., Goriely, S., Belgya, T., . . . Plujko, V. A. (2009). RIPL–reference input parameter library for calculation of nuclear reactions and nuclear data evaluations. *Nuclear Data Sheets, 110*(12), 3107-3214.

Chadwick, M. B., Talou, P., & Kawano, T. (2005). Reducing uncertainty in nuclear data. *Los Alamos Science, 29*, 26-41.

Chapra, S. C., & Canale, R. P. (2015). *Numerical Methods for Engineers*. New York, USA: McGraw-Hill.

Coetzee Paul, P., & Peisach, M. A. X. (1972). Activation cross-sections for deuteron-induced reactions on some elements of the first transition series, up to 5.5 MeV *Radiochimica Acta*, *17*(1), 1-6.

Cogneau, M., Gilly, L. J., & Cara, J. (1967). Absolute cross-sections and excitation functions for deuteron-induced reactions on the nickel isotopes between 2 and 12 MeV. *Nuclear Physics A, 99*(4), 686-694.

Cohen, B. L., & Newman, E. (1955). (p,pn) and (p,2n) Cross-sections in medium weight elements. *Physical Review, 99*(3), 718.

Cohen, B. L., Newman, E., Charpie, R. A., & Handley, T. H. (1954). (p,pn) and (p,an) excitation functions. *Physical Review, 94*(3), 620-625.

Cottingham, W. N., & Greenwood, D. A. (2001). *An introduction to nuclear physics.* UK: Cambridge University Press.

Daraban, L., Abbas, K., Simonelli, F., Adam-Rebeles, R., & Gibson, N. (2008). Experimental study of excitation functions for the deuteron induced reactions $^{64}Zn(d,2p)^{64}Cu$ and $^{64}Zn(d,\alpha n)^{61}Cu$ using the stacked-foil technique. *Applied Radiation and Isotopes, 66*(2), 261-264.

Daum, E. (1997). Investigation of light ion induced activation cross-sections in iron proton induced activation cross-sections. *Progress Report on Nuclear Data Research in the Federal Republic of Germany, NEA/NSC/DOC-13, INDC -043,* 4-8.

Deutsch, E., Libson, K., Vanderheyden, J.-L., Ketring, A. R., & Maxon, H. R. (1986). The chemistry of rhenium and technetium as related to the use of isotopes of these elements in therapeutic and diagnostic nuclear medicine. *International Journal of Radiation Applications and Instrumentation. Part B. Nuclear Medicine and Biology, 13*(4), 465-477.

Ditrói, F., Fehsenfeld, P., Khanna, A., Konstantinov, I., Majhunka, I., Racolta, P., . . . Thereska, J. (1997). The thin layer activation method and its applications in industry. *IAEA TECDOC,* 924.

Ditrói, F., Takács, S., Tárkányi, F., Fenyvesi, A., Bergman, J., Heselius, S. J., & Solin, O. (1995). Investigation of the charged particle nuclear reactions on natural boron for the purposes of the thin layer activation (TLA). *Nuclear Instruments and Methods in Physics Research Section B: Beam Interactions with Materials and Atoms, 103*(4), 389-392.

Draper, N. R., & Smith, H. (2014). *Applied regression analysis* (326). USA: John Wiley & Sons.

Druzhinin, A. A., Lbov, A. A., & Bilibin, L. P. (1967). Cross-section of the fast-neutron reactions (n,gamma) and (n,2n) for Re isotopes. *Soviet Journal of Nuclear Physics-USSR, 5*(1), 13.

Duchemin, C., Guertin, A., Haddad, F., Michel, N., & Métivier, V. (2015). Cross-section measurements of deuteron induced nuclear reactions on natural tungsten up to 34 MeV. *Applied Radiation and Isotopes, 97*, 52-58.

Eary, J. F., Durack, L., Williams, D., & Vanderheyden, J. L. (1990). Considerations for imaging Re-188 and Re-186 isotopes. *Clinical Nuclear Medicine, 15*(12), 911-916.

Enqvist, T., Wlazło, W., Armbruster, P., Benlliure, J., Bernas, M., Boudard, A., . . . Volant, C. (2001). Isotopic yields and kinetic energies of primary residues in 1 A GeV 208Pb+p reactions. *Nuclear Physics A, 686*(1–4), 481-524.

EXFOR, (2017). Available from International Atomic Energy Agency (IAEA) Experimental Nuclear Reaction Data (EXFOR) Retrieved on 10 March 2017, from The International Network of Nuclear Reaction Data Centres. https://www-nds.iaea.org/exfor/exfor.htm.

EXFOR, (2018). Available from International Atomic Energy Agency (IAEA) Experimental Nuclear Reaction Data (EXFOR) Retrieved on 20 May 2018, from The International Network of Nuclear Reaction Data Centres. https://www-nds.iaea.org/exfor/exfor.htm.

Fenyvesi, A., Tárkányi, F., & Heselius, S. J. (2004). Excitation functions of nuclear reactions induced by ^{3}He-particles on cobalt. *Nuclear Instruments and Methods in Physics Research Section B: Beam Interactions with Materials and Atoms, 222*(3), 355-363.

Firestone, R. B. (1998). *Table of Isotopes*. USA: Wiley.

Firestone, R. B., Baglin, C. M., & Chu, F. S. Y. (1998). *Update to the 8th Table of Isotopes on CD*. USA: John Wiley and Sons.

Froehlich, K. (2009). *Environmental radionuclides: Tracers and timers of terrestrial processes* (Vol. 16). Vienna, Austria: Elsevier.

Fulmer, C. B., & Williams, I. R. (1970). Excitation functions for radioactive nucleides produced by deuteron-induced reactions in copper. *Nuclear Physics A, 155*(1), 40-48.

Gadioli, E., Gadioli Erba, E., Asher, J., & Parker, D. J. (1984). Analysis of ^{59}Co (α, x p y n z α) reactions up to 170 MeV incident α energy. *Zeitschrift für Physik A: Atoms and Nuclei, 317*(2), 155-168.

Ghosh, R., Badwar, S., Lawriniang, B., Jyrwa, B., Naik, H., Naik, Y., . . . Ganesan, S. (2017). Measurement of ^{58}Fe(p,n)^{58}Co reaction cross-section within the proton energy range of 3.38 to 19.63 MeV. *Nuclear Physics A, 964*, 86-92.

Gibbs, B. P. (2011). *Advanced Kalman filtering, least-squares and modeling: A practical handbook.* USA: John Wiley & Sons.

Goethals, P., Volkaert, A., Vandewielle, C., Dierckx, R., & Lameire, N. (2000). ^{55}Co-EDTA for renal imaging using positron emission tomography (PET): a feasibility study. *Nuclear Medicine and Biology, 27*(1), 77-81.

Grassi, I., Nanni, C., Allegri, V., Morigi, J. J., Montini, G. C., Castellucci, P., & Fanti, S. (2012). The clinical use of PET with (11) C-acetate. *American Journal of Nuclear Medicine and Molecular Imaging, 2*(1), 33-47.

Grütter, A. (1982). Excitation functions for radioactive isotopes produced by proton bombardment of Cu and Al in the energy range of 16 to 70 MeV. *Nuclear Physics A, 383*(1), 98-108.

Guertin, A., Duchemin, C., Haddad, F., Michel, N., & Métivier, V. (2014). Measurements of ^{186}Re production cross-section induced by deuterons on ^{nat}W target at ARRONAX facility. *Nuclear Medicine and Biology, 41*, e16-e18.

Gyürky, G., Fülöp, Z., Halász, Z., Kiss, G., & Szücs, T. (2014). Direct study of the α-nucleus optical potential at astrophysical energies using the ^{64}Zn(p,α)^{61}Cu reaction. *Physical Review C, 90*(5), 052801.

Heinle, R., Welch, A., Scharf, V., Meacham, G., & Prusoff, W. (1952). Studies of excretion (and absorption) of ^{60}Co labeled vitamin B12 in pernicious anemia. *Transactions of the Association of American Physicians, 65*, 214.

Herman, M., Capote, R., Carlson, B., Obložinský, P., Sin, M., Trkov, A., . . . Zerkin, V. (2007). EMPIRE: nuclear reaction model code system for data evaluation. *Nuclear Data Sheets, 108*(12), 2655-2715.

Hermanne, A., Szelecsényi, F., Sonck, M., Takács, S., Tárkányi, F., & Van den Winkel, P. (1999). New cross-section data on ^{68}Zn(p, 2n)^{67}Ga and ^{nat}Zn(p,xn)^{67}Ga nuclear reactions for the development of a reference data base. *Journal of Radioanalytical and Nuclear Chemistry, 240*(2), 623-630.

Hermanne, A., Takács, S., Adam-Rebeles, R., Tárkányi, F., & Takács, M. P. (2013). New measurements and evaluation of database for deuteron induced reaction on Ni up to 50 MeV. *Nuclear Instruments and Methods in Physics Research Section B: Beam Interactions with Materials and Atoms, 299*, 8-23.

Hermanne, A., Tárkányi, F., Takács, S., Kovalev, S. F., & Ignatyuk, A. (2007). Activation cross-sections of the ^{64}Ni(d,2n) reaction for the production of the medical

radionuclide ^{64}Cu. *Nuclear Instruments and Methods in Physics Research Section B: Beam Interactions with Materials and Atoms, 258*(2), 308-312.

Hilgers, K., Stoll, T., Skakun, Y., Coenen, H. H., & Qaim, S. M. (2003). Cross-section measurements of the nuclear reactions ^{nat}Zn(d,x)^{64}Cu, ^{66}Zn(d,α)^{64}Cu and ^{68}Zn(p,αn)^{64}Cu for production of ^{64}Cu and technical developments for small-scale production of ^{67}Cu via the ^{70}Zn(p,α)^{67}Cu process. *Applied Radiation and Isotopes, 59*(5), 343-351.

Hisakazu, M., Etsuko, S., Hiromichi, N., & Yukio, M. (1978). Alpha particle bombardment of natural nickel target for the production of ^{61}Cu. *The International Journal of Applied Radiation and Isotopes, 29*(11), 611-614.

Hodgson, P. E. (1971). *Nuclear reactions and nuclear structure.* Oxford, UK: Clarendon Press.

Holt, J., & Young, C. (1950). The Angular Distribution of Protons from the Reaction ^{27}Al(d,p)^{28}Al. *Proceedings of the Physical Society. Section A, 63*(8), 833-838.

Hussain, M., Sudár, S., Aslam, M. N., Malik, A. A., Ahmad, R., & Qaim Syed, M. (2010). Evaluation of charged particle induced reaction cross-section data for production of the important therapeutic radionuclide ^{186}Re *Radiochimica Acta International Journal for Chemical Aspects of Nuclear Science and Technology, 98*(7), 385-395.

IAEA. (2007). from International Atomic Energy Agency. Retrieved on 25 October 2016, from https://www-nds.iaea.org/medical/cup65zn0.html.

IAEA. (2017). from International Atomic Energy Agency. Retrieved on 10 march 2018, https://www-nds.iaea.org/medical/monitor_reactions.html.

Ishioka, N. S., Watanabe, S., Osa, A., Koizumi, M., Matsuoka, H., & Sekine, T. (2002). Excitation Functions of Rhenium Isotopes on the ^{nat}W(d,xn) Reactions and Production of No-carrier-added ^{186}Re. *Journal of Nuclear Science and Technology, 39*(Supplement 2), 1334-1337.

IUPAC, (2016). Periodic table of elements. Retrived on 20 June 2018, from https://iupac.org/what-we-do/periodic-table-of-elements.

Jadvar, H., & Parker, J. A. (2006). *Clinical PET and PET/CT*. London, UK: Springer Science & Business Media.

Jalilian, A. R., Rostampour, N., Rowshanfarzad, P., Shafaii, K., Kamali-Dehghan, M., & Akhlaghi, M. (2009). Preclinical studies of [^{61}Cu]ATSM as a PET radiopharmaceutical for fibrosarcoma imaging. *Acta Pharmaceutica, 59*(1), 45-55.

Jalilian, A. R., Rowshanfarzad, P., Sabet, M., & Shafiee, A. (2006). Preparation of [^{61}Cu]-2-acetylpyridine thiosemicarbazone complex as a possible PET tracer for malignancies. *Applied Radiation and Isotopes, 64*(3), 337-341.

Jansen, H., Pruim, J., Vliet, A., Paans, A., Hew, J., Franssen, E., . . . Korf, J. (1994). Visualization of damaged brain tissue after ischemic stroke with cobalt-55 positron emission tomography. *Journal of Nuclear Medicine, 35*, 456-456.

Jansen, H., Willemsen, A., Sinnige, L., Paans, A., Hew, J., Franssen, E., . . . Korf, J. (1995). Cobalt-55 positron emission tomography in relapsing-progressive multiple sclerosis. *Journal of the Neurological Sciences, 132*(2), 139-145.

Jastrzebski, J., Singh, P. P., Mroz, T., Vigdor, S. E., Fatyga, M., & Karwowski, H. J. (1986). Interaction of 5-50 MeV/nucleon ^{3}He and ^{4}He with ^{59}Co. *Physical Review C Nuclear Physics, 34*(1), 60-79.

Jenkins, I., & Wain, A. (1970). Excitation functions for the bombardment of ^{56}Fe with protons. *Journal of Inorganic and Nuclear Chemistry, 32*(5), 1419-1425.

Junde, H. (2008). Nuclear data sheets *109*, 787. Retrieved on 20 Sep 2016, from http://www.nndc.bnl.gov/nudat2.

Karol, P. J., & Miller, J. M. (1968). Nuclear-structure effects in simple high-energy spallation reactions. *Physical Review, 166*(4), 1089-1096.

Kawano, T., Matsunobu, H., & Murata, T. (2000). Evaluation of fission cross-sections and covariances for ^{233}U, ^{235}U, ^{238}U, ^{239}Pu, ^{240}Pu, and ^{241}Pu. JAERI-Research 2000-004, 2000 Japan Atomic Energy Research Institution.

Kelley, J., Kwan, E., Purcell, J., Sheu, C., & Weller, H. (2012). Energy levels of light nuclei A= 11. *Nuclear Physics A, 880*, 88-195.

Khandaker, Kim, K., Kim, G., & Otuka, N. (2010). Cyclotron production of the ^{105,106m}Ag, ^{100,101}Pd, ^{100,101m,105}Rh radionuclides by ^{nat}Pd(p,x) nuclear processes. *Nuclear Instruments and Methods in Physics Research Section B: Beam Interactions with Materials and Atoms, 268*(14), 2303-2311.

Khandaker, M. U., Ali, S. K. I., Kassim, H. A., & Yusof, N. (2017). Evaluated cross-sections of ^{55}Co radionuclide, a non-standard positron emitter for clinical applications. *Radiation Physics and Chemistry, 140*(Supplement C), 511-520.

Khandaker, M. U., Nagatsu, K., Minegishi, K., Wakui, T., Zhang, M.-R., & Otuka, N. (2017). Study of deuteron-induced nuclear reactions on natural tungsten for the production of theranostic ^{186}Re via AVF cyclotron up to 38 MeV. *Nuclear Instruments and Methods in Physics Research Section B: Beam Interactions with Materials and Atoms, 403*, 51-68.

Khandaker, M. U., Uddin, M. S., Kim, K., Lee, M. W., Kim, K. S., Lee, Y. S., . . . Lee, Y. O. (2008). Excitation functions of proton induced nuclear reactions on ^{nat}W up to 40 MeV. *Nuclear Instruments and Methods in Physics Research Section B: Beam Interactions with Materials and Atoms, 266*(7), 1021-1029.

Kim, E. J., Nakamura, T., Uwamino, Y., Nakanishi, N., Imamura, M., Nakao, N., . . . Tanaka, S. (1999). Measurements of Activation Cross-sections on Spallation Reactions for ^{59}Co and ^{nat}Cu at Incident Neutron Energies of 40 to 120 MeV. *Journal of Nuclear Science and Technology, 36*(1), 29-40.

Kim, K., Khandaker, M. U., Naik, H., & Kim, G. (2014). Excitation functions of proton induced reactions on ^{nat}Fe in the energy region up to 45 MeV. *Nuclear Instruments and Methods in Physics Research Section B: Beam Interactions with Materials and Atoms, 322*, 63-69.

Kinuya, S., Yokoyama, K., Izumo, M., Sorita, T., Obata, T., Mori, H., . . . Tonami, N. (2005). Locoreginal radioimmunotherapy with ^{186}Re-labeled monoclonal antibody in treating small peritoneal carcinomatosis of colon cancer in mice in comparison with ^{131}I-counterpart. *Cancer Letters, 219*(1), 41-48.

Kinuya, S., Yokoyama, K., Kawashima, A., Izumo, M., Sorita, T., Obata, T., . . . Michigishi, T. (2002). Radioimmunotherapy with ^{186}Re-labeled monoclonal antibody to treat liver metastases of colon cancer cells in nude mice. *Cancer Biotherapy and Radiopharmaceuticals, 17*(6), 681-687.

Klett, R., Lange, U., Haas, H., Voth, M., & Pinkert, J. (2007). Radiosynoviorthesis of medium-sized joints with rhenium-186-sulphide colloid: a review of the literature. *Rheumatology, 46*(10), 1531-1537.

Knapp Jr, F. R., Beets, A., Pinkert, J., Kropp, J., Lin, W., & Wang, S. (1998). Rhenium radioisotopes for therapeutic radiopharmaceutical development. *IAEA Safety Reports Series, 209*(11)*,* 156-159.

Knut, L. (2015). Radiosynovectomy in the therapeutic management of arthritis. *World journal of Nuclear Medicine, 14*(1), 10.

Kolesnikov-Gauthier, H., Carpentier, P., Depreux, P., Vennin, P., Caty, A., & Sulman, C. (2000). Evaluation of toxicity and efficacy of ^{186}Re-hydroxyethylidene diphosphonate in patients with painful bone metastases of prostate or breast cancer. *Journal of Nuclear Medicine, 41*(10), 1689-1694.

Koning, Rochman, D., & Sublet, J. C. (2017). TALYS-based evaluated nuclear data library. Retrieved on 12 Feb 2018 , from https://tendl.web.psi.ch/tendl_2017/tendl2017.html.

Koning, A. J., & Rochman, D. (2012). Modern Nuclear Data Evaluation with the TALYS Code System. *Nuclear Data Sheets, 113*(12), 2841-2934.

Krajčiová, D., Melník, M., Havránek, E., Forgácsová, A., & Mikuš, P. (2014). Copper compounds in nuclear medicine and oncology. *Journal of Coordination Chemistry, 67*(9), 1493-1519.

Kuno, A., Matsuo, M., Takano, B., Yonezawa, C., Matsue, H., & Sawahata, H. (1997). Neutron induced prompt gamma-ray and instrumental neutron activation analyses of urban estuarine sediments. *Journal of Radioanalytical and Nuclear Chemistry, 218*(2), 169-176.

Laforest, R., Dehdashti, F., Lewis, J. S., & Schwarz, S. W. (2005). Dosimetry of $^{60/61/62/64}$Cu-ATSM: a hypoxia imaging agent for PET. *European Journal of Nuclear Medicine and Molecular Imaging, 32*(7), 764-770.

Lagunas-Solar, M., & Jungerman, J. (1979). Cyclotron production of carrier-free cobalt-55, a new positron-emitting label for bleomycin. *The International Journal of Applied Radiation and Isotopes, 30*(1), 25-32.

Lam, M. G., de Klerk, J. M., & van Rijk, P. P. (2004). ^{186}Re-HEDP for metastatic bone pain in breast cancer patients. *European Journal of Nuclear Medicine And Molecular Imaging, 31*(1), S162-S170.

Lapi, S., Mills, W. J., Wilson, J., McQuarrie, S., Publicover, J., Schueller, M., . . . Ruth, T. J. (2007). Production cross-sections of $^{181–186}$Re isotopes from proton bombardment of natural tungsten. *Applied Radiation and Isotopes, 65*(3), 345-349.

Lederer, C. M., Hollander, J. M., & Perlman, I. (1967). *Table of lsotopes*. New York, USA: John Wiley & Sons.

Lederer, C. M., & Shirley, V. S. (1978). *Table of lsotopes*. New York, USA: John Wiley & Sons.

Leo, W. R. (2012). *Techniques for nuclear and particle physics experiments: a how-to approach*. New York, USA. Springer Science & Business Media.

Levkovskij, V. N. (1991a). *Activation cross section nuclides of average masses (A= 40–100) by protons and alpha-particles with average energies (E= 10–50 MeV)*. Moscow, USSR: Inter-Vesi.

Levkovskij, V. (1991b). *Activation Cross-sections of Medium Mass Nuclide (A= 40–100) by Medium Energy Protons and Alpha Particles (E= 10–50 MeV).* Moscow, USSR: Inter-Vesi.

Li, Q., Li, R., Ji, K., & Dai, W. (2015). Kalman Filter and Its Application. *1-3 Nov 2015 International Conference on Intelligent Networks and Intelligent Systems (ICINIS)*. Tianjin, China, 74-77.

Manenti, S., Persico, E., Abbas, K., Bonardi Mauro , L., Gini, L., Groppi, F., . . . Simonelli, F. (2014). Excitation functions and yields for cyclotron production of radiorhenium via deuteron irradiation: ^{nat}W(d,xn)$^{181,182(A+B),183,184(m+g),186g}$Re nuclear reactions and tests on the production of ^{186g}Re using enriched ^{186}W *Radiochimica Acta*, *102*(8), 669-680.

Mannhart, W., & Messreaktor, B. F. (1981). *A small guide to generating covariances of experimental data*. Germany: Physikalisch-Technische Bundesanstalt.

Mannheim, J. G., Schmid, A. M., Schwenck, J., Katiyar, P., Herfert, K., Pichler, B. J., & Disselhorst, J. A. (2018). PET/mri hybrid systems. *Seminars in Nuclear Medicine, 48*(4),332-347.

Martens, U., & Schweimer, G. W. (1970). Production of ^{7}Be,^{22}Na,^{24}Na and^{28}Mg by irradiation of ^{27}Al with 52 MeV deuterons and 104 MeV alpha particles. *Zeitschrift für Physik A Hadrons and Nuclei, 233*(2), 170-177.

Martens, U., & Zyklotron-Laboratorium, G. S. (1969). Kernforschungszentrum KFK 1083. Karlsruhe, Germany.

Matters, D. A., Lerch, A. G., Hurst, A. M., Szentmiklósi, L., Carroll, J. J., Detwiler, B., . . . Belgya, T. (2016). Investigation of ^{186}Re via radiative thermal-neutron capture on ^{185}Re. *Physical Review C, 93*(5), 054319.

Maxon, H. R., Thomas, S. R., Hertzberg, V. S., Schroder, L. E., Englaro, E. E., Samaratunga, R., . . . Deutsch, K. F. (1992). Rhenium-186 hydroxyethylidene diphosphonate for the treatment of painful osseous metastases. *Seminars in Nuclear Medicine, 22*(1), 33-40.

Maziere, B., Stulzaft, O., Verret, J., Comar, D., & Syrota, A. (1983). [55 Co]-and [64 Cu] DTPA: New radiopharmaceuticals for quantitative tomocisternography. *The International Journal of Applied Radiation And Isotopes, 34*(3), 595-601.

McCarthy, D. W., Bass, L. A., Cutler, P. D., Shefer, R. E., Klinkowstein, R. E., Herrero, P., . . . Welch, M. J. (1999). High purity production and potential applications of copper-60 and copper-61. *Nuclear Medicine and Biology, 26*(4), 351-358.

McCutchan, E. (2012). Nuclear data sheets for A= 68. *Nuclear Data Sheets, 113*(6-7), 1735-1870.

McGowan, F., Stelson, P., & Smith, W. (1964). Cross-sections for the ^{58}Ni(α, p), ^{58}Ni(α, γ), and ^{59}Co(α, n) Reactions. *Physical Review, 133*(4B), B907-910.

McGowan, F. K., Milner, W. T., & Kim, H. J. (1964). *Nuclear Cross-sections for Charged-Particle Induced Reactions Ni, Cu*. Tennessee, USA: Oak Ridge National Laboratory.

Melcher, C. L. (2000). Scintillation crystals for PET. *The Journal of Nuclear Medicine, 41*(6), 1051-1055.

Menapace, E., Bonardi, M., Groppi, F., Persico, E., & Alfassi, Z. (2007, April). *Experimental and calculated nuclear reaction data relevant to innovative production of medical radioisotopes.* Paper presented at the International Conference on Nuclear Data for Science and Technology (pp.1403-1406), Nice, France.

Metrohm, Herisau, (2015). Pharmaceutical analysis (8.000.5139EN) (pp. 20), Switzerland, Retrieved on 21 February 2019, from https://www.metrohm.com/en/documents /80005139.

Miah, M. H., Kuhnhenn, J., Herpers, U., Michel, R., & Kubik, P. (2002). Production of residual nuclides by proton-induced reactions on target W at an energy of 72 MeV. *Journal of Nuclear Science and Technology, 39*(2), 369-372.

Michel, R., & Brinkmann, G. (1980). Alpha-induced reactions on cobalt. *Nuclear Physics A, 338*(1), 167-189.

Michel, R., Brinkmann, G., & Stück, R. (1983). Integral excitation functions of α-induced reactions on titanium, iron and nickel. *Radiochimica Acta, 32*(4), 173-190.

Michel, R., Brinkmann, G., Weigel, H., & Herr, W. (1979). Measurement and hybrid-model analysis of proton-induced reactions with V, Fe and Co. *Nuclear Physics A, 322*(1), 40-60.

Michel, R., & Galas, M. (1983). ^{3}He-induced reactions on cobalt. *Nuclear Physics A, 404*(1), 77-92.

Michel, R., Hansmann, D., Neumann, S., Glasser, W., Schuhmacher, H., Dangendorf, V., . . . Meulders, J. P. (2015). Excitation functions for the production of radionuclides by neutron-induced reactions on C, O, Mg, Al, Si, Fe, Co, Ni, Cu, Ag, Te, Pb, and U up to 180 MeV. *Nuclear Instruments and Methods in Physics Research Section B: Beam Interactions with Materials and Atoms, 343*, 30-43.

Moustapha, M. E., Ehrhardt, G. J., Smith, C. J., Szajek, L. P., Eckelman, W. C., & Jurisson, S. S. (2006). Preparation of cyclotron-produced ^{186}Re and comparison with reactor-produced ^{186}Re and generator-produced ^{188}Re for the labeling of bombesin. *Nuclear Medicine and Biology, 33*(1), 81-89.

Nagame, Y., Nakamura, Y., Takahashi, M., Sueki, K., & Nakahara, H. (1988). Pre-equilibrium process in ^{3}He-induced reactions on ^{59}Co, ^{109}Ag, ^{181}Ta and ^{209}Bi. *Nuclear Physics A, 486*(1), 77-90.

Nakao, M., Ochiai, K., Kubota, N., Sato, S., Yamauchi, M., Nishitani, T., . . . Sudo, H. (2006). Evaluation of deuteron-induced activation for IFMIF accelerator structural materials. *JAEA-Research--2006-071*. Japan: Japan Atomic Energy Agency.

Nassiff, S., & Münzel, H. (1973). Cross-sections for the Reactions ^{66}Zn(d,)^{67}Ga, ^{52}Cr(d,2n)^{52g}Mn and ^{186}W(d,2n)^{186}Re. *Radiochimica Acta, 19*(3), 97-99.

Nichols, A., & Tuli, J. (2007, April). *The aims and activities of the International Network of Nuclear Structure and Decay Data Evaluators*. Paper presented at the International Conference on Nuclear Data for Science and Technology (pp. 37-42). Nice, France.

Nichols, A. L., Singh, B., & Tuli, J. K. (2012). Nuclear data sheets for A= 62. *Nuclear Data Sheets, 113*(4), 973-1114.

Nieweg, O., Piers, D., Beekhuis, H., Paans, A., Welleweerd, J., Vaalburg, W., & Woldring, M. (1981). Bleomycin-Co-55 in the detection of lung-cancer and brain metastases. *Journal of Nuclear Medicine, 22*(6), 50.

NNDC. (2018). Q-value Calculator Retrieved on 5 January 2018, from Brookhaven National Laboratory. https://www.nndc.bnl.gov/qcalc.

Nozaki, T., & Hazue, M. (1995). Advantage of accelerator produced radionuclides. *Principles of Nuclear Medicine. 2nd ed. Philadelphia WB Saunders*, 144-150.

NuDat 2.7. (2018). NNDC. from National Nuclear Data Center, Brookhaven National Laboratory.

Ochiai, K., Kubota, N., Sato, S., Yamauchi, M., Ishioka, N.H., Nishitani, T., Konno, C., & Nakao, M. Bersillon, O.Bauge, E., Bauge, E.Gunsing, F., Gunsing, F.Leray, S., Leray, S., & Jacqmin, R. (2007, April). *Deuteron induced activation cross-section measurement for IFMIF*. Paper presented at the International Conference on Nuclear Data for Science and Technology (pp. 1011-1014). Nice, France.

Ogawa, K., Mukai, T., Asano, D., Kawashima, H., Kinuya, S., Shiba, K., . . . Saji, H. (2007). Therapeutic effects of a ^{186}Re-complex–conjugated bisphosphonate for the palliation of metastatic bone pain in an animal model. *Journal of Nuclear Medicine, 48*(1), 122-127.

Otuka, N., Dupont, E., Semkova, V., Pritychenko, B., Blokhin, A., Aikawa, M., . . . Dunaeva, S. (2014). Towards a more complete and accurate experimental nuclear reaction data library (EXFOR): international collaboration between nuclear reaction data centres (NRDC). *Nuclear Data Sheets, 120*, 272-276.

Otuka, N., Lalremruata, B., Khandaker, M. U., Usman, A. R., & Punte, L. R. M. (2017). Uncertainty propagation in activation cross-section measurements. *Radiation Physics and Chemistry, 140*, 502-510.

Özcan, Z. (2014). Radiosynovectomy in Hemophilic Synovitis. *Molecular Imaging and Radionuclide Therapy, 23*(1), 1-4.

Palmedo, H., Rockstroh, J. K., Bangard, M., Schliefer, K., Risse, J., Menzel, C., & Biersack, H.-J. (2001). Painful Multifocal Arthritis: Therapy with Rhenium 186 Hydroxyethylidenedi-phosphonate (^{186}Re HEDP) after Failed Treatment with Medication—Initial Results of a Prospective Study. *Radiology, 221*(1), 256-260.

Paul, R. L., Harris, L. J., Englert, P. A. J., Goldman, I. D., Jackson, C., Larimer, R.-M., . . . Sur, B. (1995). Production of cosmogenic nuclides in thick targets by alpha bombardment. Part I — short-lived radioisotopes. *Nuclear Instruments and Methods in Physics Research Section B: Beam Interactions with Materials and Atoms, 100*(4), 464-470.

Pement, F. W., & Wolke, R. L. (1966). Compound-statistical features of deuteron-induced reactions. *Nuclear Physics, 86*(2), 429-442.

Pichard, A., Mrázek, J., Assié, M., Hass, M., Honusek, M., Lhersonneau, G., . . . Šimečková, E. (2011). A new cross-section measurement of reactions induced by ^{3}He particles on a carbon target. *The European Physical Journal A, 47*(6), 72.

Qaim, S., Khatun, S., & Wölfle, R. (1980). Integral cross-section measurements on (n,x) reactions induced by 30 MeV d (Be) break-up neutrons on FRT wall and structural materials (DOE/NDC-21/L(2)) New York, USA.

Qaim, S. M. (2017). Nuclear data for production and medical application of radionuclides: Present status and future needs. *Nuclear Medicine and Biology, 44*, 31-49.

Rahmim, A., & Zaidi, H. (2008). PET versus SPECT: strengths, limitations and challenges. *Nuclear Medicine Communications, 29*(3), 193-207.

Read, J. B. (1968). (p,xn) Reactions of ^{56}Fe, ^{57}Fe and ^{58}Fe at 370 MeV. *Journal of Inorganic and Nuclear Chemistry, 30*(8), 2039-2046.

Rejmund, F., Mustapha, B., Armbruster, P., Benlliure, J., Bernas, M., Boudard, A., . . . Leray, S. (2001). Measurement of isotopic cross-sections of spallation residues in 800 A MeV ^{197}Au+ p collisions. *Nuclear Physics A, 683*(1), 540-565.

Remsberg, L. P., & Miller, J. (1963). Study of (p,pn) reactions in medium weight nuclei at 370 MeV. *Physical Review, 130*(5), 2069.

Reus, U., & Westmeier, W. (1983). Catalog of gamma rays from radioactive decay part II. *Atomic Data and Nuclear Data Tables*, *29*(2), 193-406.

Rowshanfarzad, P., Sabet, M., Reza Jalilian, A., & Kamalidehghan, M. (2006). An overview of copper radionuclides and production of ^{61}Cu by proton irradiation of ^{nat}Zn at a medical cyclotron. *Applied Radiation and Isotopes, 64*(12), 1563-1573.

Schmorak, M. (1974). Nuclear data sheets for A= 186. *Nuclear Data Sheets, 13*(2), 267-303.

Schnabel, R. B., & Eskow, E. (1999). A revised modified Cholesky factorization algorithm. *SIAM Journal on Optimization, 9*(4), 1135-1148.

Scott, N. E., Cobble, J. W., & Daly, P. J. (1968). A comparison of reactions induced by medium-energy ^{3}He and ^{4}He ions in heavy target nuclei. *Nuclear Physics A, 119*(1), 131-145.

Sharma, H., Zweit, J., Smith, A., & Downey, S. (1986). Production of cobalt-55, a short-lived, positron emitting radiolabel for bleomycin. *International Journal of Radiation Applications and Instrumentation. Part A. Applied Radiation and Isotopes, 37*(2), 105-109.

Shashank, K., Ravi, N., Mukunda Rao, R., & V. Alamelu, J. (2013). *Implementation of Kalman Filter to Monitor the Level Fluctuations in a Dam Using FPGA* (vol. 188). India: Springer.

Shigeta, N., Matsuoka, H., Osa, A., Koizumi, M., Izumo, M., Kobayashi, K., . . . Lambrecht, R. M. (1996). Production method of no-carrier-added ^{186}Re. *Journal of Radioanalytical and Nuclear Chemistry, 205*(1), 85-92.

Silva, M., Luck Jr, J. V., & Llinás, A. (2004). Chronic hemophilic synovitis: the role of radiosynovectomy. *Treatment of Hemophilia. World Federation of Hemophilia, 33*, 1-10.

Siemens Healthcare, (2018). published by Siemens Medical Solutions, USA. Retrieved on 21 February 2019, from https://www.healthcare.siemens.com.my/molecular-imaging/pet-ct/biograph-mct.

Singh, N., Mukherjee, S., & Gadkari, M. (2005). Excitation functions of alpha induced reactions on natural nickel up to 50 MeV. *International Journal of Modern Physics E, 14*(04), 611-629.

Singh, N. L., Agarwal, S., & Rao, J. R. (1993). Excitation function for α-particle-induced reactions in light-mass nuclei. *Canadian Journal of Physics, 71*(3-4), 115-121.

Skulski, W., Fornal, B., Broda, R., Jastrzebski, J., Koczon, P., Kownacki, J., . . . Wrzesiński, J. (1992). Mass and charge release by the evaporation of particles from compound nuclei around mass. *Zeitschrift für Physik A Hadrons and Nuclei, 342*(1), 61-66.

Smith, D. (2008). *A Unified Monte Carlo approach to fast neutron cross-section data evaluation* (No. ANL/NDM-166). Argonne National Laboratory. Argonne, IL USA.

Spellerberg, S., Reimer, P., Blessing, G., Coenen, H., & Qaim, S. (1998). Production of ^{55}Co and ^{57}Co via proton induced reactions on highly enriched ^{58}Ni. *Applied Radiation and Isotopes, 49*(12), 1519-1522.

Srivastava, S. C., Mausner, L. F., Mease, R. C., Kolsky, K. L., Meinken, G. E., Joshi, V., ... & Fowler, J. S. (1993, May). Co-55 Labeled Monoclonal-Antibodies (Mabs) for Tumor Imaging with Pet. (1850 Samuel Morse Dr, Reston, VA 20190-5316: Society of Nuclear Medicine). *Journal of Nuclear Medicine* 34(5), 237..

Sterns, C. M. (1962). "NO TITLE". *Report series No.34* (pp. 63). New York, USA: Columbia University.

Stevens, H., Jansen, H. M., De Reuck, J., Lemmerling, M., Strijckmans, K., Goethals, P., . . . Korf, J. (1999). ^{55}Cobalt (Co) as a PET-tracer in stroke, compared with blood flow, oxygen metabolism, blood volume and gadolinium-MRI. *Journal of the Neurological Sciences, 171*(1), 11-18.

Szelecsényi, F., Kovács, Z., Suzuki, K., Okada, K., Fukumura, T., & Mukai, K. (2004). Formation of ^{60}Cu and ^{61}Cu via Co+^{3}He reactions up to 70 MeV: Production possibility of ^{60}Cu for PET studies. *Nuclear Instruments and Methods in Physics Research Section B: Beam Interactions with Materials and Atoms, 222*(3), 364-370.

Szelecsényi, F., Kovács, Z., Suzuki, K., Okada, K., van der Walt, T. N., Steyn, G. F., & Mukherjee, S. (2005). Production possibility of ^{61}Cu using proton induced nuclear reactions on zinc for PET studies. *Journal of Radioanalytical and Nuclear Chemistry, 263*(2), 539-546.

Szelecsényi, F., Steyn, G. F., Kovács, Z., Vermeulen, C., van der Meulen, N. P., Dolley, S. G., . . . Mukai, K. (2005). Investigation of the ^{66}Zn(p,2pn)^{64}Cu and 68Zn(p,x)64Cu nuclear processes up to 100 MeV: Production of ^{64}Cu. *Nuclear Instruments and Methods in Physics Research Section B: Beam Interactions with Materials and Atoms, 240*(3), 625-637.

Szelecsényi, F., Suzuki, K., Kovács, Z., Takei, M., & Okada, K. (2002). Production possibility of ^{60,61,62}Cu radioisotopes by alpha induced reactions on cobalt for PET studies. *Nuclear Instruments and Methods in Physics Research Section B: Beam Interactions with Materials and Atoms, 187*(2), 153-163.

Szelecsényi, F., Takács, S., Tárkányi, F., Sonck, M., & Hermanne, A. (1997, September). *Study of production possibility of no-carrier-added ^{186}Re via proton induced reaction on tungsten for use in radiotherapy.* (Heys, J. R., Melillo, D. G., eds.) Paper presented at the Proceedings of the sixth international symposium: synthesis and applications of isotopically labeled compounds, (pp. 701–703) John Wiley & Sons, Philadelphia, USA.

Szymanski, P., Fraczek, T., Markowicz, M., & Mikiciuk-Olasik, E. (2012). Development of copper based drugs, radiopharmaceuticals and medical materials. *Biometals, 25*(6), 1089-1112.

T.S.Soewarsono, Y. U., T.Nakamura. (1992). Neutron activation cross-section measurement from Li-7(p,n) in the proton energy region of 20 MeV to 40 MeV (pp. 354). Japan: JAERI.

Takács, S., Sonck, M., Azzam, A., Hermanne, A., & Tárkányi, F. (1997). Activation gross-section measurements of deuteron induced reactions on ^{nat}Ni with special reference to beam monitoring and production of for ^{61}Cu medical purpose. *Radiochimica Acta, 76*(1-2), 15-24.

Takács, S., Szelecsényi, F., Tárkányi, F., Sonck, M., Hermanne, A., Shubin, Y., . . . Youxiang, Z. (2001). New cross-sections and intercomparison of deuteron monitor reactions on Al, Ti, Fe, Ni and Cu. *Nuclear Instruments and Methods in Physics Research Section B: Beam Interactions with Materials and Atoms, 174*(3), 235-258.

Takács, S., Tárkányi, F., Király, B., Hermanne, A., & Sonck, M. (2007). Evaluated activation cross-sections of longer-lived radionuclides produced by deuteron induced reactions on natural nickel. *Nuclear Instruments and Methods in Physics Research Section B: Beam Interactions with Materials and Atoms, 260*(2), 495-507.

Takács, S., Tárkányi, F., & Kovács, Z. (1996). Excitation function of alpha-particle induced nuclear reactions on natural nickel. *Nuclear Instruments and Methods in Physics Research Section B: Beam Interactions with Materials and Atoms, 113*(1), 424-428.

Takács, S., Tárkányi, F., Sonck, M., & Hermanne, A. (2002). Investigation of the ^{nat}Mo (p, x)^{96mg}Tc nuclear reaction to monitor proton beams: New measurements and consequences on the earlier reported data. *Nuclear Instruments and Methods in Physics Research Section B: Beam Interactions with Materials and Atoms, 198*(3), 183-196.

Tárkányi, F., Ditrói, F., Csikai, J., Takács, S., Uddin, M. S., Hagiwara, M., . . . Dityuk, A. I. (2005). Activation cross-sections of long-lived products of proton-induced nuclear reactions on zinc. *Applied Radiation and Isotopes, 62*(1), 73-81.

Tárkányi, F., Hermanne, A., Takács, S., Ditrói, F., Kovalev, F., & Ignatyuk, A. V. (2007). New measurement and evaluation of the excitation function of the ^{186}W(p,n) nuclear reaction for production of the therapeutic radioisotope ^{186}Re. *Nuclear Instruments and Methods in Physics Research Section B: Beam Interactions with Materials and Atoms, 264*(2), 389-394.

Tarkanyi, F., Takács, S., Gul, K., Hermanne, A., Mustafa, M., Nortier, F., . . . Youxiang, Z. (2001). Beam monitor reactions. In: Charged particle cross-section database for medical radioisotope production: Diagnostic radioisotopes and monitor reactions. *IAEA,Vienna., IAEA-TECDOC-1211*.

Tárkányi, F., Takács, S., Szelecsényi, F., Ditrói, F., Hermanne, A., & Sonck, M. (2003). Excitation functions of deuteron induced nuclear reactions on natural tungsten up to 50 MeV. *Nuclear Instruments and Methods in Physics Research Section B: Beam Interactions with Materials and Atoms, 211*(3), 319-330.

Tárkányi, F., Takács, S., Szelecsényi, F., Ditrói, F., Hermanne, A., & Sonck, M. (2006). Excitation functions of proton induced nuclear reactions on natural tungsten up to 34 MeV. *Nuclear Instruments and Methods in Physics Research Section B: Beam Interactions with Materials and Atoms, 252*(2), 160-174.

Tebib, J., Manil, L., Modder, G., Verrier, P., De Rycke, Y., Bonmartin, A., . . . Kahan, A. (2004). Better results with rhenium-186 radiosynoviorthesis than with cortivazol in rheumatoid arthritis (RA): a two-year follow-up randomized controlled multicentre study. *Clinical and Experimental Rheumatology, 22*, 609-616.

Thereska, J. (2004). Radioisotope applications for troubleshooting and optimizing industrial processes. *Analytical Applications of Nuclear Techniques* 129-137. Vienna.

Tilley, D., Weller, H., Cheves, C., & Chasteler, R. (1995). Energy levels of light nuclei A= 18–19. *Nuclear Physics A, 595*(1), 1-170.

Titarenko, Y. E., Batyaev, V. F., Titarenko, A. Y., Butko, M. A., Pavlov, K. V., Florya, S. N., . . . Gudowski, W. (2011). Measurement and simulation of the cross-sections for nuclide production in ^{nat}W and ^{181}Ta targets irradiated with 0.04- to 2.6-GeV protons. *Physics of Atomic Nuclei, 74*(4), 551-572.

Titarenko, Y. E., Borovlev, S. P., Butko, M. A., Zhivun, V. M., Pavlov, K. V., Rogov, V. I., . . . Koldobskiy, A. B. (2011). Cross-sections for monitor reactions ^{27}Al(p,x)^{24}Na, ^{27}Al(p,x)^{22}Na, and ^{27}Al(p,x)^{7}Be at proton energies in the range 0.04–2.6 GeV. *Physics of Atomic Nuclei, 74*(4), 507.

Treytl, W. J., & Caretto, A. A. (1966). Study of (p,n) Reactions between 100 and 400 MeV. *Physical Review, 146*(3), 836-840.

Tuli, J. (2003). Nuclear data sheets for A= 82. *Nuclear Data Sheets, 98*, 209-334.

Tuli, J. K. (2005). Nuclear wallet cards: Brookhaven National Laboratory. NewYork, USA.

Turner, J. E. (2008). *Atoms, radiation, and radiation protection.* USA: John Wiley & Sons.

Uddin, M. S., Khandaker, M. U., Kim, K. S., Lee, Y. S., & Kim, G. N. (2007). Excitation functions of the proton induced nuclear reactions on ^{nat}Zn up to 40 MeV. *Nuclear Instruments and Methods in Physics Research Section B: Beam Interactions with Materials and Atoms, 258*(2), 313-320.

Usman, A. R., Khandaker, M. U., Haba, H., Murakami, M., & Otuka, N. (2016). Measurements of deuteron-induced reaction cross-sections on natural nickel up to 24 MeV. *Nuclear Instruments and Methods in Physics Research Section B: Beam Interactions with Materials and Atoms, 368*, 112-119.

Uwamino, Y., Sugita, H., Kondo, Y., & Nakamura, T. (1992). Measurement of neutron activation cross-sections of energy up to 40 MeV using semimonoenergetic p-Be neutrons. *Nuclear Science and Engineering, 111*(4), 391-403.

Vera Ruiz, H., & Lambrecht, R. M. (1998, June). *Trends in Cyclotrons for Radionuclide Production.* Paper presented at the Proceedings of the International Conference on Cyclotrons and their Applications, (pp. 28-30), Caen, France.

Vlieks, A., Morgan, J., & Blatt, S. (1974). Total cross-sections for some (α,n) and (α,p) reactions in medium-weight nuclei. *Nuclear Physics A, 224*(3), 492-502.

Vrzalová, J., Svoboda, O., Krása, A., Kugler, A., Majerle, M., Suchopár, M., & Wagner, V. (2013). Studies of (n,xn) cross-sections in Al, Au, Bi, Cu, Fe, I, In, Mg, Ni, Ta, Y, and Zn by the activation method. *Nuclear Instruments and Methods in Physics Research Section A: Accelerators, Spectrometers, Detectors and Associated Equipment, 726*, 84-90.

Wadsak, W., & Mitterhauser, M. (2010). Basics and principles of radiopharmaceuticals for PET/CT. *European Journal of Radiology, 73*(3), 461-469.

Wenrong, Z., Hanlin, L., & Weixiang, Y. (1993). Measurement of cross-sections by bombarding Fe with protons up to 19 MeV. *Chinese Journal of Nuclear Physics, 15*(4), 337-340.

Wigner E.P. (1995) *On the Development of the Compound Nucleus Model. In: Mehra J. (eds) Philosophical Reflections and Syntheses. The Collected Works of Eugene Paul Wigner* (Part B Historical, Philosophical, and Socio-Political Papers), vol B6,459-475. Heidelberg, Berlin, Germany: Springer.

Wikimedia Commons, the free media repository, (2017). Table isotopes en.svg. (2017, May 18). Retrieved on 21 February 2019 , frpm https://commons.wikimedia.org/w/index.php?title=File:Table_isotopes_en.svg&oldid=244525910

Williams, H. A., Robinson, S., Julyan, P., Zweit, J., & Hastings, D. (2005). A comparison of PET imaging characteristics of various copper radioisotopes. *European Journal of Nuclear Medicine and Molecular Imaging, 32*(12), 1473-1480.

Williams, I., & Fulmer, C. (1967). Excitation functions for radioactive isotopes produced by protons below 60 MeV on Al, Fe, and Cu. *Physical Review, 162*(4), 1055-1061.

Y.Uno, S. M., S.Chiba, T.Fukahori, Y.Kasugai, O.Iwamoto, P.Siegler, Y.Ikeda. (1996). *Measurements of activation cross-sections for the neutron dosimetry at an energy range from 17.5 to 30 MeV by using the ^{7}Li(p,n) quasi-mono-energetic neutron source*. International Symposium on Reactor Dosimetry. Prague, Czech Republic.

Yadav, A., Singh, P. P., Sharma, M. K., Singh, D. P., Unnati, Singh, B. P., . . . Musthafa, M. M. (2008). Large pre-equilibrium contribution in α + ^{nat}Ni interactions at ≈8–40 MeV. *Physical Review C, 78*(4), 044606.

Yeong, C.-H., Cheng, M.-h., & Ng, K.-H. (2014). Therapeutic radionuclides in nuclear medicine: current and future prospects. *Journal of Zhejiang University. Science. B, 15*(10), 845-863.

Yoshio, H., & Yukio, M. (1976). production of ^{61}Cu by α- and ^{3}He bombardments on cobalt target. *Chemistry Letters, 5*(5), 397-400.

Zaman, M., & Qaim, S. (1996). Excitation Functions of (d,n) and (d,α) Reactions on ^{54}Fe: Relevance to the Production of High Purity ^{55}Co at a Small Cyclotron. *Radiochimica Acta, 75*(2), 59-64.

Zarchan, P., & Musoff, H. (2013). *Fundamentals of Kalman filtering: a practical approach*. USA: American Institute of Aeronautics and Astronautics.

Zerkin, V. (2009). ZV View tool (Version Ver. 9.2) [web tool]. Kiev,Vienna: IAEA - NDS. Retrieved on 10 September 2016, from https://www-nds.iaea.org/public/zvview/web-zvview.

Zhang, T., Das, S. K., Fels, D. R., Hansen, K. S., Wong, T. Z., Dewhirst, M. W., & Vlahovic, G. (2013). PET With (62)Cu-ATSM and (62)Cu-PTSM Is a Useful Imaging Tool for Hypoxia and Perfusion in Pulmonary Lesions. *AJR. American Journal of Roentgenology, 201*(5), W698-W706.

Zhang, X., Li, Q., Li, W., Sheng, R., & Shen, S. (2001). Production of no-carrier-added ^{186}Re via deuteron induced reactions on isotopically enriched ^{186}W. *Applied Radiation and Isotopes, 54*(1), 89-92.

Zhang, X., Li, W., Fang, K., He, W., Sheng, R., Ying, D., & Hu, W. (1999). Excitation functions for ^{nat}W(p,xn)$^{181-186}$Re reactions and production of no-carrier-added ^{186}Re via ^{186}W(p,n)^{186}Re reaction. *Radiochimica Acta, 86*(1-2), 11-16.

Zhenlan, T., Fuying, Z., Huiyuan, Q., & Gongqing, W. (1981). Excitation functions for W-182-186 (d, 2n) Re-182-186 and W-186 (d, p) W-187 reactions. *Chinese Journal of Nuclear Physics (Beijing), 3*(3), 242-248.

Zhukova, O. A., Kanashevich, V. I., Laptev, S. V., & Chursin, G. P. (1972). Nuclear Reactions Produced by α Particles on ^{59}Co Nuclei. *Yadernaya Fizika, 16*, 242.

Zhuravlev, B., Grusha, O., Ivanova, S., Trykova, V., & Shubin, Y.-N. (1984). Analysis of neutron spectra in interaction of 22- MeV protons with nuclei. *Soviet Journal of Nuclear Physics 39*(2), 164-168.

Ziegler, J. F. (2004). SRIM-2003. *Nuclear Instruments and Methods in Physics Research Section B: Beam Interactions with Materials and Atoms, 219*, 1027-1036.

Zuber, K., & Singh, B. (2015). Nuclear Data Sheets 125, 1. Retrieved on 12 February 2018, from http://www.nndc.bnl.gov/nudat2.

Zweit, J., Smith, A. M., Downey, S., & Sharma, H. L. (1991). Excitation functions for deuteron induced reactions in natural nickel: Production of no-carrier-added 64Cu from enriched ^{64}Ni targets for positron emission tomography. *International Journal of Radiation Applications and Instrumentation. Part A. Applied Radiation and Isotopes, 42*(2), 193-197.

LIST OF PUBLICATIONS AND PAPERS PRESENTED

Publications:

Ali, S. K., Khandaker, M. U., Dababneh, S., & Kassim, H. A. (2018). Evaluation of production cross-sections for 61Cu non-standard PET radionuclide via light-ion-induced nuclear reactions on Co, Ni, Zn targets. *Nuclear Instruments and Methods in Physics Research Section B: Beam Interactions with Materials and Atoms*, *436*, 221-235.

Ali, S. K. I., Khandaker, M. U., & Kassim, H. A. (2018). Evaluation of production cross-sections for ^{186}Re theranostic radionuclide via charged-particle induced reactions on Tungsten. *Applied Radiation and Isotopes, 135*, 239-250.

Khandaker, M. U., **Ali, S. K. I.**, Kassim, H. A., & Yusof, N. (2017). Evaluated cross-sections of ^{55}Co radionuclide, a non-standard positron emitter for clinical applications. *Radiation Physics and Chemistry, 140*(Supplement C), 511-520.

Nuclear Inst. and Methods in Physics Research B 436 (2018) 221–235

Contents lists available at ScienceDirect

Nuclear Inst. and Methods in Physics Research B

journal homepage: www.elsevier.com/locate/nimb

Evaluation of production cross-sections for ^{61}Cu non-standard PET radionuclide via light-ion-induced nuclear reactions on Co, Ni, Zn targets

Samer K.I. Ali[a,b], Mayeen Uddin Khandaker[a,c,*], Saed Dababneh[b], H.A. Kassim[a]

[a] Department of Physics, University of Malaya, 50603 Kuala Lumpur, Malaysia
[b] Department of Physics, Faculty of Science, Al Balqa Applied University, P.O. Box 2587, Amman 11941, Jordan
[c] Centre for Biomedical Physics, School of Healthcare and Medical Sciences, Sunway University, 47500 Bandar Sunway, Selangor Darul Ehsan, Malaysia

ARTICLE INFO

Keywords:
^{61}Cu PET radionuclide
Charged particle-induced production route
Cross-sections evaluation
SOK code
KALMAN filter
Model calculation

ABSTRACT

Production cross-sections of ^{61}Cu, a promising radionuclide for PET imaging applications, were evaluated for the light-ion-induced nuclear reactions on Co, Ni, Zn targets. Simultaneous Evaluation on KALMAN (SOK) code combined with least squares concept was used to obtain the evaluated data together with covariances. The various production routes of ^{61}Cu were compared, and recommended excitation functions were derived using a well-defined statistical procedure. The evaluated data were also compared with the predictions of the nuclear reaction model codes TALYS and EMPIRE, and found a partial agreement among them. This study indicates that the ^{58}Ni(d,n)^{61}Cu reaction is the method of choice for ^{61}Cu production; however, the ^{58}Ni(α,p)^{61}Cu and ^{59}Co (α,2n)^{61}Cu reactions also appears to have great potential.

1. Introduction

During the last few decades numerous efforts have been devoted to study the nuclear reaction cross-sections for various purposes (as for instance production of medical radionuclides) via the use of accelerator and reactor facilities worldwide. Among the different studied pathways, neutron activation and charged-particles-induced reactions for production of medically and technologically important radionuclides received more attention to the scientific community. For the convenience of end user, the International Atomic Energy Agency (IAEA) has developed an online database entitled EXFOR, where most of the published nuclear reactions data including reference materials, charts, tables etc. are updated and maintained in a timely manner. In brief, EXFOR is the EXchange FORmat for the transmission of experimental nuclear reaction data between national and international nuclear data centres for the benefit of data users in all countries [1]. However, a careful observation on the archived cross-sections for a particular reaction in the EXFOR database often show a significant discrepancy among the different measurements even at the same energy region. Although it is very difficult to identify the real reason of discrepancy, but it is generally assumed that such discrepancy is attributed to many known/unknown sources of uncertainties such as monitor cross-sections, calibration sources, detector efficiency etc. However, a reliable and/or agreed set of data for a particular reaction can be obtained via a rigorous process called data evaluation. Thus, it is not feasible to use the raw data available in the EXFOR in practical applications without any pre-treatment or further processing. Beside this, an accurate form of nuclear reaction cross-section is important not only for optimization of production route of a particular radionuclide but also for a better understanding of nuclear reaction mechanisms and validation of different nuclear models.

On the other hand, following the development of sophisticated technology together with various imaging procedures, the necessity on the development of new radio tracers show a great demand. In the category of promising radionuclides, the ^{61}Cu ($T_{1/2} = 3.339h$, $E_{mean}(\beta^+) = 523keV$, $I_{total}(\beta^+) = 61.0\%$) offers appropriate radioactive properties to be used in Positron Emission Tomography (PET) and molecular imaging [2], and has already been used for labelling of PET radio-pharmaceuticals such as (^{61}Cu-ATSM) Cu-diacetyl-bis(N4-methylthiosemicarbazone) and (^{61}Cu-ATPS) [^{61}Cu]-2-acetylpyridine thiosemicarbazone [3]. The relatively long half-life of ^{61}Cu compared to the conventional PET radionuclides such as ^{18}F($T_{1/2}$ = 110 min), ^{15}O($T_{1/2}$ = 2 min), ^{13}N($T_{1/2}$ = 10 min) and ^{11}C($T_{1/2}$ = 20 min) allows producers to finalize chemical separation, radiolabelling without losing much of ^{61}Cu activity and gives chance to image slower metabolic processes in the body [4].

Jalilian, Rowshanfarzad, Sabet and Shafiee [5] showed interesting results in cancer treatment procedures, since various types of human

* Corresponding author at: Centre for Biomedical Physics, School of Healthcare and Medical Sciences, Sunway University, 47500 Bandar Sunway, Selangor Darul Ehsan, Malaysia.
E-mail address: mu_khandaker@um.edu.my (M. Uddin Khandaker).

https://doi.org/10.1016/j.nimb.2018.09.025
Received 1 August 2018; Received in revised form 16 September 2018; Accepted 19 September 2018
Available online 07 October 2018
0168-583X/

Applied Radiation and Isotopes 135 (2018) 239–250

Contents lists available at ScienceDirect

Applied Radiation and Isotopes

journal homepage: www.elsevier.com/locate/apradiso

Evaluation of production cross-sections for ^{186}Re theranostic radionuclide via charged-particle induced reactions on Tungsten

Samer K.I. Ali[a], Mayeen Uddin Khandaker[a,b,*], H.A. Kassim[a]

[a] Department of Physics, University of Malaya, 50603 Kuala Lumpur, Malaysia
[b] Center for Radiation Sciences, School of Healthcare and Medical Sciences, Sunway University, 47500 Bandar Sunway, Selangor, Malaysia

HIGHLIGHTS

- Cross-sections of ^{186}W(p,n)^{186}Re and ^{186}W(d,2n),^{186}Re reactions are collected in the energy range of 5–55 MeV.
- Data were renormalized based on the latest decay data and monitor reactions.
- Experimental correlation matrices were constructed using systematic and statistical uncertainties.
- SOK code combined with least-squares method was applied to the corrected data.
- Evaluated data with covariance matrix are generated and report herein.

ARTICLE INFO

Keywords:
Theranostic ^{186}Re radioisotope
β^- + γ-ray emitter
SOK code
Cross-section evaluation
Covariance estimation

ABSTRACT

^{186}Re ($T_{1/2}$ = 89.24 h, $E(\beta^-)_{mean}$= 346.7 keV, $I(\beta^-)_{total}$ = 92.59%), an intense beta-emitter shows great potential to be used as an active material in therapeutic radiopharmaceuticals due to its suitable physico-chemical properties. ^{186}Re can be produced in several ways, however charged-particle induced reactions show to be promising towards no carrier added production. In this work, production cross-sections of ^{186}Re were evaluated following the light-charged particle induced reactions on tungsten. An effective evaluation technique such as Simultaneous Evaluation on KALMAN code combined with least squares concept was used to obtain the evaluated data together with covariances. Knowledge of the underlying uncertainties in evaluated nuclear data, i.e., covariances are useful to improve the accuracy of nuclear data.

1. Introduction

As a result of the similarity in electron configuration of technetium (Tc) and its neighboring element rhenium (Re) in the periodic table, both the Tc and Re compounds have the similar chemical properties such as lipophilicity, ionic mobility, dipole moment and formal charge. Thus, the widely used Tc can be replaced by Re in some radiopharmaceuticals (Deutsch et al., 1986). The isotope ^{186}Re has a 3.7183 days half-life and decays by emitting beta particles with end point energy of 1069.5 keV ($I(\beta^-)_{total}$ = 92.59%) which followed by emission of gamma photons with energy of 137.157 keV (Iγ = 9.47%) and populate to the stable nucleus ^{186}Os and by EC (7.47%) to ^{186}W (Baglin, 2003). Due to the emission of relatively high energetic beta particles E_{max} = 1069.5 keV, ^{186}Re can be used as an active material in radiopharmaceuticals to treat various types of tumors, and also recommended for routine clinical usage (Tebib et al., 2004). For example, HEDP[HEDP = (1-hydroxyethylidene) diphosphonate] (Deutsch et al., 1986) labeled with ^{186}Re was used for long time as palliative therapy of bone metastases from prostatic cancer (Maxon et al., 1992) or breast cancer (Lam et al., 2004), and for more than one painful metastatic site (Kolesnikov-Gauthier et al., 2000). Furthermore, ^{186}Re-sulfide colloid can be used in intra-articular corticotherapy especially medium joints (Klett et al., 2007; Knut, 2015; Özcan, 2014). In order to avoid bleeding during surgical synovectomies, Radiosynovectomy can be applied using ^{186}Re on patients who suffer from hemophilia for rheumatoid arthritis and it shows interesting results in pain reduction in the infected joints (Özcan, 2014; Silva et al., 2004). Furthermore, its appropriate gamma energy and intensity allow to track inside the patient body using SPECT modality or gamma camera, therefore, a better evaluation of the dose that has been delivered to the desired site can be done (Bary et al., 1990; Knapp et al., 1998; Palmedo et al., 2001). One of the promising applications for ^{186}Re is the radio immunotherapy using monoclonal antibodies labeled with ^{186}Re, since such radiolabeled antibodies succeed in suppressing tumor from growing up after been administered

* Corresponding author at: Department of Physics, University of Malaya, 50603 Kuala Lumpur, Malaysia.
E-mail addresses: mu_khandaker@um.edu.my, mu_khandaker@yahoo.com (M.U. Khandaker).

https://doi.org/10.1016/j.apradiso.2018.01.035
Received 22 September 2017; Received in revised form 20 January 2018; Accepted 23 January 2018
Available online 31 January 2018
0969-8043/

Radiation Physics and Chemistry 140 (2017) 511–520

Contents lists available at ScienceDirect

Radiation Physics and Chemistry

journal homepage: www.elsevier.com/locate/radphyschem

Evaluated cross-sections of ^{55}Co radionuclide, a non-standard positron emitter for clinical applications

Mayeen Uddin Khandaker*, Samer K.I. Ali, Hasan Abu Kassim, Norhasliza Yusof

Department of Physics, Faculty of Science, University of Malaya, 50603 Kuala Lumpur, Malaysia

ARTICLE INFO

Keywords:
Cobalt-55 radioisotope
β⁺-emitter
Data evaluation
Covariance
Medical applications

ABSTRACT

Production cross-sections of Cobalt-55 ($T_{1/2}$ = 17.53 h, $E_{\beta^+}^{max}$ = 570 keV, $I_{\beta^+}^{rad}$ = 76%), a non-standard positron emitter have been evaluated in the energy range of 40 MeV down to the threshold energy of the ^{56}Fe(p,2n)^{55}Co nuclear reaction due to its significance as a potential PET imaging agent in medical applications. Experimental cross-sections of ^{55}Co radionuclide that lies within the scope of this work were collected from the EXFOR database, and renormalized using the latest agreed values of decay data and monitor cross-sections. Simultaneous Evaluation on KALMAN (SOK) code combined with least-squares method was applied to the corrected cross-sections to obtain evaluated cross-sections together with the covariance information. Knowledge of the underlying uncertainties in evaluated nuclear data, i.e., covariances are useful to improve the accuracy of nuclear data.

1. Introduction

Nuclear data, especially cross-sections and decay data play an important role in the choice of a radionuclide for various applications. Decay profile such as decay energy, radiation type and half-life of a particular radionuclide determines the suitability of that radionuclide for possible applications in nuclear medicine. On the other hand, data of nuclear reaction cross-sections determine the possibility of producing a radionuclide in pure form or in no carrier added (NCA) form. Updated information of nuclear decay data can be obtained without significant deviation from established data bases such as the ENSDF library (Nichols and Tuli, 2007) and National Nuclear Data Center NUDAT-2.6 data base (NUDAT-2, 2008). But production cross-sections for a particular radionuclide measured by different authors and/or in laboratories mostly show considerable discrepancies. In general, discrepancies among the different measurements may come due to various reasons: variations of monitor reactions, inappropriate cooling time, counting geometry and so on. However, it is possible to overcome the existing discrepancies among the data sets, if the experimental data could be evaluated precisely. Specifically, a more accurate form of nuclear reaction cross-sections can be obtained by evaluating reported cross-sections considering all relevant parameters with respect to the updated ones, i.e., latest agreed values of standards.

Positron emission tomography (PET) is an optimal noninvasive imaging technique, and the relatively short-lived positron emitters ^{11}C ($T_{1/2}$ = 20.3 min), ^{13}N ($T_{1/2}$ = 10.0 min), ^{15}O ($T_{1/2}$ = 2.0 min) and ^{18}F ($T_{1/2}$ = 110 min) are commonly used in this technique. However, the drawback of these conventional PET radionuclides is that they are very short-lived, and therefore, the user has to be near to production facilities such as cyclotron. Moreover, for any targeting molecules having distribution times of several hours to days, conventional PET radionuclides are not always usable and alternative positron emitting radionuclides with matching half-lives and suitable labeling properties are thus necessary. In fact, the longest-lived radionuclides are suitable to be transported and used up to day after their production, although it is noted that the fraction of radioactive impurities and/or daughter nuclides may grow as the desired radionuclide decays. The relatively long-lived radionuclide ^{55}Co ($T_{1/2}$ = 17.53 h) investigated here, is a promising candidate for PET imaging procedures, especially in diagnosing slower metabolic processes. It also plays a greater role as a Label for bleomycin in diagnostic nuclear medicine (Heinle et al., 1952; Sharma et al., 1986), and more recently, in some cardiac and cerebral studies (Speltherberg et al., 1998). Several authors (Jansen et al., 1994; Stevens et al., 1999) successfully applied ^{55}Co radioisotope as a PET imaging agent in the studies of ischemic stroke, and suggested its effective clinical use is limited up to 48 h after the production due to the co-produced ^{56}Co ($T_{1/2}$=78.8 d, $I_{\beta+}$=19%) contaminant. Maziere et al. (1983) also used ^{55}Co nuclide for quantification of cerebrospinal fluid kinetics in different areas of the brain using PET imaging. prepared for quantitation of cerebrospinal fluid (CSF) kinetics in different areas of the brain using positron emission tomography. The radionuclides are prepared by for quanti-

* Corresponding author.
E-mail address: mu_khandaker@yahoo.com (M.U. Khandaker).

http://dx.doi.org/10.1016/j.radphyschem.2017.01.011
Received 30 September 2016; Received in revised form 10 January 2017; Accepted 17 January 2017
Available online 17 January 2017
0969-806X/